

The University of Nottingham

Chemical Engineering

The Continuous Manufacture of Dispersant Coated Bioresorbable Nanoparticles

Kirsty Walton, MSci

Thesis submitted to the University of Nottingham for the degree of Doctor of Philosophy

SEPTEMBER 2017

Declaration

Except where specific reference has been made to other sources, the work presented in this thesis is the original work of the author. It has not been submitted, in whole, or in part, for any other degree or professional qualification.

Signed……. Date…….

Kirsty Walton

Acknowledgements

Firstly, I would like to thank my supervisor Professor Derek Irvine for his continuous support, patience and guidance throughout my PhD and his continued support in my current industrial endeavours.

I am extremely grateful for the opportunity to have worked with all of the people involved in the BENcH project in particular my fellow PhD students Mike ward and Magdalena Patel. I would like to thank Professor Ed Lester who kindly provided access to the hydrothermal synthesis rig and TGA equipment. I would also like to thank Dr Andy Parsons, Professor Davide De Focatiis and Professor David Grant for their in depth knowledge and support throughout the project.

I would like to express my gratitude to the technical staff at the University of Nottingham's Nanoscale and Microscale Research Centre (NMRC), in particular Elizabeth Steer and Dr Mike Fay. Without the excellent facilities and staff at the NMRC much of the analytical work conducted throughout my PhD would not have been possible.

Amongst the excellent analytical facilities at the university there are also specialist research groups who gave up their time to support my work and provide valuable results and expertise. I am indebted to Professor Jeremy Titman and his team for providing the opportunity to explore solid state NMR analysis, for their support with all things NMR related and for allowing me to reside in their office whilst writing this thesis.

I have had the opportunity to work with a number of amazing research groups throughout my time at Nottingham but none more so than Professor Steve Howdle's Polymers & Supercritical Fluid group. I am extremely thankful for their support throughout not only my PhD but also my undergraduate work.

Finally, I would like to thank my partner Darian Shurville for his unlimited patience, motivation and support.

Abstract

This thesis investigates the continuous synthesis and coating of hydroxyapatite nanoparticles (HA NP's). A range of dispersant molecules were produced and subsequently used in this continuous coating process. Starting with small aliphatic hydrocarbon chains attached to various functional groups a basic understanding of the interactions occurring between the dispersant molecule, the hydroxyapatite surface and a solvent medium was built. It became clear that the length of the hydrocarbon chain, the nature of the functional group and the morphology of the dispersant all had a role to play in the effectiveness and extent of the coating. Using this fundamental understanding the work progressed into the realm of polymeric dispersants. The biodegradable and bioresorbable polymer, polylactic acid (PLA) was utilised in the coating process with the aim of producing HA NP's that could be dispersed within a polymer matrix. These low molecular weight (M_w) polymers were based on similar chain size and functional groups chemistry. Similar linear morphologies were investigated along with a new six armed, branched morphology. It was concluded that molecular weight of the polymer (chain length), the functional head group (initiator) and morphology of the polymer were all responsible for the dispersant to successfully coat the HA NP's. However, results indicated that different surface interactions were occurring between the polymeric dispersant chain and HA than those occurring between the hydrocarbon chain and HA. The conclusion that had been drawn from our hydrocarbon coated HA NP's was that the interaction between dispersant and surface primarily resulted from the functional group. The aliphatic carbon chain would not form any significant surface bonds. This was not the same conclusion drawn from the results of our polymeric dispersants, which appeared to interact favourably with the highly charged nanoparticle surface.

A wide range of analytical techniques have been employed in this thesis to fully understand the surface chemistry occurring between dispersant and nanoparticle surface. Gel-permeation chromatography (GPC), thermogravimetric analysis (TGA), Fourier transform infrared (FTIR) and nuclear magnetic resonance (NMR) spectroscopy have been used to explore the chemistry and morphology of the dispersants. Understanding the interactions between the hydroxyapatite surface and the dispersant molecule proved more challenging. Multiple electron microscopy techniques, including scanning electron microscopy (SEM), tunnelling electron microscopy (TEM), electron energy loss (EEL) spectroscopy along with TGA and FTIR spectroscopy provided an insight into the dispersant-surface interactions. Elemental analysis, such as X-ray powder diffraction (XRD) and energy-dispersive X-ray spectroscopy (EDX) also provided support to the theories developed throughout the project. It was vital that such a wide range of analytical techniques were explored as no one technique could provide the full picture of the surface chemistry.

Whilst the many conventional analytical approaches directed our focus to a combination of functional groups and chain lengths, the exact nature of the bonds between dispersant and nanoparticle surface remained elusive. Often NMR spectroscopy, being one of the most powerful tools in understanding chemical bonds, would be able to provide such information. Due to the physical nature of our final nanocomposite material, solution state NMR spectroscopic analysis was not possible leading our investigation into the realm of solid-state NMR spectroscopy. With the help of the Nottingham University's solid-state NMR research group ^{1}H-^{31}P correlation experiments were used to investigate the interactions between the dispersant molecules and the surface of HA NP's. The spectra revealed that hydrocarbon based dispersant primarily interacted with the surface *via* their functional head group. PLA based dispersant spectra were dominated by resonances

arising from polymer chain – hydroxyapatite surface interactions. Dynamic nuclear polarization (DNP) solid-state NMR selectively enhanced the surface interactions and supported the conclusions drawn from the standard solid-state NMR correlation spectroscopy. Solid-state NMR spectroscopy was able to provide the final crucial piece of evidence that supported the conclusions drawn from Chapter's 2 and 3.

Abbreviations

DNP	Dynamic Nuclear Polarisation
DDSA	Dodecenylsuccinic Anhydride
DUMBO	Decoupling Using Mind-Boggling Optimization
DRI	Differential Refractometer
DSC	Differential scanning calorimetry
EDX	Energy-dispersive X-ray
EE	Extraction Efficiency
EELS	Electron Energy Loss Spectroscopy
FTIR	Fourier Transform Infrared
GPC	Gel Permeation Chromatography
HA	Hydroxyapatite
HPLC	High Performance Liquid Chromatography
IPA	Isopropyl Alcohol
IR	Infrared
MALLS	Multiangle Light Scattering Detector
MAS	Magic Angle Spinning
M_n	Number Average Molecular Weight

M_w	Weight Average Molecular Weight
NMR	Nuclear Magnetic Resonance
NP's	Nanoparticles
PDI	Polydispersity Index
PLGA	Poly(lactide-co-glycolide)
PLA	Polylactic Acid
PLLA	Poly(L-lactic acid)
PDLA	Poly(D-lactic acid)
PDLLA	Poly(D,L-lactic acid)
PTFE	Polytetrafluoroethylene
RI	Refractive Index
ROP	Ring Opening Polymerisation
SEM	Scanning Electron Microscopy
TEM	Transmission Electron Microscopy
TGA	Thermogravimetric Analysis
THF	Tetrahydrofuran
XRD	X-ray Diffraction

Contents

DECLARATION II
ACKNOWLEDGEMENTS III
ABSTRACT IV
ABBREVIATIONS VII
CONTENTS IX
LIST OF FIGURES, SCHEMES, TABLES AND EQUATIONS XI
1 CHAPTER 1: LITERATURE REVIEW 1
1.1 Introduction to Polymers 1
1.2 Polyesters 6
1.2.1 Poly (lactic acid) (PLA) 7
1.2.2 Ring Opening Polymerisation (ROP) 9
1.2.3 Anionic ROP 10
1.2.4 Cationic ROP 11
1.2.5 Coordination-Insertion ROP 11
1.3 Introduction to Dispersants 13
1.4 Hydroxyapatite (HA) Nanoparticles 15
1.4.1 Supercritical water continuous hydrothermal synthesis (scWCHS) reactor 16
1.5 Aims and Objectives 17
1.6 References 19
2 CHAPTER 2: CONTINUOUS FLOW, SINGLE STAGE SYNTHESIS OF DISPERSANT-STABILISED HYDROXYAPATITE PLATELET NANOPARTICLES - HYDROCARBON DISPERSANT OPTIMISATION 21
2.1 Aims and Objectives 21
2.2 Introduction 21
2.3 Experimental 26
2.3.1 Dispersant Synthesis 26
2.3.2 Material Characterisation 29
2.4 Results and Discussion 31
2.5 Conclusions 56
2.6 References 57
3 CHAPTER 3: CONTINUOUS FLOW, SINGLE STAGE SYNTHESIS OF DISPERSANT-STABILISED HYDROXYAPATITE PLATELET NANOPARTICLES - POLYLACTIC ACID (PLA) DISPERSANT OPTIMISATION 60
3.1 Aims and Objectives 60
3.2 Introduction 60
3.3 Experimental 62
3.3.1 Dispersant Synthesis 63
3.3.2 Material Characterisation 66
3.4 Results and Discussion 68
3.5 Material Analysis 108

3.6 CONCLUSIONS 118
3.7 REFERENCES 120

4 CHAPTER 4: CONTINUOUS FLOW, SINGLE STAGE SYNTHESIS OF DISPERSANT-STABILISED HYDROXYAPATITE PLATELET NANOPARTICLES - SOLID-STATE NMR SPECTROSCOPIC ANALYSIS 122

4.1 AIMS AND OBJECTIVES 122
4.2 INTRODUCTION 123
4.3 EXPERIMENTAL SETUP 124
4.4 RESULTS AND DISCUSSION 125
4.5 DNP SOLID-STATE NMR 134
4.5.1 DNP Experimental Method 136
4.5.2 4.5.2 DNP: Results and Discussion 137
4.6 CONCLUSIONS 141
4.7 REFERENCES 143

5 CHAPTER 5: SUMMARY AND OUTLOOK 145

5.1 REFERENCES 149

6 APPENDIX 150

6.1 FURTHER ANALYSIS OF THE ESTERIFIED HYDROCARBON DISPERSANTS 151
6.2 FURTHER ANALYSIS OF THE POLYMERIC DISPERSANTS 152
6.3 POLYMER DSC 155

List of Figures, Schemes, Tables and Equations

Figure 1.1 A diagram of basic homopolymer and copolymer structures. 2
Figure 1.2 A basic graph of average molecular weight *vs.* conversion for step-growth and chain-growth polymerisation. 4
Figure 1.3 Lactide stereoisomers. 7
Figure 1.4 Dispersant molecules interacting with a small hydrophilic particle. 14
Figure 1.5 The scWCHS reactor developed by Lester et al. [32] which is used in the BENcH project. Pumps are Gilson® HPLC pumps with the entire system composed of Swagelok stainless steel 316. [34, 36] 16
Figure 2.1 Schematic diagram of the continuous flow hydrothermal reactor.[25] 24
Figure 2.2a and 2.3b Schematic representation of the potential bonding methods for each head group with the HA surface. 'R' group represents a hydrocarbon chain of variable length. From left to right in 2.3a: hydrocarbon-carboxylic acid, hydrocarbon-sodium carboxylate and hydrocarbon-isosorbide. 2.3b shows other bonding options for the hydrocarbon-carboxylic acid to the HA surface and the entrainment of the isosorbide head group. 32
Figure 2.3 Molecular structure of isosorbide with endo and exo hydroxyl groups indicated. 33
Figure 2.4. 2.4a shows a 3D model of the isosorbide molecule (created in ChemBio3D Ultra) in its lowest energy state as calculated using the MM2 theorem. The distances between the three oxygen atoms in the hydroxyl group and the two ether groups depicted as a triangle. 2.4b is a diagrammatic representation of the cavity (blue) between the three oxygen atoms (red). The triangle established between the three oxygen atoms in 2.5a was used to calculate the radius of the cavity. 34
Figure 2.5 A 3D model of di-esterified lauric isosorbide in a low energy state (created in ChemBio3D Ultra) with the three oxygen atoms highlighted in yellow (2 contained in the ring structure and the third being the hydroxyl group). The distances between the 3 oxygen atoms are indicated. 36
Figure 2.6 Shows a 3D model of di-esterified lauric isosorbide in a low energy state (created in ChemBio3D Ultra) interacting with the HA surface (as a cross-section) *via* interaction through the surface Ca^{+2} ion and the cavity created by the three oxygen groups (highlighted in yellow) indicated in Figures 2.4 and 2.5. The red arrow indicates where the Ca^{2+} ion would interact, and the dashed line represents the surface of HA which should be viewed as being in the plane of the paper. 37
Figure 2.7 A molecular diagram of di-esterified laurate isosorbide with electron lone pairs shown. A red box indicates the potential interaction point of this molecule with the surface of HA. 38
Figure 2.8 A basic representation of the stearic conformations of two armed linear dispersants on the HA surface. Red spheres represent the head groups and the black lines the hydrocarbon chain. 39
Figure 2.9 TGA plots of total recorded mass loss (weight %) *vs* temperature for the hydrocarbon dispersants (inset) and coated NP's. 40

Figure 2.10 TGA plots of total recorded mass loss as a derivative of weight%/temperature *vs.* temperature for the hydrocarbon dispersant coated NP's. 41
Figure 2.11. FTIR Absorbance spectrum for unmodified HA NP with relevant absorbance bands labelled.[40] 48
Figure 2.12. FTIR Absorbance spectra for HA NP's coated with C12 hydrocarbon dispersants. Absorbance bands related to the dispersant are labelled. 49
Figure 2.13. FTIR Absorbance spectra for HA NP's coated with C16 hydrocarbon dispersants. Absorbance bands related to the dispersant are labelled. 51
Figure 2.14. FTIR Absorbance spectra for HA NP's coated with C18 hydrocarbon dispersants. Absorbance bands Peaks related to the dispersant are labelled. 53
Figure 2.15 XRD patterns for uncoated HA and coated HA for each dispersant. Highlighted marks on the x-axis indicate the predicted peak positions for hexagonal phase hydroxyapatite. 54
Figure 2.16. SEM images of modified HA. From left to right, top to bottom: HA-lauric acid, HA-palmitic acid, HA-stearic acid, HA-sodium laurate, HA-sodium palmitate, HA-sodium stearate, HA-lauric isosorbide, HA-palmitic isosorbide and HA-stearic isosorbide. 55
Figure 2.17 TEM images of modified HA. From left to right, top to bottom: HA-lauric acid, HA-palmitic acid, HA-stearic acid, HA-sodium laurate, HA-sodium palmitate, HA-sodium stearate, HA-lauric isosorbide, HA-palmitic isosorbide and HA-stearic isosorbide. 56
Figure 3.1a and 3.1b. Schematic representation of the potential bonding methods for each head group with the HA surface. 'R' group represents a PLA chain of variable length. From left to right in 1a: PLA-sodium, PLA-isosorbide alcohol group interaction and PLA-isosorbide entrained (one armed isosorbide initiated PLA). 1b shows the interaction mode for the 6-armed star PLA. 70
Figure 3.2 ^{1}H NMR spectrum of isosorbide initiated PLA, 1269 Da (20 °C, 400 MHz, $(CD_3)_2CO$). The molecular structure with corresponding labelled peaks is also depicted. . 71
Figure 3.3. Molecular diagram of the PLA chain ended with the isosorbide head group in its lowest energy configuration using a MM2 energy minimisation calculation. R represents another PLA chain initiated from the second isosorbide hydroxyl group. 79
Figure 3.4a. Basic representation of the possible steric conformations linear dispersants can form on the surface of HA. 3.4b. basic representation of the steric conformations of two armed linear dispersants on the HA surface. Red spheres represent the head groups/initiator and the black lines the PLA chain. 80
Figure 3.5. Top: mall amounts of dispersant (black lines) creating bridges between the NP's (blue spheres). Bottom: Excess of polymer fully coating the NP surface to create a steric barrier.[34] 84
Figure 3.6 TGA plots of total recorded mass loss (weight %) *vs.* temperature for the IsPLA dispersants (top graph) and IsPLA (0.005M) coated NP's (bottom). 86
Figure 3.7. TGA plot of total recorded mass loss as a derivative of weight%/temperature vs temperature for the IsPLA dispersants and IsPLA (0.005M) coated NP's. 86
Figure 3.8. TGA plots of total recorded mass loss (weight %) vs. temperature for the NaPLA dispersants (top graph) and NaPLA (0.005M) coated NP's (bottom). 87

Figure 3.9. TGA plot of total recorded mass loss as a derivative of weight%/temperature *vs.* temperature for the NaPLA dispersants and NaPLA (0.005M) coated NP's. 88
Figure 3.10. TGA plots of total recorded mass loss (weight %) *vs.* temperature for the sorbitol PLA (1000DA) and sorbitol PLA (3000Da) dispersants (top graph) and sorbitol PLA (0.005M) coated NP's (bottom)..... 89
Figure 3.11. Basic representation of the possible steric conformations branched dispersants can form on the surface of HA. Black lines represent polymer chains with dashed lines representing chains going into the plane of the paper. Red spheres represent the alcohol hydroxyl chain end group. 90
Figure 3.12. TGA plot of total recorded mass loss as a derivative of weight%/temperature *vs*. temperature for the sorbitol PLA (1000 Da) and sorbitol PLA (3000 Da) dispersants and sorbitol PLA coated NP's. 90
Figure 3.13. TGA plots of total recorded mass loss (weight %) *vs*. temperature for IsPLA (16) coated NP's (top graph) and TGA plot of total recorded mass loss as a derivative of weight%/temperature *vs.* temperature (bottom graph). The dispersant was dosed into the hydrothermal rig at varying concentrations as indicated. 94
Figure 3.14. TGA plots of total recorded mass loss (weight %) *vs.* temperature for sorbitol PLA (3000Da) coated NP's (top graph) and TGA plot of total recorded mass loss as a derivative of weight%/temperature *vs.* temperature (bottom graph). The dispersant was dosed into the hydrothermal rig at varying concentrations as indicated. 95
Figure 3.15. TGA plots of total recorded mass loss (weight %) *vs*. temperature for sorbitol PLA (6000Da) coated NP's (top graph) and TGA plot of total recorded mass loss as a derivative of weight%/temperature *vs*. temperature (bottom graph). The dispersant was dosed into the hydrothermal rig at varying concentrations as indicated. 97
Figure 3.16. TGA plots of total recorded mass loss (weight %) *vs.* temperature for IsPLA (16) coated NP's (top graph) and TGA plot of total recorded mass loss as a derivative of weight%/temperature vs temperature (bottom graph). 99
Figure 3.17. FTIR Absorbance spectrum for unmodified HA NP with relevant absorbance bands labelled. 102
Figure 3.18. FTIR Absorbance spectra for HA NP's coated with IsPLA dispersants. Absorbance bands related to the dispersant are labelled. 103
Figure 3.19. FTIR Absorbance spectra for HA NP's coated with NaPLA dispersants. Absorbance bands related to the dispersant are labelled. 104
Figure 3.20. FTIR Absorbance spectra for HA NP's coated with IsPLA (16) dispersant in varying reaction conditions. Absorbance bands related to the dispersant are labelled. 105
Figure 3.21. FTIR Absorbance spectra for HA NP's coated with the sorbitol PLA (1000 Da) dispersant. Absorbance bands related to the dispersant are labelled. 106
Figure 3.22. FTIR Absorbance spectra for HA NP's coated with sorbitol PLA (3000 Da) dispersant in varying reaction conditions. Absorbance bands related to the dispersant are labelled. 107
Figure 3.23. FTIR Absorbance spectra for HA NP's coated with sorbitol PLA (6000 Da) dispersant in varying reaction conditions. Absorbance bands related to the dispersant are labelled. 108

Figure 3.24. XRD patterns for uncoated HA and coated HA for a selection of PLA dispersants. Highlighted marks on the x-axis indicate the predicted peak positions for hexagonal phase hydroxyapatite. Further XRD analysis can be found in the appendix (1a). 109
Figure 3.25. SEM images of modified HA. From left to right, top to bottom: HA-IsPLA (8), HA- IsPLA (16), HA- IsPLA (24), HA-NaPLA (8), HA-NaPLA (16), HA-NaPLA (24), HA-Sorbitol PLA (1000Da), HA-Sorbitol PLA (3000Da) and HA- Sorbitol PLA (6000Da) 0.0025M. 110
Figure 3.26. TEM images of modified HA. From left to right, top to bottom: HA-IsPLA (8), HA- IsPLA (16), HA- IsPLA (24), HA-NaPLA (8), HA-NaPLA (16), HA-NaPLA (24), HA-Sorbitol PLA (1000Da), HA-Sorbitol PLA (3000Da) and HA- Sorbitol PLA (6000Da) 0.0025M. Scale bar bottom right is equivalent to 500nm. More TEM images can be found in the appendix 1b. 111
Figure 3.27. TEM image of IsPLA (16) coated HA before any post synthesis processing. 113
Figure 3.28. EEL analysis of HA-IsPLA (8) with EEL's carbon % mapping image, TEM image of the area examined and a normalised EEL graph or eV *vs.* counts with relevant peaks labelled. With the red line signifying uncoated HA (for reference) and the blue line being the sample. 114
Figure 3.29. EEL analysis of HA-IsPLA (16) with EEL's carbon mapping image, TEM image of the area examined (green box) and a normalised EEL graph or eV *vs.* counts with relevant peaks labelled. With the red line signifying uncoated HA (for reference) and the blue line being the sample. 116
Figure 3.30. EEL analysis of HA-Sorbitol PLA (3000Da) 0.0025M with EEL's carbon mapping image, TEM image of the area examined (green box) and a normalised EEL graph or eV *vs*. counts with relevant peaks labelled. With the red line signifying uncoated HA (for reference) and the blue line being the sample.....118
Figure 4.1**.** Pulse sequence used to acquire the ^{1}H-^{31}P spectra. 125
Figure 4.2**.** ^{1}H spectrum of HA NP's.....127
Figure 4.3. ^{1}H-^{31}P correlation spectrum of the HA nanoparticles. Skyline projections of both dimensions are also displayed. 128
Figure 4.4. ^{1}H-^{31}P correlation spectrum of the HA nanoparticles coated with DDSA. Skyline projections of both dimensions are also displayed. 129
Figure 4.5. Dispersant molecules interacting with a small hydrophilic particle to form a micellar type structure. 130
Figure 4.6. ^{1}H-^{31}P correlation spectrum of the HA nanoparticles coated with Laurate Isosorbide (C12). Skyline projections of both dimensions are also displayed. 131
Figure 4.7. ^{1}H-^{31}P correlation spectrum of the HA nanoparticles coated with NaPLA (8) Skyline projections of both dimensions are also displayed. 132
Figure 4.8. ^{1}H-^{31}P correlation spectrum of the HA nanoparticles coated with IsPLA (8) Skyline projections of both dimensions are also displayed. 133
Figure 4.9. ^{1}H-^{31}P correlation spectrum of the HA nanoparticles coated with IsPLA (24) Skyline projections of both dimensions are also displayed. 134

Figure 4.10. Pulse sequence used to acquire the DNP enhanced ^{1}H-^{31}P correlation spectra. $[R_{\varphi}][R^{-}_{\varphi}] = [90_{45}90_{135}90_{45}][90_{-45}90_{-135}90_{-45}]$. 136
Figure 4.11b. ^{31}P spectra of HA-IsPLA (8) recorded with the microwaves off (blue) and the microwaves on (red). 138
Figure 4.12. ^{1}H-^{31}P correlation spectrum of HA-DDSA acquired using DNP. Skyline projections of both dimensions are also displayed. 140
Figure 4.13. ^{1}H-^{31}P correlation spectrum of HA-IsPLA (8) acquired using DNP. Skyline projections of both dimensions are also displayed. 141
Figure 6.1 DSC trace of IsPLA(16) 155

Scheme 1.1 Two routes leading to the polymerisation of lactic acid. 8
Scheme 1.2 Anionic ROP mechanism.[26] 10
Scheme 1.3 An example of cationic ROP mechanism.[26] 11
Scheme 1.4 Coordination-Insertion mechanism with Tin (II) Octanoate as the catalyst, L representing the catalysts ligands and the ROH representing an initiator containing an alcohol functional group. 12
Scheme 2.1 Schematic representation of the DDSA ring opening reaction.[24] 25
Scheme 2.2. Resonance form of carboxylate and reaction schematic this functional groups interaction with the HA surface. 51

Table 2.1 Ratio of singly esterified isosorbide (A) to doubly esterified isosorbide (B) for each sample. Ratios were calculated using the GPC derived mass fractions data. 35
Table 2.2 Weight losses in varying temperature regions TGA and level of Extraction efficiency achieved for the dispersant modified HA. 42
Table 3.1 Polymeric dispersant sample abbreviations, molar ratios of reactants and reaction conditions. All reactions were carried out under a Ar atmosphere for 20 minutes. 64
Table 3.2 Summary of the GPC and NMR analysis of isosorbide initiated PLA (IsPLA(16)) with 50 ppm catalyst added. Samples were taken at various intervals during the polymerisation. 72
Table 3.3 Summary of the GPC and NMR spectroscopic analysis of sodium hydroxide initiated PLA (NaPLA) at 180°C with samples being taken at various intervals during the polymerisation. The polymer had a target of 16 polymer units (molecular weight target: 1192 Da). 74
Table 3.4 Summary of the GPC and NMR analysis of sodium hydroxide initiated PLA (NaPLA) at 140 °C with samples being taken at various intervals during the polymerisation. The polymer had a target of 16 polymer units (molecular weight target: 1192 Da). 75
Table 3.5a Summary of the GPC analysis of sorbitol initiated PLA (Sorbitol PLA) using 40 ppm of tin octanoate and targeting a Mn of 1000 Da. Samples were taken at various intervals during the polymerisation. Initiator: monomer ratio was 1:6. 76
Table 3.6 Weight losses in varying temperature regions TGA for the dispersant modified HA. 91

Table 3.7 Weight losses in varying temperature regions TGA for the dispersant modified HA. 101
Table 3.8 Average carbon % values and Ca/P ratios for the dispersant modified HA. Results were obtained using EDX analysis. 112

Equation 1 Calculation of Mn (NMR):..... 72
Equation 2 Calculation of the Mn of Arms (NMR): 73
Equation 3 Calculation of conversion (NMR):..... 73
Equation 4 Einstein's law of diffusion: 83
Equation 5 Stokes law: 83

1 Chapter 1: Literature Review

1.1 Introduction to Polymers

Polymers are molecules of high relative molecular mass made up of simple repeating units of low relative molecular mass molecules (monomers). Polymers can be found throughout nature in cellulose, proteins and DNA. These polymers fall into the category of biopolymers. Many more polymers are purely synthetic such as polytetrafluoroethylene (PTFE) and Kevlar. Others are synthesised from naturally occurring, renewable resources like polylactic acid (PLA) and are often classed as biopolymers.[1] Many of the polymers seen and used today are synthetic polymers such as nylon, polystyrene and Teflon. Whilst people have been utilising various natural biopolymers, like rubber, as far back as the early South American Aztecs it was not until the early 19th century that first truly synthetic polymer, Bakelite, was formally announced to the science community. Baekeland had successfully synthesised this thermosetting polymer from the condensation reaction of phenol with formaldehyde. Whilst poly(vinyl chloride) had been synthesised 30 years earlier it was not until 1926 that this synthetic polymer was also recognised. During this early period of polymer chemistry Staudinger reported polymerisation to be all processes that combine two or more molecules to produce a product of the same composition but with a higher molecular weight. Staudinger also went on to define the two basic polymerisation processes; condensation polymerisation where polymers are formed by step wise reactions between functional groups and addition polymerisation involving double or triple carbon-carbon bonds breaking and linking together to form a polymer.[2] In 1935 Carothers famously carried out the reaction of hexamethylene diamine and adipic acid to form polyamide 6-6, also known as nylon. From there this exciting area of organic chemistry grew rapidly with DuPont pioneering the first industrial effort to investigate

these novel durable and versatile materials.[3, 4] Today polymers have replaced many materials, such as metal and wood, in a wide range of applications.[5]

Polymerisation is the term given to the synthesis process in which monomer units are reacted together to form chains (or three-dimensional networks) to form polymers. If only a few monomers are present in the chain, i.e. less than 10, then the resulting molecule of intermediate relative molecular mass is called an oligomer.[6]

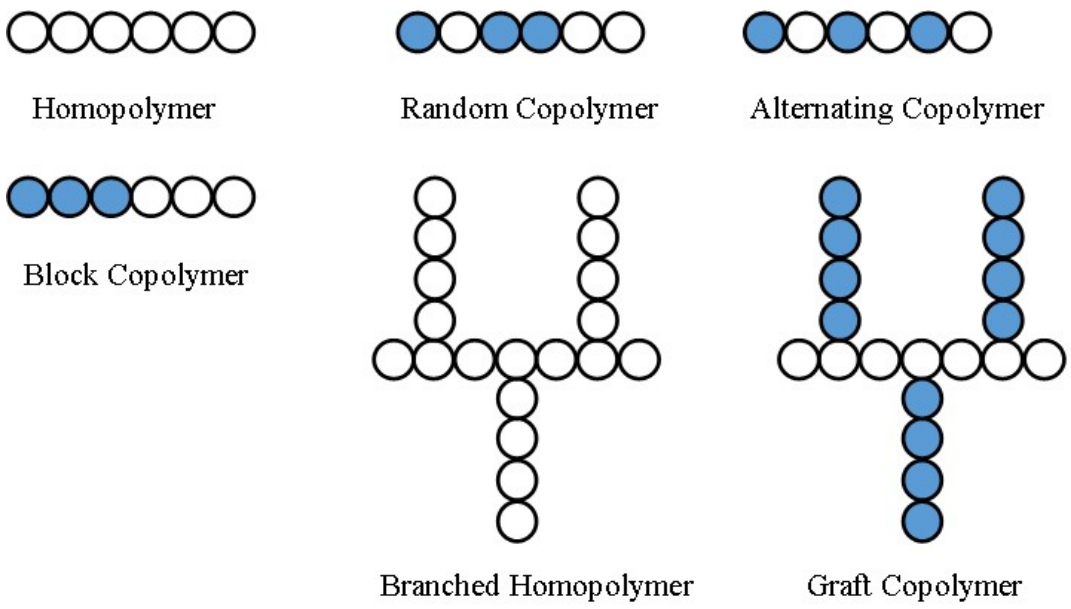


Figure 1.1 A diagram of basic homopolymer and copolymer structures.

A polymer comprised of only one type of monomer is known as homopolymer and those made of two or more monomers are called copolymers.[3] The addition of different monomer units to the polymerisation process to create a copolymer enables a tailoring of the properties of the final material. It is possible to alter glass transition temperatures, rheological properties and solubility of the polymer through the addition of different monomer units.[7-9] Altering the arrangement of the monomer units also affects these

properties and leads to the formation of random, alternating or block copolymer materials. As these polymers contain pieces of chemical structure from both polymers they can exhibit a combination of properties found in both polymers. If specifically tailored block copolymers can interact with multiple phases of a composite material or solution making for excellent surfactant properties.[10] Branched polymers contain multiple polymer chains growing randomly from a main linear backbone. This change in morphology also leads to changes in the physical properties of the final polymeric material.[11] Graft copolymers consist of a linear backbone of one homopolymer composition on which a number of branches of a different homopolymer are grafted.[10]

There are two main categories in which polymerisation reactions fall into: addition and condensation. Condensation polymers contain bifunctional or polyfunctional monomers which react together in a step-wise fashion to form a polymer. Often condensation reactions will eliminate small molecules (such as water) in the polymerisation process and are classed as reversible reactions. Addition polymerisation consists of the sequential addition of bi/polyfunctional monomer units to a growing polymer chain without the elimination of part of the monomer molecules. However, certain polymerisation reactions do not fall into either category. For example, the polymerisation of polyurethane does not produce a small molecule despite the kinetics of the polymerisation being that of a condensation polymerisation. Therefore, two distinct classifications for polymerisation mechanisms were introduced; chain-growth and step-growth polymerisation.[11] Figure 1.2 displays a basic overview of the kinetic differences between the two different polymerisations.

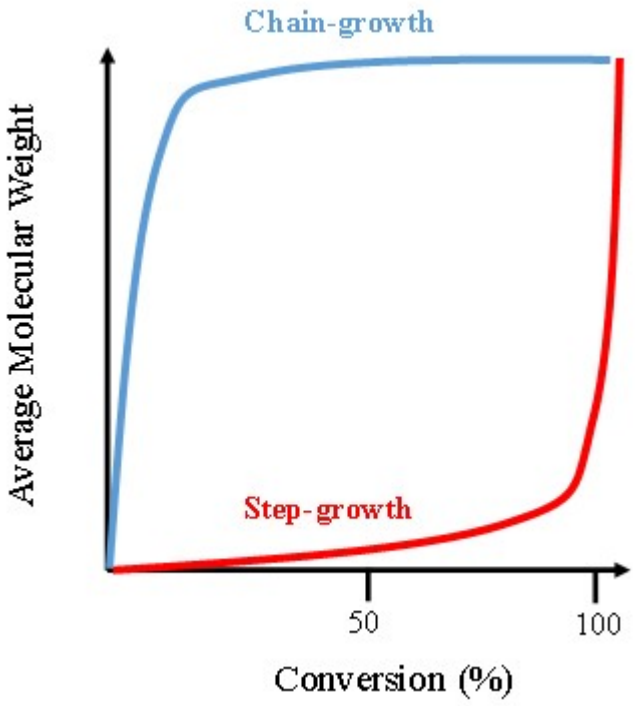


Figure 1.2 A basic graph of average molecular weight *vs.* conversion for step-growth and chain-growth polymerisation.

Step growth polymerisation has its origins in condensation polymerisation with polymer linkages occurring between the reactive functional groups in the monomer molecules. The main characteristic of this type of polymerisation is that any two species containing the appropriate functional groups will react with each other to produce a polymer with a molecular weight that increases gradually with functional group conversion. This results in a high conversion of monomer to polymer in the early stages of the reaction to produce low molecular weight oligomers. After this step, an exponential increase in molecular weight is observed as these oligomers combine to form the desired polymer. A well-known example of step growth polymerisation has been mentioned previously with the reaction of a diamine and dicarboxylic acid to form nylon.[12]

Chain growth polymerisation involves the successive addition of monomers onto the end of growing polymer chains. This differs from step growth polymerisation where species of

all sizes in the reaction will react with each other leading to the exponential growth in molecular weight towards the higher % conversions. Chain growth polymerisation is known as addition polymerisation as its primary characteristic is the successive addition of monomers onto a growing chain. Usually this polymerisation process will involve the breaking of carbon-carbon double bonds instead of utilising the reaction of two functional groups.[13] The basic kinetic profile of chain growth polymerisation is displayed in Figure 1.2 where we see that high molecular weights are achieved at low conversions as the polymer chains grow rapidly. The molecular weight then remains steady as more and more monomer units are added to the growing polymer chain until the polymerisation process terminates.

In this thesis, our work is focused on the ring opening polymerisation (ROP) of lactide to make polylactic acid (PLA) which is discussed in more detail further on in this chapter. This polymerisation process involves the successive addition of monomers to a growing chain and therefore falls under the category of chain growth polymerisation. Chain growth polymerisations have three distinct steps: initiation, propagation and termination (detailed below) and are related to the mechanisms observed in ROP process.

- During the initiation step an active centre is formed on the monomer. In ROP this could be the introduction of an anion, cation or the introduction of a nucleophilic site.
- Propagation involves the successive addition of monomers to the active site created in the initiation step.
- Termination of the polymerisation can occur through a chain transfer mechanism where the active centre is transferred to another molecule. This molecule could be another polymer or a chain transfer agent. In the case of certain ROP mechanisms termination can occur upon removal of the catalyst situated at the end of the

growing chain via hydrolysis. The active end of a chain may also 'backbite' the growing chain leading to the formation of a macrocycle. [14, 15]

1.2 Polyesters

Polyesters are polymers containing many ester functional groups in their main chain as a major structural component. The general formula for polyesters can be depicted as $–(COOR)_2–$ with the R groups differing in properties which would affect the overall behaviour of the final polymer.[2] Early work in this field of polymer chemistry was conducted by Carothers and led to the synthesis of the well-known polyester, poly(ethylene terephthalate (PET).[16] PET is a thermoplastic polymer resin containing an aromatic ring within its main structure. It is generally used in the form of synthetic fibres and is not biodegradable.[2]

The traditional synthesis of polyesters involved polycondensation using diols and diacids. However, a high degree of conversion and thus a high molecular weight is difficult to achieve using this method. High temperatures, long reaction times and the need to remove by-products are some of the drawbacks of condensation (step-growth) polymerisation. The ring opening of lactones, ketene acetals and cyclic diesters as an alternative to the difficult polycondensation route has been successfully deployed in industry to synthesise high molecular weight polyesters.[17]

Many polyesters are biodegradable, with the primary route of degradation occurring with the hydrolysis of the ester linkages. Such linkages are common in nature and it was suspected that structures containing esters linkages would be biodegradable.[17]

1.2.1 Poly (lactic acid) (PLA)

PLA is a biodegradable thermoplastic aliphatic polyester that can be made from renewable resources such as corn starch. PLA can be processed through a variety of different methods including extrusion and injection moulding enabling its use in an array of different applications from packaging to medical implants.[18] Due to the chirality of the lactide monomer different forms of PLA can exist such as poly-L-lactic acid (PLLA), poly-D-lactic acid (PLDA) and poly-D,L-lactic acid (PDLLA). The three stereoisomers of lactide are shown in Figure 1.3 *Meso*-lactide has both a D and an L stereocentre.

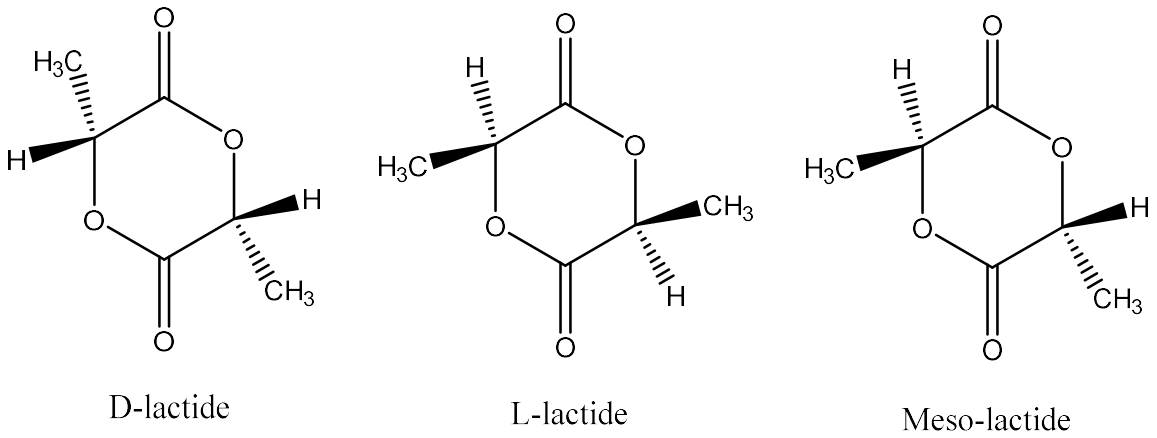
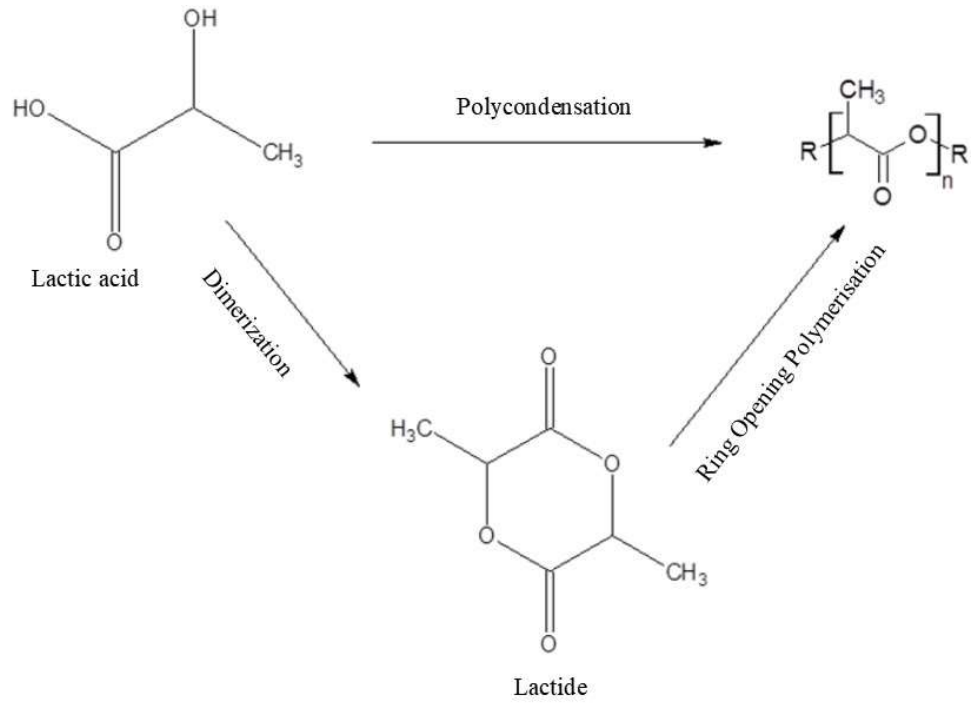


Figure 1.3 Lactide stereoisomers.

PLLA and PLDA are generally crystalline in nature and PDLLA amorphous. The degree of crystallisation and associated properties, such as the mechanical strength and thermal resistance, in PLA is controlled by varying the ratio of the D and L enantiomers of lactide.[2] The ROP of an enantiopure monomer will result in an isotactic polymer structure with all the stereocentres aligned on the same side of the polymer chain (i.e. all the CH_3 groups will be on the same side). The stereocontrolled ROP of *meso*-lactide can lead to either syndiotactic PLA (alternating steriocentres, -LDLDLDLD-) or heterotactic PLA

(doubly alternating centres, -LLDDLLDD-).[19] The ROP of none enantiopure monomer mixtures (*rac*-lactide) can lead to the formation of an atactic polymer where the stereocentres are randomly aligned throughout the chain. The utilisation of different isomeric polymer structures can lead to changes in the thermal stability. Atactic arms were found to be less thermally stable than there isotactic counterparts.[19, 20]

Degradation of PLA occurs *via* hydrolysis reactions that break down the ester bonds found throughout the polymer, making the aliphatic polyester backbone sensitive to water. The main by-product of this degradation process is lactic acid, a nontoxic molecule that can be processed by the body. PLA is a widely recognised biodegradable and biocompatible polymer that can be sourced from renewable materials making it highly attractive to the medical field.[18]



Scheme 1.1 Two routes leading to the polymerisation of lactic acid.

Error! Reference source not found.1 depicts the two main mechanisms by which PLA can be produced. The polycondensation route (step-growth polymerisation) is the most direct method of synthesising PLA from lactic acid but cannot easily produce stereo-regular high molecular weight polymers and is therefore, not commonly used in industry. This route also requires reduced pressures and catalysts; to reach higher molecular weights azeotropic conditions or coupling agents have to be employed. These synthesis conditions are often costly to set up, maintain and use safely at large scale. The second route to polymerising lactic acid involves dimerization to form the commercially available lactide followed by ring opening polymerisation (ROP). Dimerization occurs with the condensation polymerisation of lactic acid and removal of water to produce the 'prepolymer'. A catalyst, commonly tin (II) octoate, is added to the mixture of lactic acid oligomers at high temperatures (>200 °C) to produce crude lactide monomer through the thermal catalytic depolymerisation of lactic acid oligomers. The crude lactide is then purified by distillation or solvent crystallisation. Lactide can then be polymerised to high molecular weights using multiple ROP mechanisms.[21] The most commonly used ROP is coordination-insertion ROP which is discussed in detail further on in this chapter. This route is able to produce high molecular weights of stereo-regular PLA without the need for azeotropic conditions or coupling agents. This synthesis route is widely used in the industrial production of high molecular weight PLA. [22, 23]

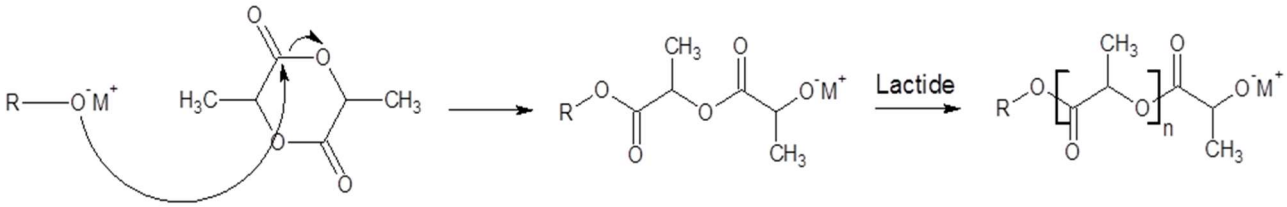
1.2.2 Ring Opening Polymerisation (ROP)

As previously discussed ROP falls under a type of polymerisation known as chain growth polymerisation in which the active centre of the polymer chain reacts and opens up the cyclic lactide monomer in order to increase in length. ROP of lactide was first demonstrated by Carothers in 1932 and over the past 40 years the ROP of cyclic esters has

been extensively investigated due to its ability to produce polyesters in a controlled manner.[24] Many different initiators, mechanisms and catalysts have been explored with the resulting products exhibiting useful properties such as biodegradability. There are three main mechanisms by which ROP can be achieved: anionic, cationic and coordination-insertion.[23, 25] Our focus in this work is on the anionic and coordination –insertion mechanisms.

1.2.3 Anionic ROP

In the polymerisation of lactide, anionic ROP is initiated upon the nucleophilic attack of the carbonyl group, resulting in the cleavage of the carbonyl – endocyclic oxygen bond which opens the ring and creates a reactive anionic centre on the end of the growing polymer chain (Scheme 1.2).

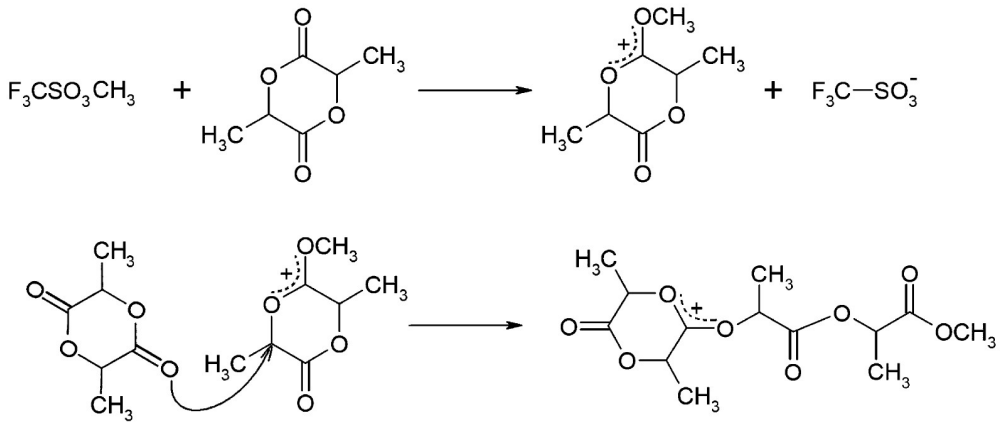


Scheme 1.2 Anionic ROP mechanism.[26]

In this mechanism the initiator can be any nucleophile, however initiators that are strongly nucleophilic tend to deprotonate the monomer instead of initiating the polymerisation. This mechanism is also prone to inter and intra-molecular back-biting and other side reactions that have the potential to significantly hinder chain propagation resulting in low molecular weights.[23, 25]

1.2.4 Cationic ROP

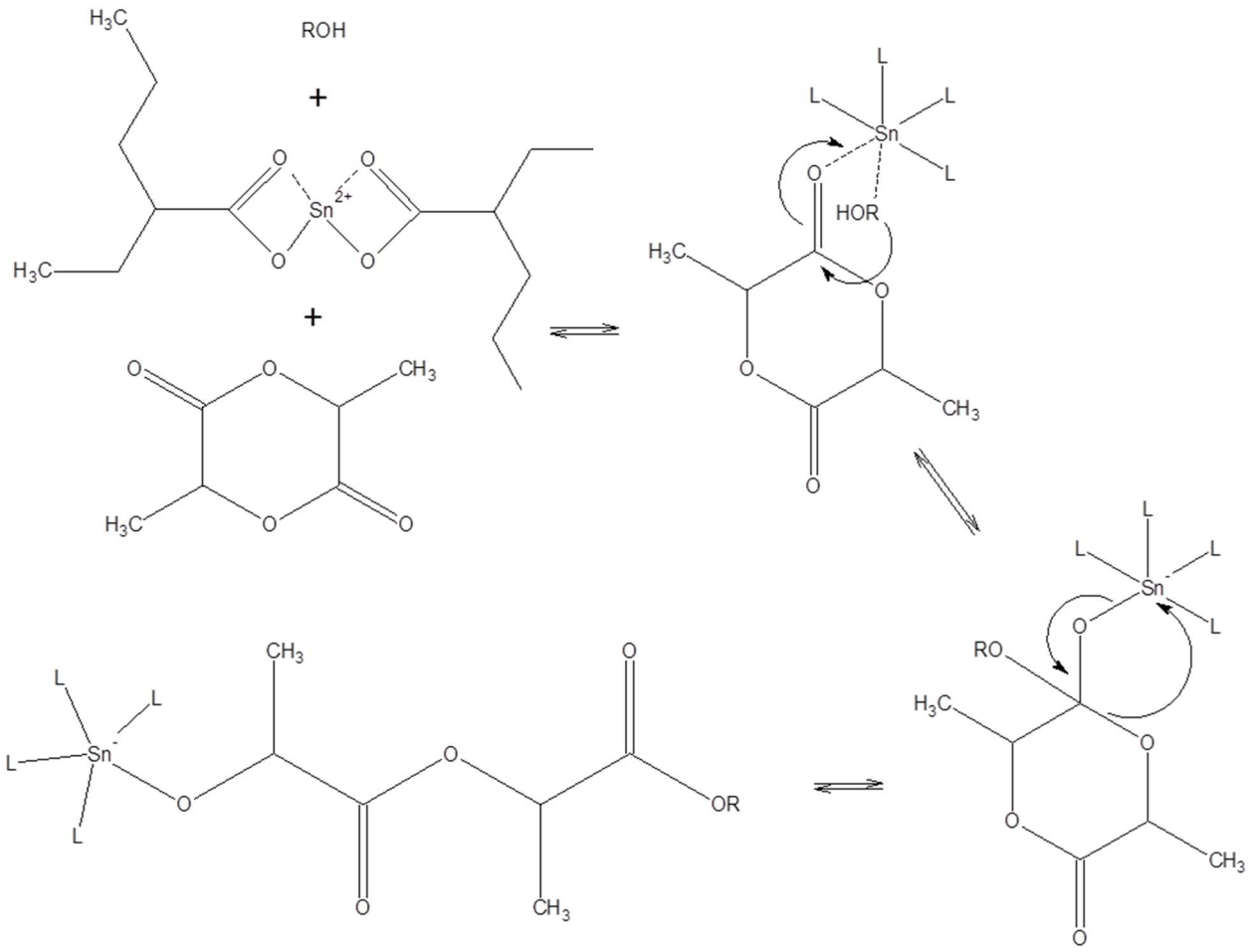
Cationic ROP involves the protonation or alkylation of one of the exocyclic oxygen groups situated on the lactide monomer. This initiation step leads to the resulting O-CH-OCH_3 bond to become positively charged. Nucleophilic attack by a second monomer unit breaks this bond to create another electrophilic carbenium ion that attacks another monomer unit and so on to create a polymer chain. This is the propagation step. Initiators for this ROP will usually consist of carbenium ion donors or strong acids.[26]



Scheme 1.3 An example of cationic ROP mechanism.[26]

1.2.5 Coordination-Insertion ROP

This method is the most widely utilised as it is able to produce controlled high molecular weight polymers through the use of a metal-alkoxide catalyst.[19] These catalysts often contain free p or d orbitals and behave like Lewis Acids.



Scheme 1.4 Coordination-Insertion mechanism with Tin (II) Octanoate as the catalyst, L representing the catalysts ligands and the ROH representing an initiator containing an alcohol functional group.

Scheme 1.4 shows that the reaction proceeds by the metal catalyst first coordinating with the active ROH group and then the carbonyl group on the lactide monomer. The nucleophilic ROH group attacks the carbonyl group within the lactide ring breaking the carbonyl – endocyclic oxygen bond and opening the ring. Propagation is achieved by further insertion of more lactide monomers *via* the active catalyst situated at the end of the chain. Termination is brought about by hydrolysis which removes the catalyst from the growing chain. Living polymerisation (where chain transfer and chain termination does not occur) may also be achieved through this method.[23, 25]

There are a large number of catalysts available for coordination-insertion ROP with organometallic catalysts being the most effective at producing high molecular weights with controlled stereo-chemistry. Tin (II) octanoate is the 'standard' catalyst used in the ROP of lactide as it is soluble in molten lactide, easy to handle, commercially available and Food and Drug Administration (FDA) approved. This catalyst is highly active and capable of producing polymers within a few minutes or hours. Tin (II) octanoate is therefore the catalyst of choice in this work.[23, 27]

1.3 Introduction to Dispersants

A dispersant is a substance that is added to a suspension to improve the separation between small particles and prevent them from aggregating. They will often consist of three distinct structural features: a hydrocarbon group ('tail group'), a polar functional group ('head group') and a connecting group.[28] For example, lauric acid can be described as a dispersant with the hydrocarbon chain functioning as the tail, the acid group as the polar functional head group and the hydroxyl situated in the carboxylic acid forming the connecting group. Often the hydrocarbon group is polymeric in nature and can have a wide range of molecular weights depending on the properties needed to disperse the particle of interest.[29] Typically dispersant molecules must be able to interact with both phases in a suspension or composite material i.e. between a hydrophilic phase and a hydrophobic phase as shown in Figure 1.4 below. The behaviour of a dispersant is strongly influenced by the balance between the hydrophobic and lipophilic groups. In 1954 Griffin defined this concept as the hydrophile–lipophile balance (HLB). The HLB is a scale of 1-20 with 1 being the most lipophilic (for example, hexane) and 20 being the most hydrophilic. From 1-4 the dispersant or surfactant will not mix in water, above 13 a clear water solution will be obtained.[30]

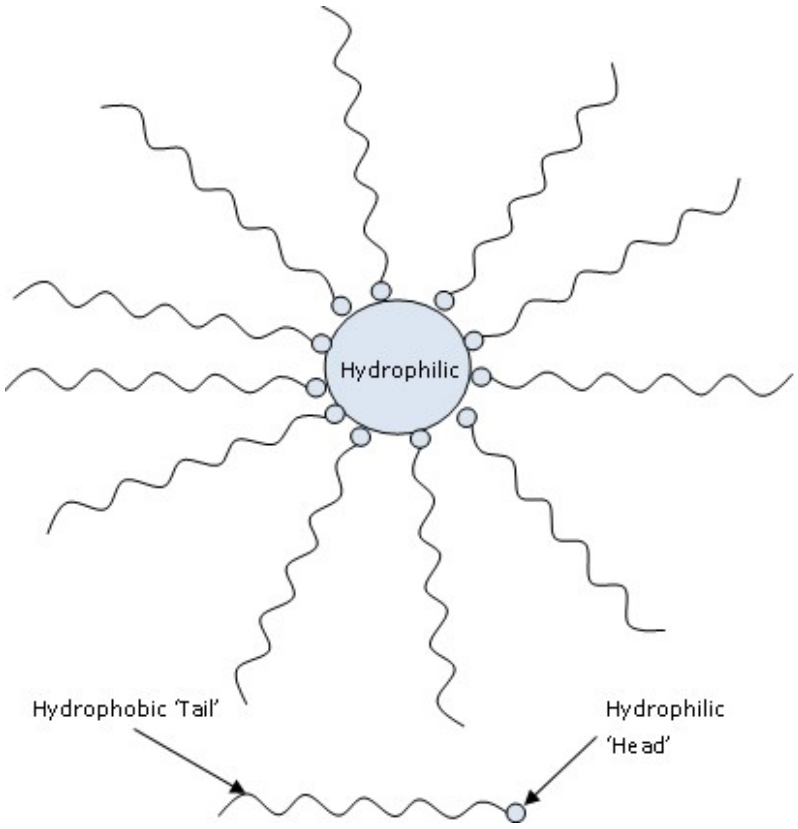


Figure 1.4 Dispersant molecules interacting with a small hydrophilic particle.

Dispersants can be found in detergents, concrete, surface coatings and in many other areas of industry. Our project will focus on stabilising nanoparticles in a polymer matrix with the effectiveness of the dispersant correlating to how well it is able to separate in an organic phase and stabilise the nanoparticles within the polymer. As the aforementioned nanoparticles will be processed into the matrix polymer via extrusion they must be able to disperse efficiently into the molten (or liquid) polymer before it sets.

Solid particles will move around in the liquid system according to Brownian motion and will inevitably collide with each other. If the nanoparticles can separate after the collision and not aggregate, they will remain stable and well-dispersed. However, due to the incredibly small nature of the nanoparticles the attractive forces between them are great; especially in a phase that is unfavourable. In order to have as little interaction with this

unfavourable phase as possible the particles will seek to reduce their collective surface area by forming a larger particle i.e. they will aggregate and form large clusters. Keeping the particles apart is the key to stabilisation and the job of a dispersant is to make sure the particles are not able to interact with each other to any great extent. Dispersants can achieve this by forming a barrier around the nanoparticles that favours the polymer matrix. This 'barrier' can also cause repulsive steric forces between the nanoparticles.[31]

1.4 Hydroxyapatite (HA) Nanoparticles

HA with a crystal structure formula of $Ca_{10}(PO_4)_6(OH)_2$ is a naturally occurring mineral and the main component of bones and teeth making it one of only a few bioactive materials. Nano-sized HA is widely used as a bio-ceramic in medical and dental applications due to its similarity with hard body tissues which enable it to integrate into bone structures without breaking down. There are several established methods of synthesising HA nanoparticles which include: wet chemical deposition, biomimetic deposition, sol-gel and electro-deposition with the most common synthesis route being precipitation. The manufacture of HA nanoparticles by hydrothermal processing has been established in both a batch and continuous forms. Lester *et al.*[32] recently developed a symmetrical counter current nozzle reactor capable of producing high quality HA nanoparticles. This hydrothermal process will be utilised in this project to not only produce but also coat the HA nanoparticles. [33-35]

1.4.1 Supercritical water continuous hydrothermal synthesis (scWCHS) reactor

As briefly mentioned in section 1.4 this work will be utilising the continuous hydrothermal process to synthesise HA nanoparticles and attach the desired dispersant molecules to the surface of HA. A schematic of the reactor is shown in Figure 1.5 below.

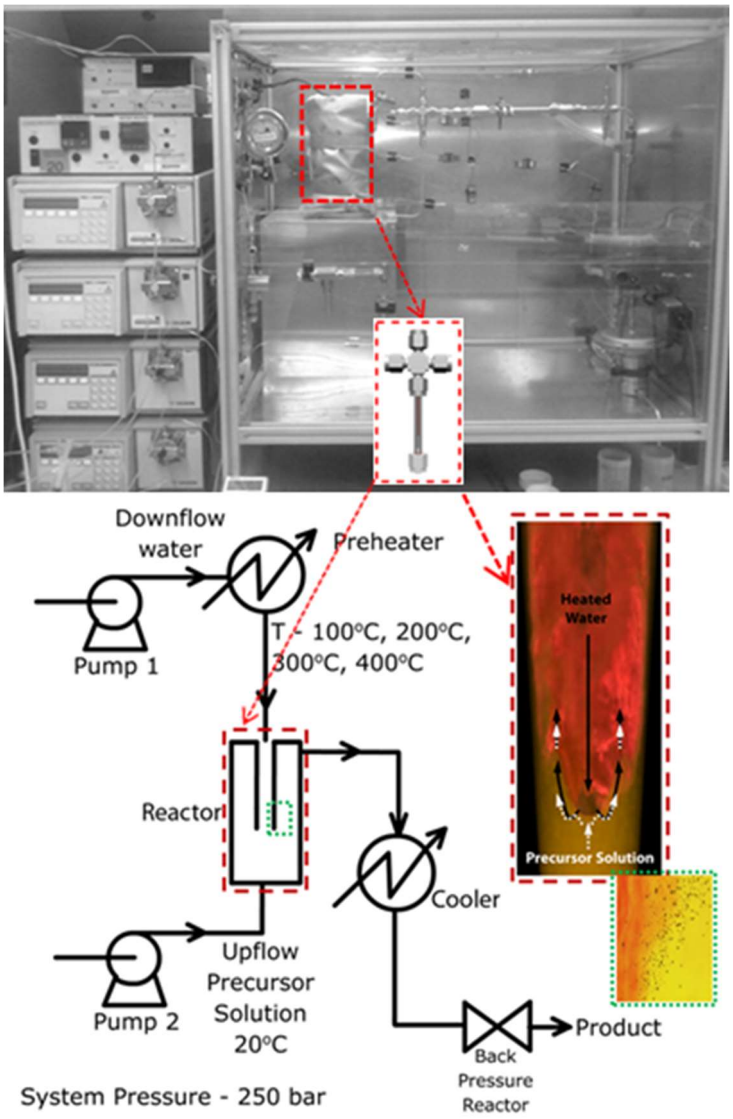


Figure 1.5 The scWCHS reactor developed by Lester et al. [32] which is used in the BENcH project. Pumps are Gilson® HPLC pumps with the entire system composed of Swagelok stainless steel 316. [34, 36]

The scWCHS reactor was developed by Lester *et al.* [32] and has been commercialised by Promethean Particles. It allows for the continuous synthesis and capping of HA

nanoparticles by using a pipe-in-pipe concentric arrangement where a hot, pressurised aqueous mixture of ammonium phosphate is passed through the inner pipe (down flow) and the up flow consisting of a room temperature organic solution containing the dispersant and calcium nitrate. The synthesis/precipitation of the HA nanoparticles and subsequent capping happens at the same point in the reactor. Different morphologies of HA can be produced by simply altering the experimental parameters. For example, altering the pH of the system can produce varying morphologies such as rods and platelets. This system also enables uniform mixing of the reactants and short residence times mean limited HA nanoparticle growth and a reduced risk of the harsh conditions decomposing the dispersant. [33, 37] It also provides a fast and continuous route to the production of coated HA nanoparticles.

1.5 Aims and Objectives

The Integrated Molecular Design of Melt-processable Bioresorbable Engineering Nanocomposites for Health-Care (BENcH) Project aims to develop the next generation of resorbable polymer nanocomposites to be used primarily in medical applications. The BENcH Project is interdisciplinary and consists of three streams:

- Stream 1 – Particle and dispersant synthesis
- Stream 2 – Rheological, degradative and structural properties
- Stream 3 - Nanocomposite manufacture

The focus in this thesis will be on Stream 1 – Particle and dispersant synthesis which consists of three main aims:

- Synthesis and preparation of platelet nanoparticles
- Synthesis of tailored dispersants and coupling agents for nanoparticles
- Continuous production of feedstock using the hydrothermal synthesis method

Substantial progress has already been made in the area of synthesis and preparation of the platelet nanoparticles. For this project platelet nanoparticles will be produced by a counter-current hydrothermal process that has already been developed by Lester *et al.* [32] and commercialised by Promethean Particles. Therefore, the aims of this study will revolve around the synthesis of tailored dispersants and the continuous production of the capped nanoparticles.

For a dispersant to be successful in the BENcH Project it needs to be able to interact with both the surface of the HA nanoparticles and the medical grade PLA which will form the matrix polymer in the final composite material. Thus, the aim is to design a head group (also regarded as the initiator) for the oligomer (dispersant) that is capable of interacting with the nanoparticle surface by utilising functionalised end groups and create a chain or 'tail' that can integrate into the matrix polymer.

In order to continuously produce the composites, the aim is to mix the dispersant with the HA nanoparticles as they precipitate out of solution in the supercritical water continuous hydrothermal synthesis (scWCHS) reactor. The dispersant must be able to withstand the rather harsh conditions of the rig. However, the short residence time of the materials in the reactor should enable most PLA oligomers to coat the HA without degrading.

As the products of the BENcH Project are designed for industrial incorporation it is also an objective to make the dispersants not only effective but simple and cost efficient to produce.

1.6 References

1. L. T. Sin, *Polylactic Acid: PLA Biopolymer Technology and Applications*, Elsevier Science, 2012.
2. S. Fakirov, *Biodegradable Polyesters*, Wiley, 2015.
3. C. E. Carraher Jr, *Introduction to Polymer Chemistry, Fourth Edition*, CRC Press, Independence, 2017.
4. G. B. Kauffman, *J. Chem. Educ*, 1988, **65**, 803.
5. D. N. Saheb and J. P. Jog, *Advances in Polymer Technology*, 1999, **18**, 351-363.
6. A. D. Jenkins, P. Kratochvil, R. F. T. Stepto and U. W. Suter, *Polimery*, 1998, **43**, 559-564.
7. M. L. O'Neill, Q. Cao, R. Fang, K. P. Johnston, S. P. Wilkinson, C. D. Smith, J. L. Kerschner and S. H. Jureller, *Industrial & Engineering Chemistry Research*, 1998, **37**, 3067-3079.
8. Y. S. Kim, C. I. Chung, S. Y. Lai and K. S. Hyun, *Journal of Applied Polymer Science*, 1996, **59**, 125-137.
9. F. P. Reding, J. A. Faucher and R. D. Whitman, *Journal of Polymer Science*, 1962, **57**, 483-498.
10. J. E. McGrath, *Journal of Chemical Education*, 1981, **58**, 914.
11. A. Kumar and R. K. Gupta, *Fundamentals of Polymer Engineering, Revised and Expanded*, CRC Press, 2003.
12. J. Asua, *Polymer Reaction Engineering*, Wiley, 2008.
13. N. A. Dotson, R. Galvan, R. L. Laurence and M. Tirrell, *Polymerization Process Modeling*, Wiley, 1995.
14. D. J. Darensbourg and O. Karroonnirun, *Macromolecules*, 2010, **43**, 8880-8886.
15. O. Nuyken and S. D. Pask, *Polymers*, 2013, **5**, 361-403.
16. J. Scheirs and T. E. Long, *Modern Polyesters: Chemistry and Technology of Polyesters and Copolyesters*, Wiley, 2005.
17. A. C. Albertsson, U. Edlund, M. Hakkarainen, S. Karlsson, Y. Liu, E. Ranucci, M. Ryner, M. S. Lindblad, K. M. Stridsberg and I. K. Varma, *Degradable Aliphatic Polyesters*, Springer Berlin Heidelberg, 2003.
18. O. Dechy-Cabaret, B. Martin-Vaca and D. Bourissou, *Chemical Reviews*, 2004, **104**, 6147-6176.
19. M. J. Stanford and A. P. Dove, *Chemical Society Reviews*, 2010, **39**, 486-494.
20. S. Corneillie and M. Smet, *Polymer Chemistry*, 2015, **6**, 850-867.
21. R. A. Auras, L. T. Lim, S. E. M. Selke and H. Tsuji, *Poly(lactic acid): Synthesis, Structures, Properties, Processing, and Applications*, Wiley, 2011.
22. D. Garlotta, *Journal of Polymers and the Environment*, 2001, **9**, 63-83.
23. V. K. A.P. Gupta, *European Polymer Journal*, 2007, **43**, 4053–4074.
24. M. Jamshidian, E. A. Tehrany, M. Imran, M. Jacquot and S. Desobry, *Comprehensive Reviews in Food Science and Food Safety*, 2010, **9**, 552-571.
25. K. M. Stridsberg, *Controlled Ring-Opening Polymerization: Polymers with designed Macromolecular Architecture*, Kista Snabbtryck AB, Stockholm, Sweden, Stockholm, 2002.
26. A. P. Gupta and V. Kumar, *European Polymer Journal*, 2007, **43**, 4053-4074.
27. B. M.-V. Odile Dechy-Cabaret, and Didier Bourissou, *Chem. Rev.*, 2004, **104**, 6147-6176.
28. L. R. Rudnick, *Lubricant Additives: Chemistry and Applications, Third Edition*, CRC Press, 2017.

29. *Oil Spill Dispersants: Mechanisms of Action and Laboratory Tests*, Taylor & Francis, 1993.
30. C. E. O. S. Dispersants, M. Board, C. E. T. Systems, D. E. P. Sciences and N. R. Council, *Using Oil Spill Dispersants on the Sea*, National Academies Press, 1989.
31. *Journal*, 2009.
32. E. H. Lester and B. J. Azzopardi, *Journal*, 2005.
33. E. Lester, S. V. Y. Tang, A. Khlobystov, V. L. Rose, L. Buttery and C. J. Roberts, *CrystEngComm*, 2013, **15**, 3256-3260.
34. M. Gimeno-Fabra, F. Hild, P. W. Dunne, K. Walton, D. M. Grant, D. J. Irvine and E. H. Lester, *Crystengcomm*, 2015, **17**, 6175-6182.
35. F. J. M. M.P. Ferraz, C.M. Manuel, *Journal of Applied Biomaterials & Biomechanics*, 2004, **2**, 74-80.
36. J. R. Hyde, E. Lester, S. Kingman, S. Pickering and K. H. Wong, *Composites Part a-Applied Science and Manufacturing*, 2006, **37**, 2171-2175.
37. M. Gimeno-Fabra, P. Dunne, D. Grant, P. Gooden and E. Lester, *Chemical Engineering Journal*, 2013, **226**, 22-29.

2 Chapter 2: Continuous Flow, Single Stage Synthesis of Dispersant-Stabilised Hydroxyapatite Platelet Nanoparticles - Hydrocarbon Dispersant Optimisation

2.1 Aims and Objectives

This chapter investigates the hydrothermal synthesis of coated hydroxyapatite nanoparticles (HA NP's) using a continuous flow method developed by Lester *et al.* [25] as previously discussed in Chapter 1. This work was carried out using a selection of tailored amphiphilic surfactants as the coating materials. These hydrocarbon based dispersants used could be produced (or bought) in sufficient quantities with relative ease and provide a good foundation for further work that would utilise oligomeric polylactic acid (PLA) as the coating material. Both the chain length and end groups of the hydrocarbons were altered to investigate the interactions and establish effective combinations capable of successfully coating the HA surface. There are two points in the hydrothermal rig where dispersants could safely be introduced into the flow system; as a pre-cursor within the cold, up-flow stream or at the capping point situated after the reactor. Therefore, it was first necessary to establish which point addition would be most effective for our process. Preliminary work carried out by Gimeno-Fabra[24] used dodecenylsuccinic anhydride (DDSA) to investigate the most efficient method of introducing the surfactant into the system and once established, all other dispersants were subsequently introduced at the same point in the process.

2.2 Introduction

Key challenges in modern healthcare have driven the need for bioactive, regenerative materials capable of repairing or replacing various bodily tissues.[1] Hydroxyapatite (HA) is an inorganic material that is both bioactive and osteoconductive, which has gained

significant attention in the medical field with its extensive use in tissue replacement, bone replacement, drug delivery, scaffolds and as a coating for metal implants.[1-4] Currently, metal implants are the dominant devices utilised in bone replacement surgery, partly because they are mechanically superior to their biopolymer counterparts. However, it is known that their use can have significant adverse effects on the strength and integrity of bone surrounding the implanted device. This can lead to a phenomenon termed stress shielding, which is related to the superior mechanical properties of the implant causing it to share the load carrying capacity of the surrounding bone, rather than just supporting its structure. As the surrounding bone is subject to a reduced load it is shielded from stress and is likely to decrease in both thickness and mass, causing unwanted side effects in the patient such as osteoporosis and an increased potential for re-fracture if the metal device is removed.[5, 6] Therefore, research is recently being focused on investigating the use of HA composites manufactured with biocompatible polymers as alternatives to conventional implants.[7-9] These materials not only have the potential to eliminate stress shielding because their mechanical properties closely match those seen in bone, but also have the capability of enhancing the integration of medical implants and so remove the need for secondary surgery for the implant to be removed.[10] HA can be obtained from natural sources or through numerous synthetic methods such as chemical precipitation, sol-gel, mechcanochemical, ultra-sonication and hydrothermal synthesis.[11-15] Addition of HA to biodegradable polymers,[16] such as poly(lactic acid) (PLA) and poly(lactide-*co*-glycolide) (PLGA), has been reported to increase the glass-transition temperature, thermal stability and mechanical properties of the polymer. However, the mechanical properties of these polymer composites rely heavily on the quality of the nanoparticle (NP) dispersion achieved.[17] Due to the ionic and hence hydrophilic nature of the HA surface, achieving the desired level of dispersion within a hydrophobic polymer matrix can be difficult.

Potential aggregation of the HA filler material, especially when the surface area is significantly large, as in the case of nanoparticulate fillers, and poor interfacial contact between the filler and the surrounding matrix polymer can lead to mechanical defects forming in the final nanocomposite when in use. These behave as microcracks and significantly increase the susceptibility of a device to catastrophic failure of the material when it is under stress. To counter this, coating the HA surface with a suitable dispersant has been shown to reduce the surface potential between the two phases within the composite and improve their contact angle.[18, 19] Dispersants are interfacial active, amphiphilic molecules consisting of two sections; a head group that is capable of forming strong interfacial interactions with one phase and a tail group that does so with the other.[14, 16] This enables them to form a thermodynamically favourable interfacial phase (typically in liquid : liquid systems, or in solid : liquid coating systems) which improves the contact angle between the two phases and stabilises the resultant emulsion or dispersion from aggregation. Previous literature has detailed the successful modification of HA NP's using amphiphilic dispersant and has shown that such surface modifications can alter the surface charge of the HA without changing the crystal structure.[18, 20-23] These changes at the surface of the filler have also been shown to increase the cellular uptake of HA and, as a consequence, increased cell proliferation has been observed. Furthermore, the surface-modified HA NP's were demonstrated to form stable dispersions in hydrophobic organic solutions.[18, 24] This data suggested that the modified HA NP's may also form stable dispersions in polymer melts.

Establishing the point of addition of the dispersant: Applying a dispersant in the manner previously described in the literature above usually constitutes an additional processing step. This step would involve a reaction after the formation of the nanoparticles in order to attach the dispersant onto the particle surface. Thus, this study aimed to define if this

dispersant could be included into the nanoparticle structure during the synthesis step. It was hypothesised that as well as reducing process stages, this approach should reduce aggregation and Oswald ripening. Additionally, the dispersant must be carefully tailored so that it does not alter the physical behaviour or over all morphology of the nanoscale filler material whilst delivering the necessary dispersion in the composite. Previous work on this project had reported the use of small amphiphilic molecules as dispersants (dodecenylsuccinic anhydride) for HA NP's prepared via a continuous flow hydrothermal flow process. A stabilised dispersion of NP's in an organic solvent was obtained in a single step, minimising waste and achieving a more efficient processing route.[13, 24, 25]

A schematic of the continuous flow hydrothermal reactor used in this work can be seen in Figure 2.1. The dispersant can be introduced at two points: as part of the upflow pre-cursor solution at pump 2 (method 1) or as a capping feed solution at pump 3 (method 2). Using method 1 ensures the dispersant is present in the reactor alongside the formation of HA NP's. Method two introduces the dispersant after the HA NP's have been formed with the flow at this point being approximately 20 °C cooler than the reactor.

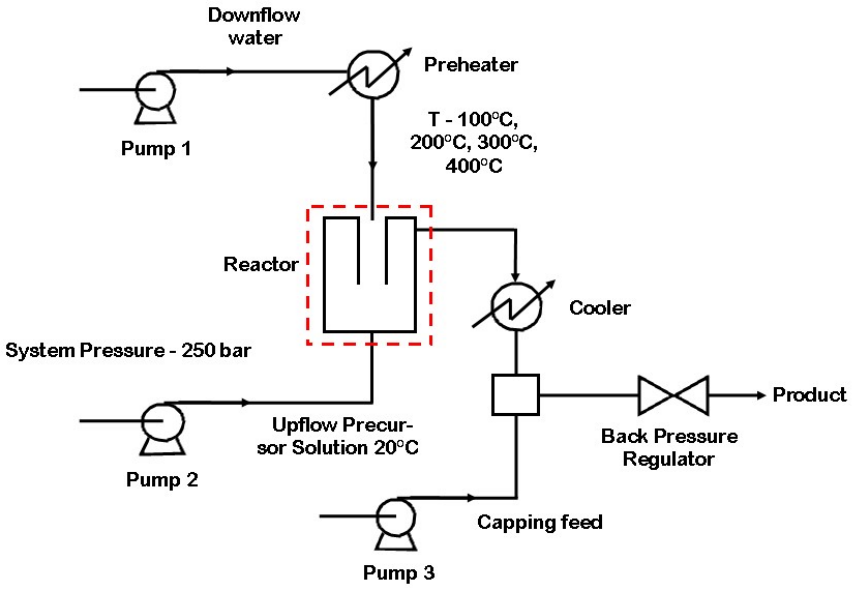
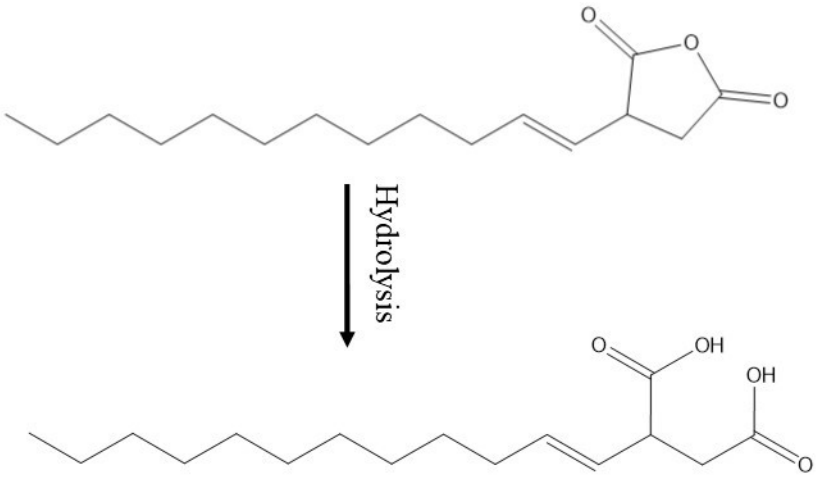


Figure 2.1 Schematic diagram of the continuous flow hydrothermal reactor.[25]



Scheme 2.1 Schematic representation of the DDSA ring opening reaction.[24]

Work on this project conducted by Gimeno-Fabra[24] investigated the addition of DDSA through both methods. It was proposed that DDSA would undergo a certain amount of hydrolysis of its ring structure within the reactor therefore, to understand the influence of ring opened structure on the coating of the HA the addition of pre-hydrolysed DDSA (H-DDSA, Scheme 2.1) was also investigated. When comparing DDSA and H-DDSA a significant difference in performance was only noted when adding the materials through the capping point (method 2) with H-DDSA providing a higher proportion of surface bound dispersant. When the reagents were added as part of the precursor solution (method 1) both performed similarly. It was concluded that the DDSA was able to undergo the hydrolysis reaction within the reactor and could bind strongly with the HA surface in a similar manner to H-DDSA; hydrolysis of the DDSA was not as efficient at the capping point leading to loosely bound DDSA molecules on the surface of the HA. Adding the dispersant during the synthesis step (method 1) was determined to be the most efficient route to successfully coat the HA NP's as this route provided higher extraction efficiency values, avoided the use of additional organic solvents and products contained a higher proportion of the HA (more efficient synthesis).[24]

In this chapter the range of dispersants with hydrocarbon tail groups that can be demonstrated to successfully stabilise dispersions of HA NP's in toluene is expanded. Both the relationship between the chain length of the tail group and the effect that steric hindrance has on the dispersant binding and nanoparticle stabilisation of the HA NP's were investigated. The length of the hydrocarbon chain was varied to include examples that featured 12, 16 and 18 carbon atoms. Three different polar head groups were also compared to determine the strongest interactions between the dispersant and HA surface. These were a protonated carboxylic acid, its sodium salt analogue and isosorbide connected to the hydrophobic tail via an ester bond. The synthesis of HA using the hydrothermal procedure shown in this paper have been successfully scaled to 200 kgs/hour production providing an industrial viable route to the manufacture of dispersible bioceramic nanoparticles.[25]

2.3 Experimental

Materials:

Calcium nitrate tetrahydrate, lauric acid and ammonium phosphate dibasic where purchased from Sigma-Aldrich and Fisher. Palmitic acid was purchased from Merc. Stearic acid was purchased from SAFC and 2-propanol (IPA) was purchased from VWR Chemicals. All materials were used as received without further purification.

2.3.1 Dispersant Synthesis

Lauric, Palmitic and Stearic sodium salts:

Sodium hydroxide (sodium laurate: 1.04 g, 0.026 mol. Sodium palmitate: 0.821 g, 0.021 mol. Sodium stearate: 0.744 g, 0.19 mol) and the chosen carboxylic acid (lauric acid: 5 g, 0.25 mol. Palmitic acid: 5g, 0.2 mol. Stearic acid: 5g, 0.18 mol) were introduced to flask

containing a mixture of 35 mL of isopropyl alcohol and 30 mL deionised water. This acid : base mixture was sonicated for 1.5 hours using a Fisherbrand FB11014 sonicator bath. The resulting white solid was filtered and washed twice with deionised water.

Lauric, Palmitic and Stearic isosorbide:

Isosorbide and the chosen carboxylic acid either (lauric, palmitic or stearic acid) in a equimolar ratio (e.g. for stearic isosorbide: stearic acid = 2.5 g, 0.008 mol and isosorbide = 1.29 g, 0.008 mol) were introduced to a flask containing *p*-toluenesulfonic acid (5% mole equivalent with respect to the carboxylic acid) and then heated to 125 °C and held at that temperature for 24 hours in total whilst the condensate water was removed by distillation. Due to the need to distil off the water produced this process consisted of three 8 hour periods with the reaction being cooled, sealed and stored at room temperature overnight. After 24 hours, a vacuum (150 mbar) was applied for 30 minutes to help facilitate the removal of any residual condensate and drive the reaction equilibrium towards 100% conversion to the target product. No further purification processes were applied. The brown solid product was analysed by GPC and shown to be a mixture of isosorbide that had been singularly and doubly esterified with the hydrocarbon acids. Further analysis can be found in Appendix 6.1.

Nanoparticle Synthesis:

HA NP's were synthesised using the continuous flow hydrothermal reactor developed by Lester and Azzopardi.[13, 24, 25] The reactor consists of a concentric pipe-in-pipe arrangement constructed of 316 stainless steel Swagelok® components. The outer tube had a 3/8 inch outer diameter (wall thickness = 0.065 inch) and the inner tube a 1/8 inch outer diameter (wall thickness = 0.035 inch). This design facilitates a counter-current flow of the two liquids, enabling rapid mixing at the exit point of the internal pipe. The short residence

time limits particle growth and degradation of any organic modifiers that may be present. Hot, pressurised ammonium phosphate/water solution was pumped through the inner pipe (down-flow) and an isopropanol solution of metal salt/organic modifier, at room temperature, was pumped through the outer tube (up-flow). The reactant solutions were prepared at ambient temperatures flowing the method detailed below in the General HA NP reagent synthesis section and the streams were flowed counter-currently with the down-flow pumped at a rate of 20 mL min^{-1} and the up-flow at 10 mL min^{-1}. The ammonium phosphate solution was heated to 200–400 °C and maintained at this temperature during the reaction. Pressure through-out the whole system was controlled by use of a manually operated back pressure regulator (BPR.) The final suspension of particles flowed out of the top of the reactor and cooled to room temperature in flow by a water cooler and was collected in a receiver tank. All NP products were centrifuged and washed with distilled water followed by isopropanol. The residual water was removed by freeze drying for 48 hours.

General HA NP reagent synthesis:

The down-flow stream (see definition above) consisted of ammonium phosphate (2.24 g, 0.015 mol) dissolved in deionised water (1 L) which had a pH = 8 and the up-flow stream (see definition above) consisted of mixture of calcium nitrate tetrahydrate (11.8 g, 0.05 mol) and the required dispersant (e.g. for stearic acid 1.42 g, 0.005 mol) dissolved in isopropanol (1L). The solutions were prepared by premixing the reagents at ambient temperature and sonicating in a Fisherbrand FB11014 sonicator bath until fully dissolved.

2.3.2 Material Characterisation

NMR:

NMR spectra were recorded at 25 °C using a Bruker AV3-400 spectrometer (^{1}H 400 MHz and ^{13}C 100 MHz). Chemical shifts were recorded in δ_H (ppm). Samples were prepared as solutions in $CDCl_3$ or D_2O and chemical shifts were referenced to the appropriate deuterated solvent. Analysis of the spectra was carried out using MestReNova software.

GPC:

Each sample was dissolved in HPLC grade THF, at a concentration of 2 mg/mL, and filtered through a 0.2 μm PTFE syringe filter. GPC analysis was performed on an Agilent 1260 HPLC with an online vacuum degasser, an Agilent online differential refractometer (DRI) and a Wyatt Helios Dawn 8 multiangle light scattering detector (MALLS.) Two Agilent 3 μm PLgel Mixed E columns (7.5 × 300 mm) were connected in series after an Agilent PLgel 3 μm Guard column (7.5 × 50 mm.) The column oven, DRI and MALLS temperature was set to 35 °C and the flow rate was set to 1 mL per minute. The sample injection volume was set to 100 μL. The specific refractive index increment (dn/dc) of L-lactide and poly(L-lactic acid) was set to 0.05 mL/g and the RI calibration constant was set to 1.5712×10^{-9}. MALLS calibration was performed using HPLC grade toluene, filtered through a 0.02 μm PTFE filter and normalisation was performed in THF using a 30 kDa linear polystyrene narrow dispersity GPC calibration standard. Analysis of the spectra was carried out using Astra software.

Extraction Efficiency (EE) Test:

The HA NP product was suspended in a water: toluene mixture (10mL: 10mL v/v mixture) *via* sonication for 30 minutes using a Fisherbrand FB11014 sonicator bath and then homogenised for 1 minute at 6100 rpm using a Silverson L5M rotor-stator homogeniser.

Following this the sample was allowed to stand for 10 minutes during which the two layers separated. The layers were collected separately using a separating funnel, the organic layer was evaporated using a rotary evaporator and stored for 24 hours in a vacuum oven set to 50 °C. The Extraction Efficiency (EE) coefficient was calculated as percentage mass of the product that was in the organic phase with respect to the initial total mass of the product that had been suspended in the two phases.

X-ray diffraction (XRD):

Powder XRD was carried out using a Bruker AXS D8 Advance diffractometer with a Cu Kα radiation (λ = 0.15418 nm) source. The samples were mounted in a poly(methyl methacrylate) (PMMA) sample holder and the range for 2θ was between 15–65°. The range interval was 0.04° and the dwell time was 5 seconds. The results were analysed using DIFFRAC.EVA software and compared to the ICDD database.

Transmission electron microscopy (TEM):

TEM imaging was conducted using a FEI Technai 12 BioTwin with an accelerating voltage of 120 kV. The suspension was dropped onto a copper grid. A suspended solution of 0.1mg ml^{-1} of HA sample in toluene was prepared using a Silverson L5M rotor-stator homogeniser and was pipetted onto the copper grid (300 lines per inch) with a holey carbon film where it was allowed to dry in air at ambient temperatures. Excess toluene was then removed by placing the grids onto filter paper.

Scanning electron microscopy (SEM):

A powder HA sample was spread onto the surface of a double-sided adhesive carbon tape mounted on an aluminium sample holder. The sample was allowed to dry overnight at room temperature. Platinum was vacuum-evaporated onto the sample using a 0.8 kV argon

plasma for 150 seconds using a Polaron SC7640 sputter coater. Images were collected using a JEOL 6400 SEM at an accelerating voltage of 15 kV.

Thermal gravimetric analysis (TGA):

TGA data was collected using a TA instruments Q500 TGA with the samples loaded onto platinum pans. The temperature limit was set to 700 °C with a heating ramp rate of 5 °C per minute. A nitrogen atmosphere was maintained at a flow of 20 mL min^{-1}.

Fourier transform infrared spectroscopy (FTIR):

FTIR data was collected using a Bruker ALPHA FTIR with an attenuated total reflectance (ATR) attachment. Each sample was recorded from 4000 – 400 cm^{-1} using 24 scans.

2.4 Results and Discussion

In this study the synthesis of the HA NP's was conducted with the prior addition of the dispersants to the up-flow reservoir such that it would be present in the reaction mixture as the nanoparticle formation occurred. A number of different interactions between the head groups and the HA surface can be proposed depending on the chemistry of the head group as well as the reaction conditions. These include electrostatic attraction, hydrogen bonding, covalent bonding or physical entrainment and examples of possible attachment modes are depicted in Figure 2.2.

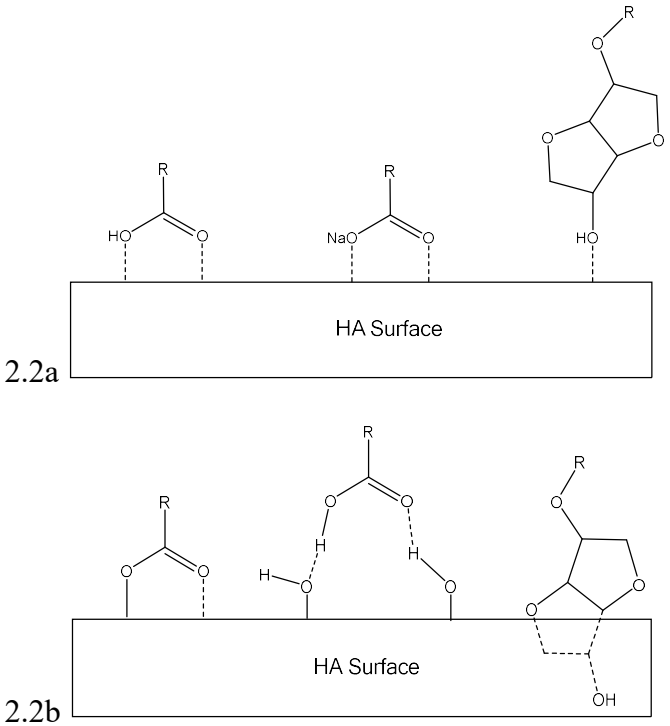


Figure 2.2a and 2.3b Schematic representation of the potential bonding methods for each head group with the HA surface. 'R' group represents a hydrocarbon chain of variable length. From left to right in 2.3a: hydrocarbon-carboxylic acid, hydrocarbon-sodium carboxylate and hydrocarbon-isosorbide. 2.3b shows other bonding options for the hydrocarbon-carboxylic acid to the HA surface and the entrainment of the isosorbide head group.

The isosorbide head group was included in the range of target head groups for the following reasons. It is derivable from low cost, agriculture sourced feedstocks, is thermally stable so was thought very likely to endure high temperature processing,[26] exhibits a high degree of structural rigidity / conformational organisation (see Figure 2.3) and contains only one obvious functional interaction/anchor point (the hydroxyl groups) however, this group alone was not considered to be a strong interaction point when compared to the highly polarised acid/sodium salt groups present in the other dispersants.

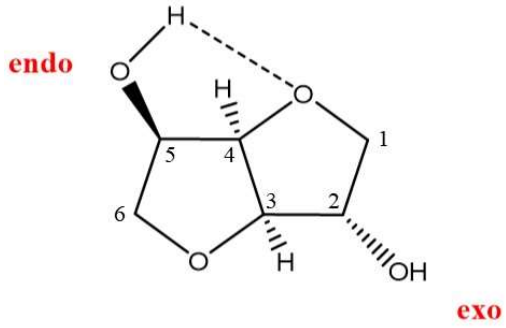
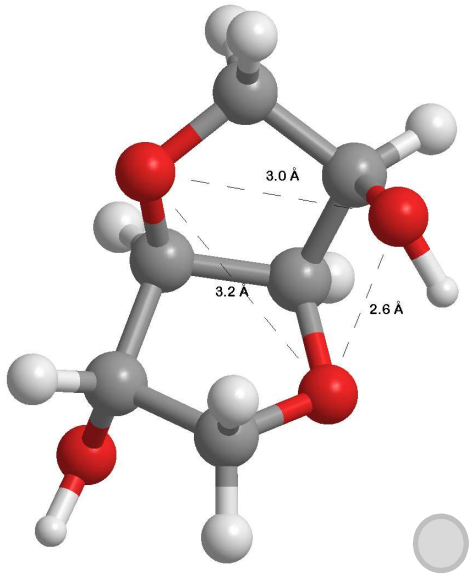


Figure 2.3 Molecular structure of isosorbide with endo and exo hydroxyl groups indicated.

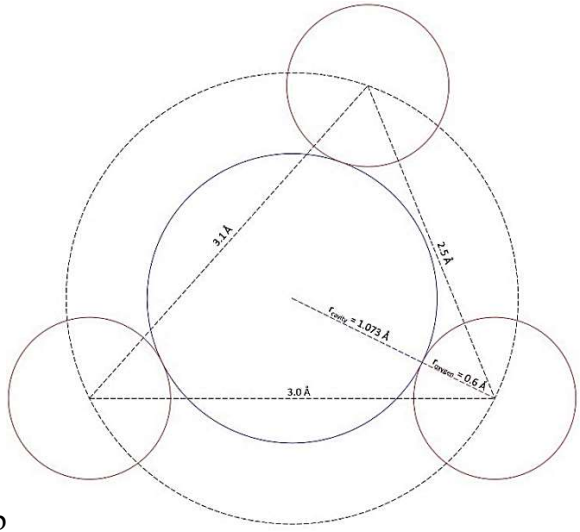
Additionally, when assessing the reactivity of isosorbide Parrott *et al.* [27] had noted that the steric surroundings of the hydroxyl groups significantly differ from each other (Figure 2.3). The endo-C5-hydroxyl group is eclipsed by the bridging oxygen atom between C-1 and C-4 whilst the exo-C2-hydroxyl group is eclipsed by hydrogen atoms. The intramolecular hydrogen bond established between the endo-hydroxyl group and the bridging oxygen atom enhances the nucleophilic nature of the group and as a consequence tends to be more reactive than its exo-2-hydroxyl counterpart.[28-31] It was hoped that this differential reactivity would lead to the exclusive preparation of mono-esterified product in an equimolar synthetic preparation.

Furthermore, the geometry of the isosorbide molecule suggests that a calcium ion could fit into a cavity formed by three oxygen molecules forming a crown ether like interaction producing a stable bonding mechanism with the surface. A 3D molecular structure of isosorbide in a low energy conformation is depicted in Figure 2.2a alongside a diagram detailing the theoretical radius of the cavity created between three oxygen atoms which was calculated by using the radius of the triangle's circumscribed circle with the radii of the three oxygen atoms also taken into account (Figure 2.4b). The MM2 calculation method was used to determine the structure of the isosorbide molecule presented in Figure

2.4a. This method uses force field calculations to determine the structure and energies of small organic molecules and hydrocarbons.



2.4a = carbon = oxygen = proton



2.4b

Figure 2.4. 2.4a shows a 3D model of the isosorbide molecule (created in ChemBio3D Ultra) in its lowest energy state as calculated using the MM2 theorem. The distances between the three oxygen atoms in the hydroxyl group and the two ether groups depicted as a triangle. 2.4b is a diagrammatic representation of the cavity (blue) between the three oxygen atoms (red). The triangle established between the three oxygen atoms in 2.5a was used to calculate the radius of the cavity.

As the radius of a calcium ion (Ca^{+2}) with a coordination state of VI is 1 Å and the radius of the cavity being 1.073 Å, therefore it is possible, especially at elevated temperatures,

that the positive calcium ion could form a stable electrostatic interaction with the negative oxygen atoms.[32, 33]

It was determined via GPC analysis that despite the differing reactivity of the two hydroxyl groups and the equimolar reaction ratio (discussed above) esterification of isosorbide occurs from both the hydroxyl groups with the reaction products consisting of a ratio of approximately 1:0.70 singly to doubly esterified isosorbide. The differing reactivity between the two hydroxyl groups can explain the ratios seen in Table 2.1 where a higher proportion of singly esterified isosorbide is observed in all the final products.

Table 2.1 Ratio of singly esterified isosorbide (A) to doubly esterified isosorbide (B) for each sample. Ratios were calculated using the GPC derived mass fractions data.

Sample	**Mass Fraction of A (%)**	**Mass Fraction of B (%)**	**Ratio of A:B**
Lauric Isosorbide	41.6	48.5	1:0.75
Palmitic Isosorbide	45.9	45.6	1.0.61
Stearic Isosorbide	42.9	49.6	1:0.7

As the ratios determined by GPC indicate that there is a significant amount of di-esterified isosorbide in our final products it is necessary to address whether this dispersant structure is also capable of interacting with the surface of the HA. A 3D molecular structure of a di-esterified lauric isosorbide in a low energy conformation is shown in Figure 2.5. Calculated distances between the three oxygen atoms that form the cavity for the Ca^{2+} show that it is of similar size to that seen in Figure 2.4 and indicates that it would still be possible for the crown ether-like interaction, mentioned previously, to occur. Figure 2.6 shows that the steric bulk of the hydrocarbon chain and the bond angles formed between the hydroxyl oxygen atom (which forms a part of the cavity) in a low energy configuration. The diagram indicates that the bond angles would be unfavourable; when

the molecule is in this energy configuration the chain prevents the cavity from getting into close proximity to the HA surface to form the desired interaction with the Ca^{2+} ion. However, hydrocarbon chains are not completely rigid and at the temperatures of the synthesis procedure it is possible for the hydrocarbon chain to orientate itself into a position that enables the isosorbide cavity to interact with the Ca^{2+} on the NP surface. A simple bond rotation between the C1 and C2 atoms on the chains could allow for a more favourable steric conformation than that shown in Figure 2.6.

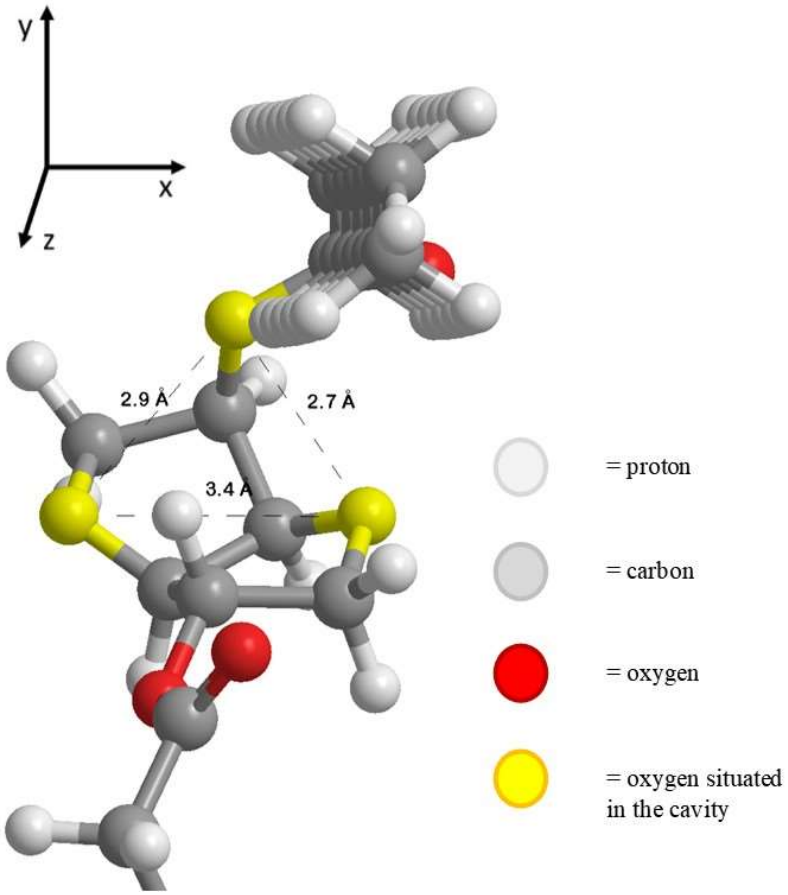


Figure 2.5 A 3D model of di-esterified lauric isosorbide in a low energy state (created in ChemBio3D Ultra) with the three oxygen atoms highlighted in yellow (2 contained in the ring structure and the third being the hydroxyl group). The distances between the 3 oxygen atoms are indicated.

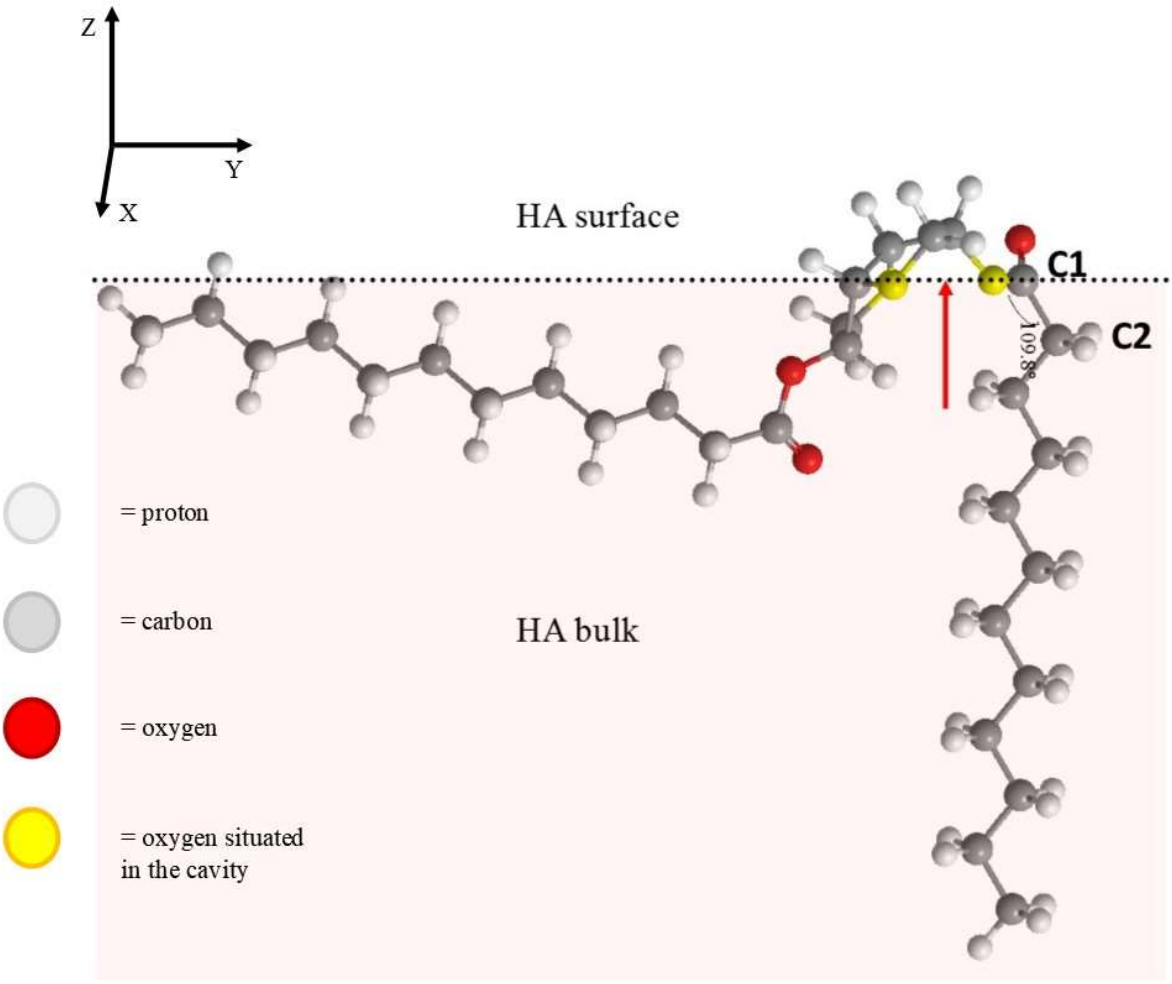


Figure 2.6 Shows a 3D model of di-esterified lauric isosorbide in a low energy state (created in ChemBio3D Ultra) interacting with the HA surface (as a cross-section) *via* interaction through the surface Ca^{+2} ion and the cavity created by the three oxygen groups (highlighted in yellow) indicated in Figures 2.4 and 2.5. The red arrow indicates where the Ca^{2+} ion would interact, and the dashed line represents the surface of HA which should be viewed as being in the plane of the paper.

The saturated hydrocarbon chains of the dispersants have no functional groups, lone pairs of electrons or reactive points (such as a double bond) and saturated hydrocarbon chains often require high temperatures, strong oxidants or metal catalysts in order to react.[34] It is unlikely, using our synthesis method, that this section of the dispersant will have any form of significant binding interaction with the HA surface. If any interaction is formed it most

likely takes place between the isosorbide functional group in the centre of the molecule and the NP surface. Figure 2.7 highlights this 'reactive' area.

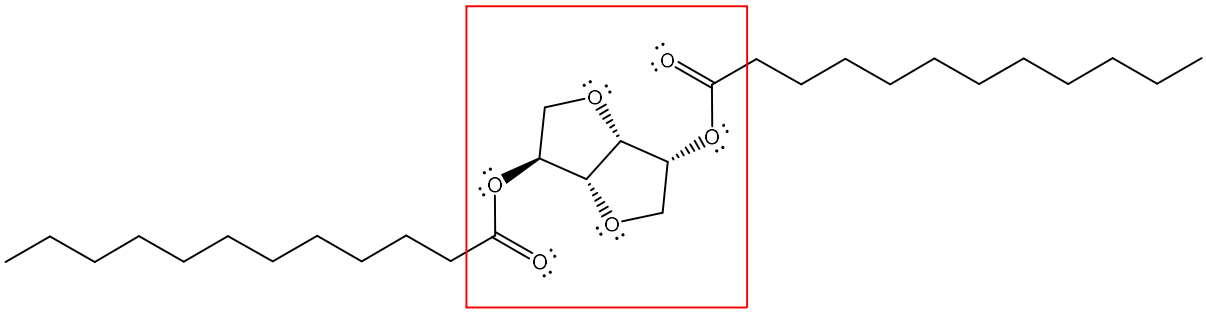


Figure 2.7 A molecular diagram of di-esterified laurate isosorbide with electron lone pairs shown. A red box indicates the potential interaction point of this molecule with the surface of HA.

The isosorbide group contained within this ABA style dispersant has multiple lone pairs of electrons on each oxygen atom. Studies conducted by Rimola *et al.*[35] use density functional theory to model the interactions between glycine and HA NP surface. Their studies suggest that interactions between the nitrogen electron lone pair contained within the glycine amino group and the Ca^{2+} ions is occurring on the surface. From this it is speculated that it could also be possible for the lone pairs on the oxygen atoms in the isosorbide-hydrocarbon based dispersants to form coordinative interaction with the Ca^{2+} ions on the surface of HA.[35]

Figure 2.8 shows a simple representation of the steric conformations that could be adopted on the surface of the HA by the di-esterified isosorbide dispersants. From the discussion above it is possible to speculate on which surface conformation is likely to be the most favoured for these di-esterified dispersants. The primary modes of interaction with the HA are contained within the isosorbide head group therefore, the conformation depicting the head group raised off the surface and the hydrocarbon chains forming the primary interaction is unlikely to be the case. The molecule lying flat on the surface with both

chain and head group interacting is possible but also not likely as not only does the hydrocarbon chain contain no modes of interaction, but it is also hydrophobic, whereas the surface of HA is highly charged and hydrophilic in nature. This leaves the final conformation with the head group as the primary point of interaction and the hydrocarbon chains angled away from the surface and the likely steric conformation adopted by this dispersant. Such a conformation will also increase the stearic bulk of the dispersant barrier enabling an enhanced performance in stability of the coated NP's.



Figure 2.8 A basic representation of the stearic conformations of two armed linear dispersants on the HA surface. Red spheres represent the head groups and the black lines the hydrocarbon chain.

Quantities of dispersant-coated and non-coated nanoparticles were prepared as detailed in the experimental section. Once collected they were subject to analysis to define the success of the incorporation of dispersant and effect this incorporation has upon the NP composition and morphology. The TGA traces (Figure 2.9) allow comparison the weight loss of the dispersants and modified/unmodified HA NP's, Table 2.2 summarises the weight losses observed for the modified and unmodified HA NP's.

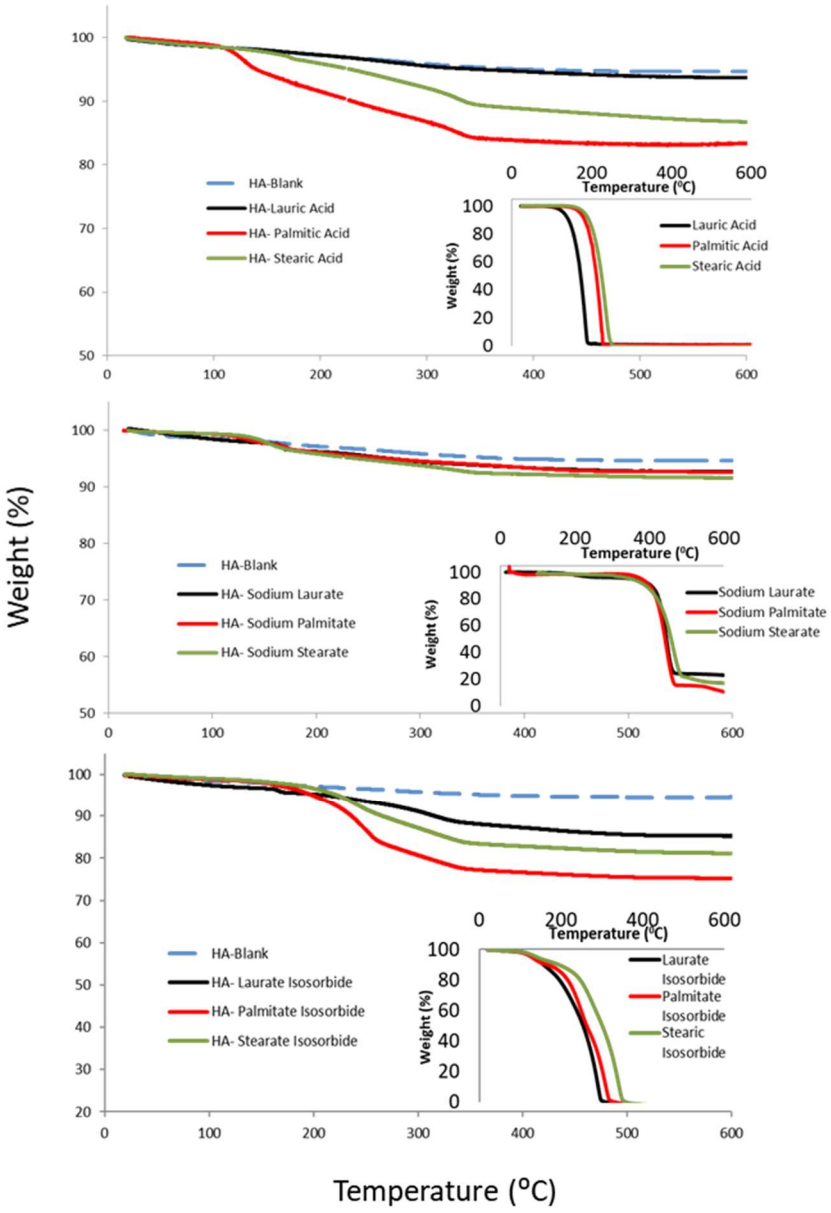


Figure 2.9 TGA plots of total recorded mass loss (weight %) *vs* temperature for the hydrocarbon dispersants (inset) and coated NP's.

Upon examining the TGA traces it was immediately clear that there were marked increases in degradation temperatures for certain dispersants and coated NP's. In particular it is interesting to note that upon altering the acid end group to produce a sodium carboxylate salt a 200 °C increase in degradation temperature was observed from the dispersants (inset graphs). This is a significant increase in thermal stability and may influence the level of

coating observed on the NP surface for these dispersants; an increase in stability this large could prevent the dispersant head group from forming stable interactions with HA at our synthesis temperature. Another marked increase in thermal stability can be seen for the HA coated with dispersants containing the isosorbide functional group compared to the acid and sodium analogues. This is seen more clearly when the derivative weight % is plotted against temperature as shown in Figure 2.10.

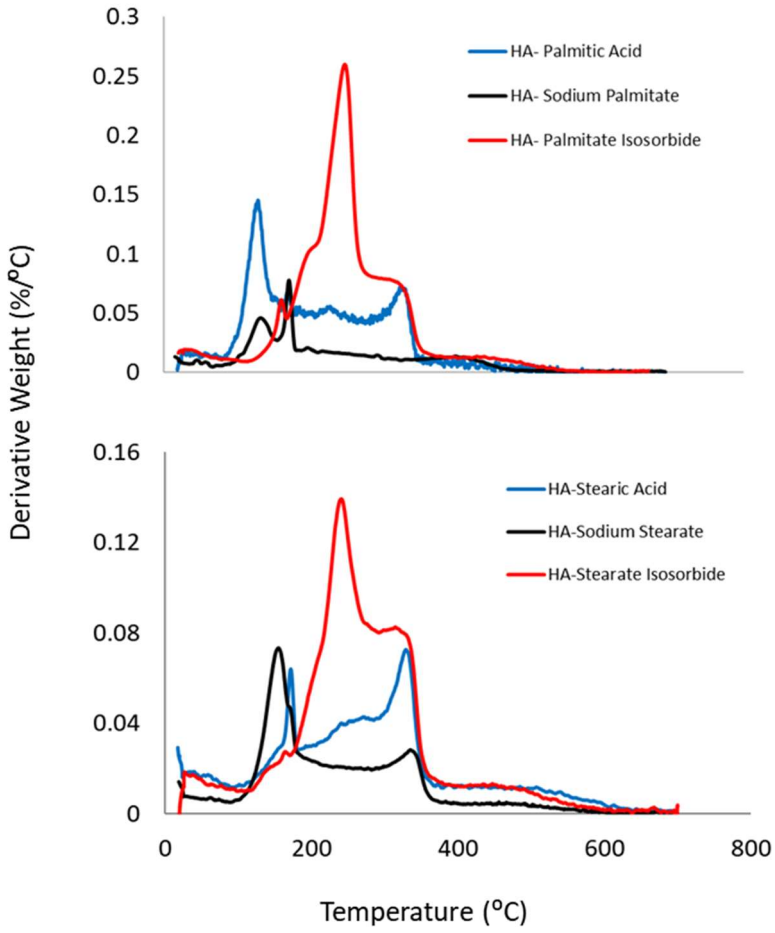


Figure 2.10 TGA plots of total recorded mass loss as a derivative of weight%/temperature *vs.* temperature for the hydrocarbon dispersant coated NP's.

The loss seen at 330-350 °C is consistent throughout all the samples shown in Figure 2.11 and can be attributed to the loss of HA lattice water.[36, 37] The peaks seen within 100-200 °C are due to a combination of evaporating surface water and loosely bound dispersant

molecules.[24, 37] Between 200-400 ºC further weight % loses for all samples is observed, with only isosorbide functionalised hydrocarbons showing a large well defined weight loss peak indicating that with this particular functional group a larger proportion of the dispersant is thermally stable on the surface of the HA. It is also noted that HA-sodium palmitate does not have a significant lattice water loss but appears to have a higher proportion of surface water evaporation weight loss: dispersant loss.

Table 2.2 Weight losses in varying temperature regions TGA and level of Extraction efficiency achieved for the dispersant modified HA.

Nanoparticle (Carbon Chain Length)	**Total Weight Loss (%)**	**Total Weight Loss (mol of dispersant)**	**Weight Loss <150^{0}C (%)**	**Weight Loss 150-200^{0}C (%)**	**Weight Loss 200-400^{0}C (%)**	**EE (weight loss %)**
HA- Lauric Acid (C12)	6.56	8.98×10^{-7}	2.017	0.74	2.68	3.89
HA- Sodium Laurate (C12)	6.55	8.26×10^{-7}	2.68	0.54	2.70	5.29
HA- Laurate Isosorbide (C12)	10.19	1.92×10^{-6}	0.97	0.72	8.08	96.59
HA- Palmitic Acid (C16)	15.84	9.33×10^{-7}	5.79	2.72	7.80	90.13
HA- Sodium Palmitate (C16)	7.51	1.71×10^{-6}	2.26	1.63	2.70	43.16
HA- Palmitate Isosorbide (C16)	24.88	1.72×10^{-6}	1.86	3.26	18.26	95.03
HA- Stearic Acid (C18)	13.06	1.27×10^{-6}	2.34	1.78	7.21	91.28
HA- Sodium Stearate (C18)	8.33	1.66×10^{-6}	2.05	2.10	3.60	97.46
HA- Stearate Isosorbide (C18)	18.84	8.38×10^{-7}	1.67	1.67	13.85	98.40
HA - Uncoated	5.34	-	1.99	0.84	2.24	7.29

The TGA analysis of the HA NP's revealed varying degrees of weight loss occurring at temperatures <400 ^{0}C. This can attributed to a combination of the loss of water, entrained process water and dispersant loss. The uncoated materials were found to contain approximately 2% surface water (<150 ^{0}C), by comparison dispersants that showed

significant weight loss above 2% in this temperature region were the palmitic acid dispersant. The weight loss in the 150-200 ºC region was related to the loss of both pore bound/entrained water in the HA structure and loosely bound dispersant molecules. The total weight loss figures defined that approximately 5% of the unmodified HA samples weight could be attributed to water and other surface contaminants related to the nanoparticle structure and synthesis procedure.[36] Comparison of this data to that of the coated samples showed that both the length of the hydrocarbon tail and the type of head group had an effect on the weight fraction of coating adhered to the HA NP's as well as the extraction efficiency (EE) achieved of the HA NP's. EE coefficients are calculated as a mass of product in the organic phase (toluene) *vs.* the mass of product in the aqueous phase after a thorough mixing of the two phases. The idea behind this technique is to quantify the level of stability the coated NP's have in a solvent that uncoated HA would not normally be stable in and therefore, give an indication of the effectiveness of the dispersant in preventing agglomeration and achieving an ideal dispersion. The more effective the coating is the more stable the NP will be in the organic phase, this will increase the amount of coated nanoparticle product that is extracted into the organic solvent leading to an increase in the EE value.[24]

Closer inspection of the data detailed that the C12 lauric chain end was shown to give almost no additional increase in weight loss and had poor EE values, with the exception of lauric isosorbide. This suggests that this hydrocarbon chain length had insufficient molecular size to achieve good partition between the NP surface and the solvent medium when synthesised using the hydrothermal process used in this study. The isosorbide molecule however, adds to the overall size of the dispersant molecule especially when the di-esterified molecular structure is considered at this structure consists of twice the amount of hydrocarbon chain. It is possible that this steric bulk also provided a more stable

interface between the NP surface and organic solvent increasing the NP's stability when dispersed leading to high EE values. The increase in the amount of coating indicates that isosorbide based dispersants are capable of being adhered better to the HA surface during synthesis. Looking at Figure 2.1 and Figure 2.5 it becomes clear that, unlike the acid and sodium salt analogues, the isosorbide functional group has multiple modes of interaction whether it is mono or di-esterified. The results suggest that these extra points of interaction could be providing a stronger surface adhesion for isosorbide based hydrocarbon dispersants.

As the chain length increases the materials demonstrate substantial increases in weight loss, indicating that a significant coating of the NP had been achieved. With the exception of sodium palmitate this difference was also reflected in the extraction efficiencies, where >90% of the C16 and C18 NP's were extracted for both the carboxylic acid and sodium salt hydrocarbons. It is also important to note that the EE values for isosorbide based dispersants remained consistently high throughout all three chain lengths. This consistent trend of high EE values for isosorbide hydrocarbons (despite the TGA results showing a decrease in the level of coating for stearate isosorbide) can be linked to Figure 2.8 and the discussion surrounding the steric conformation of the di-esterified molecule on the surface of the HA. If the dispersant adopts the stearic conformation with the chains being slightly angled from the surface, then this could explain the increased stability of the NP's within the organic solution as the stearic barrier provided by the dispersant will be enhanced by this configuration when compared to the other conformations indicated in Figure 2.8. The C16 sodium salt EE value appears as an apparent anomaly that could be explained by taking a closer look at the TGA results in Table 2.2. If the three weight percentage drops over the specified temperature ranges are considered, 59% of this loss occurs below 200^0C indicating that a significant majority of the loss is likely due to surface water and more

loosely bound dispersant molecules. The lack of strongly bound dispersant on the surface may explain why the NP's could not be as efficiently extracted as the coating was not able to provide a stable steric barrier in the organic phase. The EE value of sodium stearate rivals that of stearate isosorbide even though, at lower chain lengths the sodium carboxylate head groups did not perform as efficiently. Buszello *et al.* [38] investigated the zeta potential of oil/water emulsions using co-emulsifiers containing non-ionic polyethylene glycol fatty acids and ionic alkali fatty acids (sodium laurate and sodium stearate). They found that the zeta potential increased upon addition of the alkali fatty acids with sodium stearate providing a superior stabilization over sodium laurate. This indicates that the length of the hydrocarbon tail had an effect on the electrostatic stabilisation of the colloidal systems and to a certain extent explains the high EE value/stabilisation seen in this work for sodium stearate.[38] The trend seen in the increase in chain length with both the EE values and TGA results suggests that the chain plays a key role in the stability of NP's and also the adhesion of the dispersant to the HA surface. It is proposed that the increase in stability of the NP's with increasing chain length is a consequence of having a thicker steric barrier of dispersant between the NP surface and the solvent medium. An increase in chain length can also provide a more favourable and stable interface between the organic solvent and the HA surface. This barrier is able to prevent the NP surfaces from interacting with each other to form agglomerates more effectively due to the increase in the stearic bulk of the dispersant molecules. It is, however more difficult to explain why the chain length also affects the level of coating seen (in terms of moles) on the surface via the TGA results. It has been previously discussed that the hydrocarbon chain cannot interact with the surface of the HA in any substantial manner, so it is unlikely that the increases observed can be directly attributed to an increase in chain-surface interactions. Another possibility for this increase may lie in how the longer chain

lengths behave during the hydrothermal synthesis procedure. The two solvents used in the synthesis include water and isopropyl alcohol IPA at a 2:1 ratio with the two streams mixing within the reactor at the point of HA NP formation. The solubility of fatty acids in water decreases with increasing chain length; when the two streams mix within the reactor it is possible that the hydrocarbons with longer chain lengths will be able to precipitate out of the water/IPA solution more easily and subsequently adhere to the surface of the nano-HA (which is also precipitating out of the solution) more efficiently than the shorter fatty acid chains.[39]

Looking at the trend in head groups and the clear success of the isosorbide functional group at all chain lengths it can be proposed that the chemical nature of the head group and the morphology of the dispersants plays an influential role in the deposition of the dispersant onto the surface and its ability to adhere to that surface in a significant manner. The isosorbide dispersants were observed to deliver the best performance across the full range of chain lengths. In this case even the C12 derivative exhibits significant weight loss. This accounted for the greatest weight fraction (as a weight %) of dispersant for each corresponding chain length sample and all provided extraction efficiencies of > 95%. However, these results had to be tempered by the fact the isosorbide dispersant material contains a different molecular structure profile to both the acids and sodium salts. Firstly, the isosorbide head group has a greater molecular mass than the other dispersant head groups. Upon calculation of the total weight % as a mole fraction (as shown in Table 2.2) it is shown that the coating still increases relative to all other dispersants even when the molecular weight of the isosorbide functional group is accounted for; with the exception of stearate isosorbide. This exception poses an interesting finding as it could indicate that whilst an increase in the bulk of the dispersant is favourable it is only so until a certain point. If the molecule is too large surface adhesion could be affected, with the functional

groups containing the primary points of interaction potentially hindered from getting within close proximity of the HA surface. This may be even more pronounced in a dispersant that contains two large sterically bulky chains as is the case with isosorbide that has been di-esterified with a stearic fatty acid. However, even with a decreased amount of coating on the surface the EE value is the highest out of all the dispersants tested supporting the theory of this particular combination of mono and di-esterified dispersant morphology creating an increased steric barrier. It also highlights the importance of the length of the hydrocarbon chain in the dispersant's ability to favourably interact with the organic phase. The mono and di-esterified isosorbide dispersant morphologies have been discussed in great detail earlier in the text. It is clear from the results in Table 2.2 that this combination of functional group and different morphologies enhances the coating efficiency.

An overall conclusion from these experimental results is that the data implies that the dominating factor for achieving both dispersant deposition within the continuous hydrothermal process and dispersion stability in toluene, using these dispersants, was steric stabilization. Additionally, it was noted that when the TGA indicated that a HA sample contained at least 8% (w/w) of dispersant, the EE for the sample was above 90%. Furthermore, there was no significant variation in the EE value achieved for greater dispersant weight fractions. This suggests that an optimal level of coating of the HA surface has been achieved and that any additional dispersant did not affect the dispersion stability.

The NP materials were then analysed using Fourier transform infrared (FTIR) spectroscopy. Figure 2.11 contains example FTIR absorbance spectra of unmodified HA NP's and indicates all major IR bands for HA.

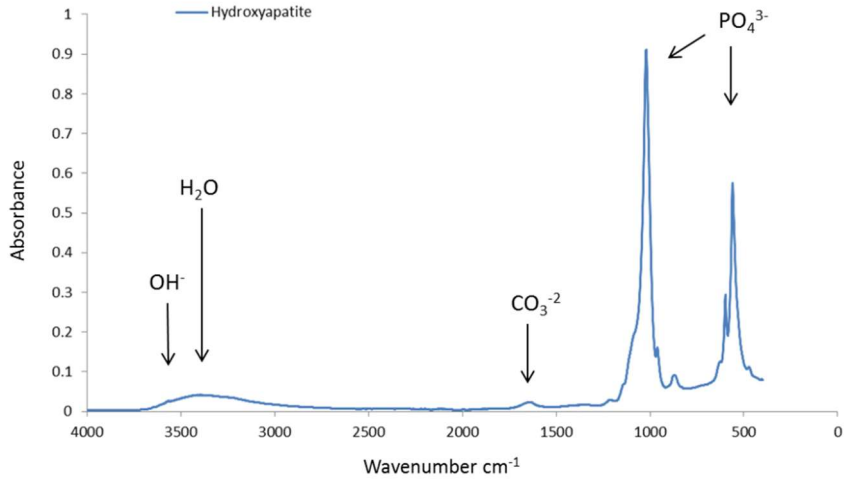


Figure 2.11. FTIR Absorbance spectrum for unmodified HA NP with relevant absorbance bands labelled.[40]

Figure 2.12 shows the FTIR spectra relating to C12 hydrocarbon chain length dispersants. Absorbance bands between 2800 and 3000 cm^{-1} were attributed to the alkyl C-H stretching and those between 1700 and 1800 cm^{-1} with the C=O stretching associated with the dispersant. It is important to note the C=O absorbance band shifts depending on the type of carbonyl functional group it is a part of, for the carboxylic acid the absorbance band is observed at 1690 cm^{-1}, for the carboxylate sodium salt the absorbance band is at 1550 cm^{-1} and for the isosorbide ester 1725-1730 cm^{-1}. This is a consistent trend seen for all the dispersants used in this study and reflects the differing strengths of the C=O bond with higher wavenumbers denoting stronger bonding in accordance to Hookes Law. For the acid functionalised hydrocarbons there is a very broad absorbance band at 2500 – 3000 cm^{-1} related to the carboxylic acid OH group which is slightly obscured by the alkyl C-H absorbance band. For the hydrocarbon containing the isosorbide head group a absorbance band at 3360 cm^{-1} is also observed and relates to the alcohol functional group found on mono-esterified isosorbide.[41, 42] Only HA- laurate isosorbide had absorbance bands (C=O and alkyl C-H) that corresponded to the dispersant which could indicate a presence of the

coating on the surface of the HA. It is interesting to note that the absorbance band relating to the alcohol OH of the mono-esterified isosorbide is not found in the FTIR of the laurate isosorbide coated HA. This absorbance band may have been obscured by surface interactions as this group is predicted to interact with the HA surface; another theory for the lack of this absorption band is that the mono-esterified isosorbide hydrocarbon may not be present at all on the surface and the coating is in fact mainly comprised of the di-esterified isosorbide dispersant. These set of results corresponds well with the TGA and EE values discussed previously and seen in Table 2.2.

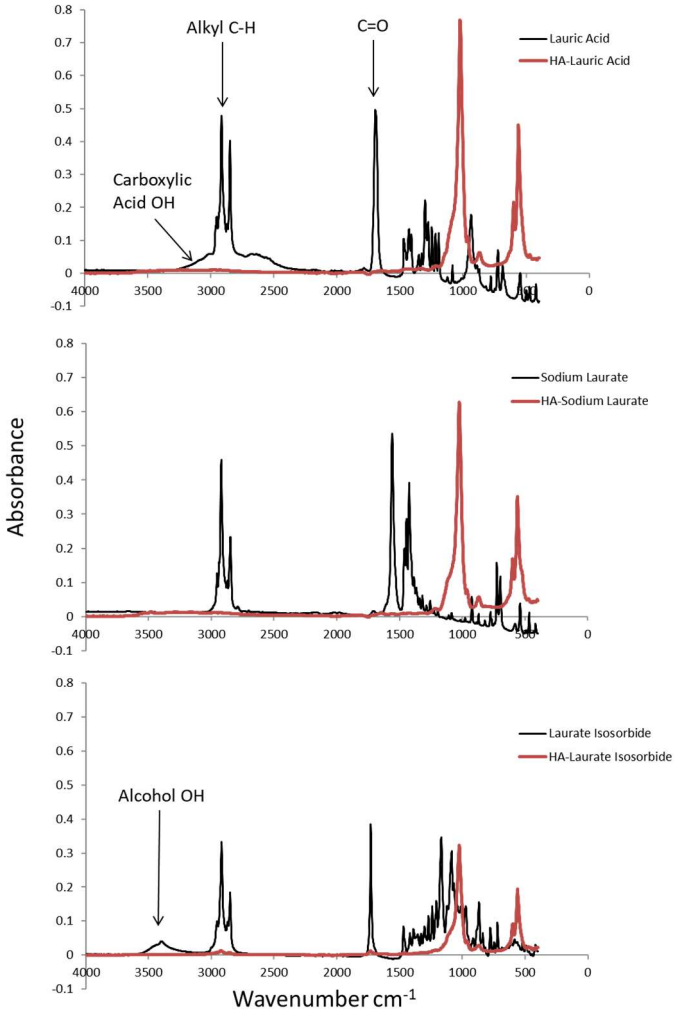
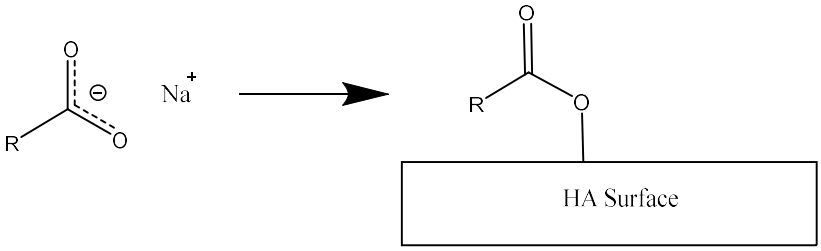


Figure 2.12. FTIR Absorbance spectra for HA NP's coated with C12 hydrocarbon dispersants. Absorbance bands related to the dispersant are labelled.

Figure 2.13 contains the FTIR spectra relating to the C16 hydrocarbon chain length dispersants. The aforementioned absorbance bands relating to the dispersants are present and labelled accordingly. All coated HA FTIR spectra for this chain length contain absorbance bands relating to the dispersant indicating its presence on the surface of the NP's and once again corresponds well with the TGA and EE values seen in Table 2.2. The FTIR spectrum of HA- sodium palmitate is particularly interesting as it contains a very broad and significant absorbance band at 3000-3700cm^{-1}. This absorbance band is seen in the uncoated HA spectrum (Figure 2.11) but not for any of the coated HA samples and is related to H_2O molecules and OH^- ions on the HA surface. Looking at the TGA/EE values shown in Table 2.2 for HA- sodium palmitate results suggested that an unusually large amount of surface water was present for this coated HA sample; the peak observed in the FTIR correlates well with this conclusion. Another absorbance band of note in this spectrum is that relating to the C=O bond within the carboxylate sodium salt. A shift in this peak from 1550cm^{-1} to 1660cm^{-1} is observed when the dispersant is bound to the surface of the HA; a shift to higher wavenumbers denotes a strengthening in the C=O bond. When the nature of this carbonyl group is considered it is apparent that the addition of the Na^+ cation weakens the C=O bond as the shift observed is lower than that of other carbonyl groups such as carboxylic acids and esters. This is due to the stable resonance form of carboxylates seen in Scheme 2.2 which shows the negative charge being stabilised over multiple bonds resulting in the electrons in the double bond being distributed across two bonds and subsequently weakening the C=O bond. Should the dispersant form an ester linkage with the HA surface this bond formation would strengthen the C=O and offers an explanation for the shift to higher wavenumbers seen for the carbonyl peak in the HA-sodium palmitate FTIR spectrum. It is of course highly likely that the carboxylic acid

groups are also capable of forming this surface bond, however a shift in the spectrum would not be observed for the HA NP's coated with this particular dispersant as there is no weakening and subsequent strengthening of the C=O bond in this reaction mechanism.



Scheme 2.2. Resonance form of carboxylate and reaction schematic this functional groups interaction with the HA surface.

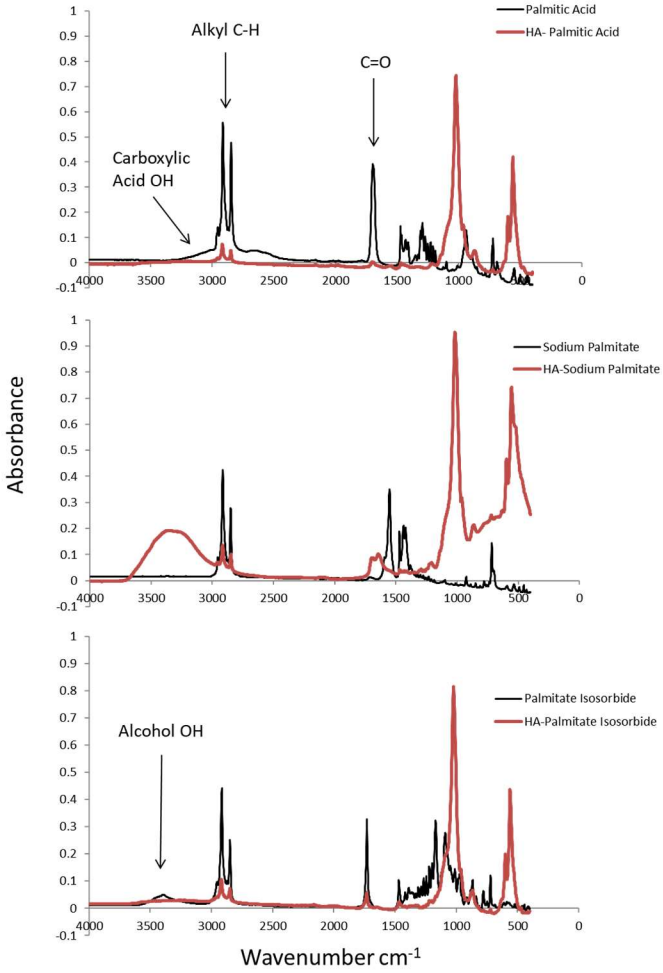


Figure 2.13. FTIR Absorbance spectra for HA NP's coated with C16 hydrocarbon dispersants. Absorbance bands related to the dispersant are labelled.

Figure 2.14 contains the FTIR spectra relating to the C18 hydrocarbon chain length dispersants. As with the previous spectra absorbance bands relating to the dispersants are present and labelled accordingly. All coated HA FTIR spectra for this chain length contains absorbance bands relating to the dispersant indicating its presence on the surface of the NP's and as with C16 FTIR spectra corresponds well with the TGA and EE values seen in Table 2.2. HA- sodium stearate does not show an excess of surface water and as a result the EE value is significantly higher than HA-sodium palmitate suggesting a much more stable dispersant coating.

The absorbance bands between 3200 and 3700 cm^{-1} for the uncoated HA spectrum in Figure 2.11 were attributed to adsorbed water but were noted to be significantly reduced or absent in all the modified HA spectra, regardless of the degree of coating (with the exception of HA-sodium palmitate). This lack of adsorbed water for the majority of the modified HA NP's indicates that the HA surface has been altered.

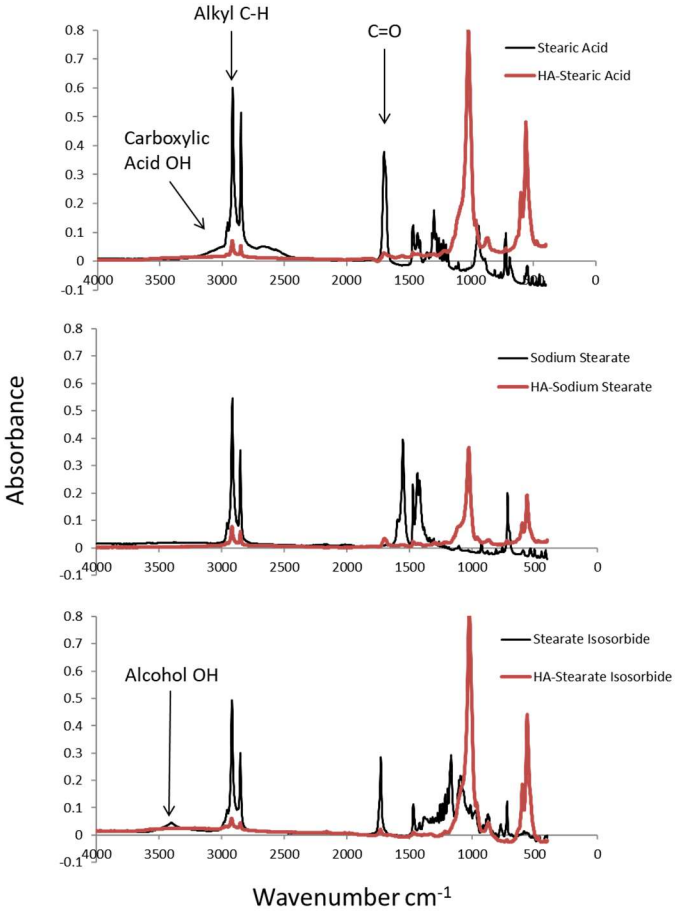


Figure 2.14. FTIR Absorbance spectra for HA NP's coated with C18 hydrocarbon dispersants. Absorbance bands Peaks related to the dispersant are labelled.

XRD data of the synthesised materials was also collected and Figure 2.15 contains the XRD patterns for unmodified HA and all the hydrocarbon modified HA. All the peaks were found to match with the HA exhibiting a hexagonal $Ca_{10}(PO_4)_6(OH)_2$ structure (ICDD ref. 01-074-0565). There were no significant changes in the relative peak intensities observed between each sample indicating similar crystal growth and orientations for each. Therefore, it can be concluded that the addition of the different dispersants to the up-flow feed of the hydrothermal process had not had a significant effect in the formation of the HA crystal structure.

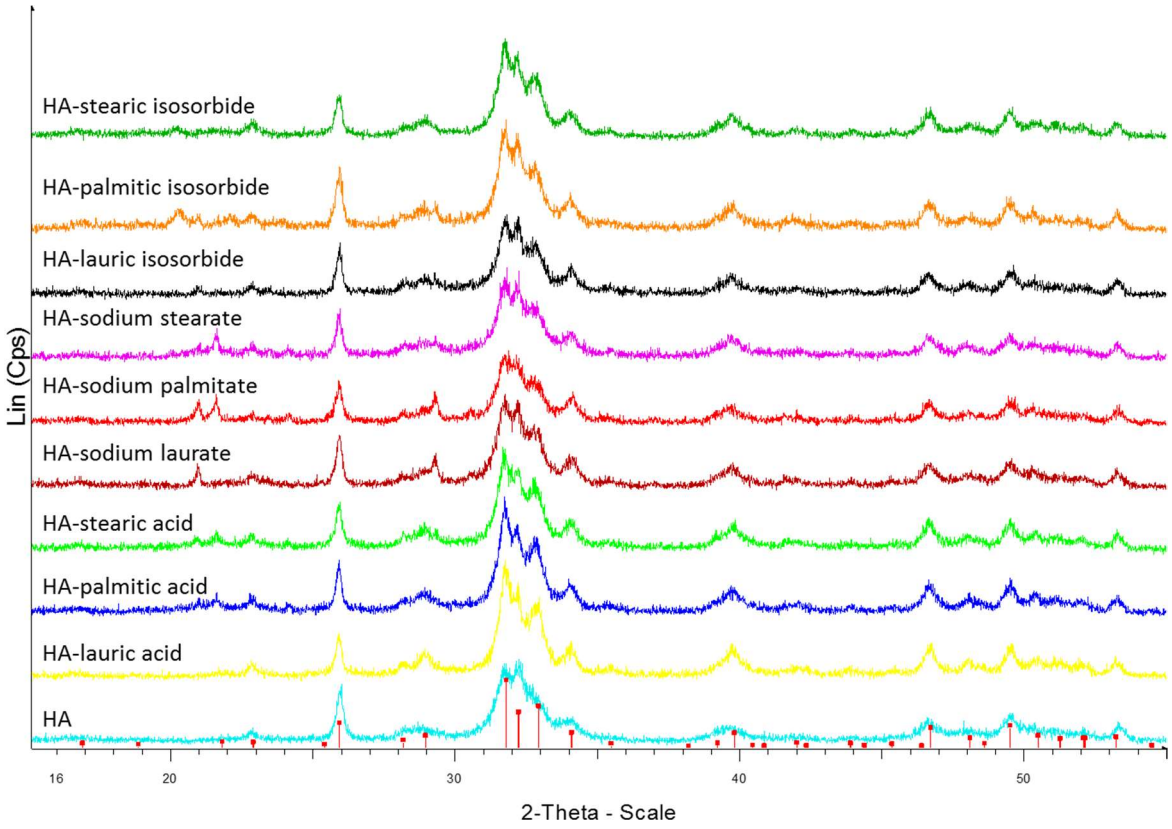


Figure 2.15 XRD patterns for uncoated HA and coated HA for each dispersant. Highlighted marks on the x-axis indicate the predicted peak positions for hexagonal phase hydroxyapatite.

TEM and SEM images indicated (see Figures 2.16 and 2.17) that all HA NP's were polydisperse with average dimensions of 300 × 115 × 20 nm. SEM indicated a similar morphology for the aggregates and EDX data determined the average ratio of Ca/P for all samples to be 1.74 ± 0.11 which was within the expected range for HA (molecular formula of HA shows Ca/P at 5:3 = 1.67).[43] The polydispersity of the samples was assessed using an ImageJ® script as described by Igathinathane *et al.*[44] It was determined that the NP's were polydispersed matching previous results reported by the Gimeno-Fabra *et al.*[24] The morphology of all the HA produced was shown to be plate-like, indicating that the dispersants had little or no effect on the morphology of the NP's produced.

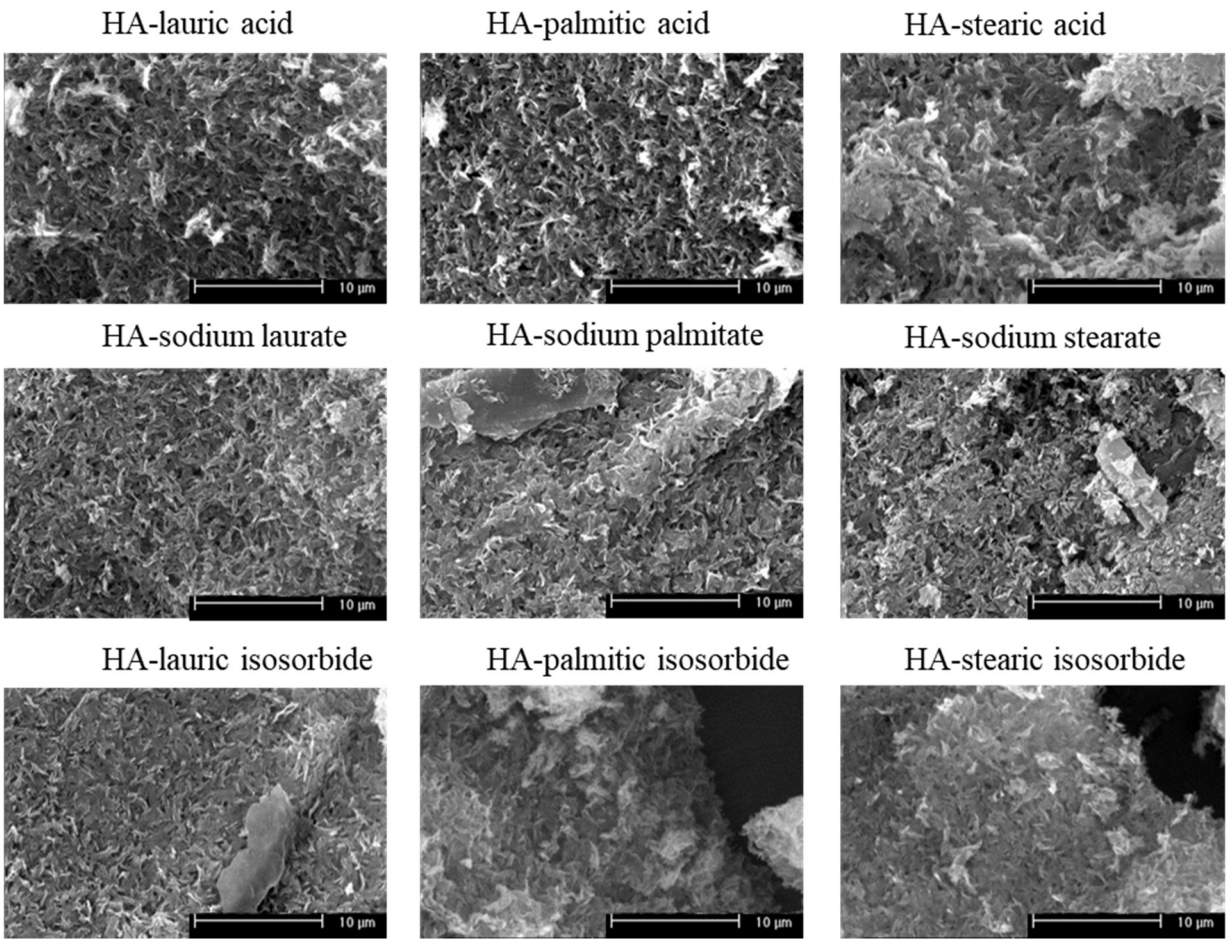


Figure 2.16. SEM images of modified HA. From left to right, top to bottom: HA-lauric acid, HA-palmitic acid, HA-stearic acid, HA-sodium laurate, HA-sodium palmitate, HA-sodium stearate, HA-lauric isosorbide, HA-palmitic isosorbide and HA-stearic isosorbide.

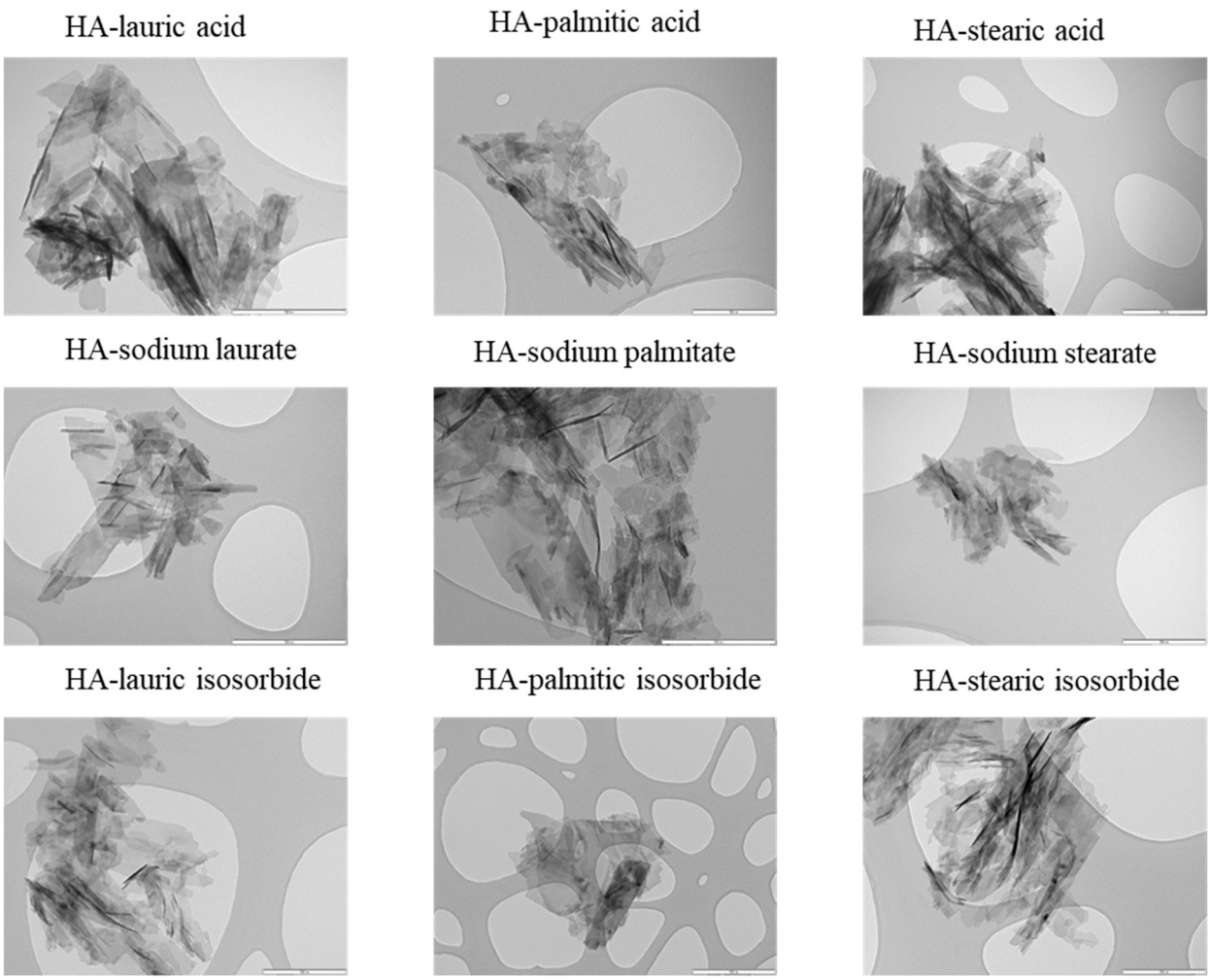


Figure 2.17 TEM images of modified HA. From left to right, top to bottom: HA-lauric acid, HA-palmitic acid, HA-stearic acid, HA-sodium laurate, HA-sodium palmitate, HA-sodium stearate, HA-lauric isosorbide, HA-palmitic isosorbide and HA-stearic isosorbide.

2.5 Conclusions

Previous work reported the first successful single step, continuous flow synthesis of surface modified HA plates using DDSA.[23] This chapter has expanded on the range of dispersants capable of modifying the surface properties of HA NP's. A selection of the modified HA NP's of varying chain lengths and functional head groups were successfully re-dispersed in toluene enabling an EE value to be determined. The successful synthesis of the modified NP's was found to be sensitive to both the chain length of the dispersant tail group, dispersant morphology and the composition of the functional head group. The most

favourable results were achieved with longer chain lengths for the carboxylic acid and sodium salts whilst the isosorbide head group performed better with shorter chain lengths. Overall the isosorbide based hydrocarbon dispersants performed most efficiently in terms of both the levels of coating and the stability achieved. It is considered that both the confined arrangement of oxygen atoms in the bicyclic isosorbide heterocycle as well as its contribution to the overall steric hindrance of this dispersant were responsible for its enhanced performance. Whilst the majority of dispersants in this study were capable of altering the structure of the HA surface they do not appear to significantly change the overall morphology or crystallinity of the HA NP's.

2.6 References

1. M. Descamps, J. C. Hornez and A. Leriche, *Journal of the European Ceramic Society*, 2009, **29**, 369-375.
2. M. Vallet-Regi, *Journal of the Chemical Society-Dalton Transactions*, 2001, DOI: 10.1039/b007852m, 97-108.
3. W. J. E. M. Habraken, J. G. C. Wolke and J. A. Jansen, *Advanced Drug Delivery Reviews*, 2007, **59**, 234-248.
4. M. Wang, *Biomaterials*, 2003, **24**, 2133-2151.
5. D. R. Sumner and J. O. Galante, *Clinical Orthopaedics and Related Research*, 1992, 202-212.
6. R. Huiskes, H. Weinans and B. Vanrietbergen, *Clinical Orthopaedics and Related Research*, 1992, 124-134.
7. K. G. Marra, J. W. Szem, P. N. Kumta, P. A. DiMilla and L. E. Weiss, *Journal of Biomedical Materials Research*, 1999, **47**, 324-335.
8. S. C. Rizzi, D. T. Heath, A. G. A. Coombes, N. Bock, M. Textor and S. Downes, *Journal of Biomedical Materials Research*, 2001, **55**, 475-486.
9. L. A. Cyster, D. M. Grant, S. M. Howdle, F. Rose, D. J. Irvine, D. Freeman, C. A. Scotchford and K. M. Shakesheff, *Biomaterials*, 2005, **26**, 697-702.
10. J. Russias, E. Saiz, R. K. Nalla, K. Gryn, R. O. Ritchie and A. P. Tomsia, *Materials Science & Engineering C-Biomimetic and Supramolecular Systems*, 2006, **26**, 1289-1295.
11. N. Demirkol, F. N. Oktar and E. S. Kayali, in *Bioceramics, Vol 25*, eds. I. Antoniac, S. Cavalu and T. Traistaru, 2014, vol. 587, pp. 147-153.
12. G. S. Khelendra Agrawal, Devendra Puri, Satya Prakash, *Journal of Minerals & Materials Characterization & Engineering*, 2011, **10**, 727-734.
13. E. Lester, S. V. Y. Tang, A. Khlobystov, V. L. Rose, L. Buttery and C. J. Roberts, *CrystEngComm*, 2013, **15**, 3256-3260.

14. S. H. Othman, S. A. Rashid, T. I. M. Ghazi and N. Abdullah, *Journal of Nanomaterials*, 2012, DOI: 10.1155/2012/718214.
15. L. Zhou, H. Zhang, H. Zhang and Z. Zhang, *Particuology*, 2013, **11**, 441-447.
16. C. Albano, G. González, J. Palacios, A. Karam and M. Covis, *Polymer Composites*, 2013, **34**, 1433-1442.
17. M. Supova, *Journal of Materials Science-Materials in Medicine*, 2009, **20**, 1201-1213.
18. Y. Li and W. Weng, *Journal of Materials Science-Materials in Medicine*, 2008, **19**, 19-25.
19. N. C. Bleach, S. N. Nazhat, K. E. Tanner, M. Kellomaki and P. Tormala, *Biomaterials*, 2002, **23**, 1579-1585.
20. L. Borum and O. C. Wilson, *Biomaterials*, 2003, **24**, 3681-3688.
21. H. W. Choi, H. J. Lee, K. J. Kim, H. M. Kim and S. C. Lee, *Journal of Colloid and Interface Science*, 2006, **304**, 277-281.
22. H. Tanaka, T. Watanabe, M. Chikazawa, K. Kandori and T. Ishikawa, *Journal of Colloid and Interface Science*, 1999, **214**, 31-37.
23. L. Borum-Nicholas and O. C. Wilson, *Biomaterials*, 2003, **24**, 3671-3679.
24. M. Gimeno-Fabra, F. Hild, P. W. Dunne, K. Walton, D. M. Grant, D. J. Irvine and E. H. Lester, *Crystengcomm*, 2015, **17**, 6175-6182.
25. E. H. Lester and B. J. Azzopardi, *Journal*, 2005.
26. G. Fleche and M. Huchette, *Starch-Starke*, 1986, **38**, 26-30.
27. A. J. Parrott, R. A. Bourne, P. N. Gooden, H. S. Bevinakatti, M. Poliakoff and D. J. Irvine, *Organic Process Research & Development*, 2010, **14**, 1428-1434.
28. D. A. Atwood, *Sustainable Inorganic Chemistry*, Wiley, 2016.
29. D. Horton, *Advances in Carbohydrate Chemistry and Biochemistry*, Elsevier Science, 1992.
30. N. El Boulifi, J. Aracil and M. Martinez, *Bioresource Technology*, 2010, **101**, 8520-8525.
31. R. U. Lemieux and A. G. McInnes, *Canadian Journal of Chemistry-Revue Canadienne De Chimie*, 1960, **38**, 136-140.
32. L. W. Du, S. Bian, B. D. Gou, Y. Jiang, J. Huang, Y. X. Gao, Y. D. Zhao, W. Wen, T. L. Zhang and K. Wang, *Crystal Growth & Design*, 2013, **13**, 3103-3109.
33. R. D. Shannon, *Acta Crystallographica Section A*, 1976, **32**, 751-767.
34. M. G. Clerici, *Applied Catalysis*, 1991, **68**, 249-261.
35. A. Rimola, Y. Sakhno, L. Bertinetti, M. Lelli, G. Martra and P. Ugliengo, *Journal of Physical Chemistry Letters*, 2011, **2**, 1390-1394.
36. C. J. Liao, F. H. Lin, K. S. Chen and J. S. Sun, *Biomaterials*, 1999, **20**, 1807-1813.
37. M. Ashok, N. M. Sundaram and S. N. Kalkura, *Materials Letters*, 2003, **57**, 2066-2070.
38. K. Buszello, S. Harnisch, R. H. Muller and B. W. Muller, *European Journal of Pharmaceutics and Biopharmaceutics*, 2000, **49**, 143-149.
39. P. Khuwijitjaru, S. Adachi and R. Matsuno, *Bioscience Biotechnology and Biochemistry*, 2002, **66**, 1723-1726.
40. I. Rehman and W. Bonfield, *Journal of Materials Science-Materials in Medicine*, 1997, **8**, 1-4.
41. G. Socrates, *Infrared and Raman Characteristic Group Frequencies: Tables and Charts*, Wiley, 2004.
42. P. Larkin, *Infrared and Raman Spectroscopy: Principles and Spectral Interpretation*, Elsevier Science, 2011.
43. S. Koutsopoulos, *Journal of Biomedical Materials Research*, 2002, **62**, 600-612.

44. C. Igathinathane, L. O. Pordesimo, E. P. Columbus, W. D. Batchelor and S. R. Methuku, *Computers and Electronics in Agriculture*, 2008, **63**, 168-182.

3 Chapter 3: Continuous Flow, Single Stage Synthesis of Dispersant-Stabilised Hydroxyapatite Platelet Nanoparticles - Polylactic Acid (PLA) Dispersant Optimisation

3.1 Aims and Objectives

This chapter builds upon the work covered in the previous Chapter 2 and expands into the realm of the application of polymer based dispersants, with a key focus on oligomeric polylactic acid (PLA) structures. This polymer was chosen as it is already used in medical applications, has a well-established synthesis route and should exhibit a high affinity towards interacting positively with the matrix polymer (medical grade PLA) in the final composite. The dispersants utilised in this chapter were synthesised using ring opening polymerisation as discussed in detail in Chapter 1. As with the hydrocarbon dispersants both the chain length and functional head groups (initiators) of the PLA were altered to investigate the interactions and establish effective combinations capable of successfully coating the HA surface. All dispersants used in this chapter were introduced in the pre-cursor stream within the hydrothermal process, such that they were present in the reactor as the nanoparticles were formed. The concentration of dispersant was also investigated with the aim of optimising the level of coating and preventing contamination of the final coated nanoparticles (NP) with excess polymer. Any excess of unattached oligomeric PLA could potentially act as a plasticiser in the extrusion process effecting the mechanical properties of the final PLA-hydroxyapatite composite product. The solvent used in the hydrothermal up-flow stream containing the polymeric dispersant was also altered to investigate the robustness of the coating process.

3.2 Introduction

The work throughout this project has been focused on the synthesis of a biocompatible nanocomposite material with aim to produce a strengthened polymer composite that aids

bone regeneration. PLA is an aliphatic biopolymer produced from naturally occurring sources of lactic acid such as corn or rice through bacterial fermentation.[1] It is a thermoplastic capable of producing a rigid material that is bioresobable making it of significant interest to the medical field.[2, 3] The degradation of PLA occurs primarily through the hydrolysis of the ester bonds situated on the polymer backbone with the degradation products consisting of H_2O, CO_2 and lactic acid, all of which are non-toxic and can be processed within the body.[4-6]

Due to PLA's greater thermal processabilty when compared to similar biopolymers a wide range of techniques such as film casting, extrusion and blow moulding can be used to form PLA into various shapes and films.[5, 7] This ease of processing combined with the lactic acid monomer being easily obtainable from inexpensive, renewable starch based materials makes it a highly attractive biopolymer.[8] The mechanical properties of PLA depend on the processing temperature, annealing time and molecular weight.[9] These properties also depend on which lactide isomer (L-lactide and D-lactide) or, indeed, what mixture of isomers are used. In the cases of poly(L-lactic acid) (PLLA) and poly(D-lactic acid) (PDLA), crystalline materials are generates whereas poly(D,L-lactic acid) (PDLLA) is an amorphous material.[5] However, both amorphous and crystalline materials are brittle in nature at room and body temperatures resulting in lowered mechanical strength, toughness and elastic modulus.[9, 10] Our study uses a 50:50 racemic mixture of D and L-lactide to produce PDLLA and will be referred to as 'PLA'.

Hydroxyapatite has excellent biocompatibility and bioactivity but has poor mechanical properties in its bulk form such as low flexural strength and fracture toughness.[11] Previous research into organic-inorganic nanocomposites has been conducted with the intention of producing nanocomposite materials with improved mechanical properties and bioactivity. These composites combine the functionality of the polymer matrix with the

unique properties of the nanoparticles. However, nanoparticles such as the highly surface-charged HA often undergo agglomeration and without being sufficiently dispersed into a polymer matrix will not impart the desired properties into the final composite material.[12] A review of the literature revealed that PLA-HA nanocomposites have been produced successfully by first dispersing the PLA and HA into separate solvents and combining the two solutions under rapid stirring.[10, 13] This method did not involve the grafting of dispersants onto the HA but relied upon the hydrogen bonding interactions between the polymer matrix and the HA surface. Further studies found that by grafting oligomeric PLA onto the surface of the HA an improvement in the mechanical properties of the PLA-HA composites were observed indicating an increase in the level of dispersion of the HA into the polymer matrix.[14] This project aimed to graft our various oligomeric PLA dispersants onto the surface of HA via our high pressure hydrothermal flow process in order to create HA NP's capable of uniformly dispersing into a PLA polymer matrix. Such dispersants would have the ability to interact with both the NP's surface and the PLA matrix preventing agglomeration and increasing dispersion uniformity throughout the matrix.

3.3 Experimental

Materials:

Calcium nitrate tetrahydrate, 3,6-dimethyl-1,4-dioxane-2,5-dione (*rac*-lactide), D-sorbitol and tin(II) 2-ethylhexanoate (tin octoate) were purchased from Sigma-Aldrich. Isosorbide was purchased from Acros Organics. Ammonium phosphate (dibasic), toluene (HPLC grade) and tetrahydrofuran (HPLC grade) were purchased from Fisher Scientific. Sodium hydroxide (pellets), methanol and 2-propanol (IPA) were purchased from VWR Chemicals. All materials were used as received without further purification.

3.3.1 Dispersant Synthesis

Polylactic Acid (PLA) polymerisation:

Rac-lactide and the appropriate initiator (D-sorbitol or sodium hydroxide or isosorbide) in the required molar ratio was placed in a 25 mL two-neck round bottom flask with a magnetic stirrer bar. The flask was sealed with rubber septa and a thermometer was inserted through the side neck. The flask was purged with Ar for several minutes. The sample was inserted into a pre-heated, 180 °C oil bath for isosorbide and D-sorbitol initiated PLA. A temperature of 140 °C was used for sodium hydroxide initiated PLA. A small positive pressure of Ar was kept within the reaction flask via the Schlenk line. A tin catalyst solution was made by adding the required quantity of tin octanoate to toluene. 100 μL of the catalyst solution was then injected and a timer was started. No catalyst solution was injected for sodium initiated PLA. The polymerisations are held at 180 °C or 140 °C for 20 minutes, cooled and the polymer collected without further purification. A summary of the dispersants used can be found in Table 3.1. Further analysis can be found in Appendix 6.2.

Table 3.1 Polymeric dispersant sample abbreviations, molar ratios of reactants and reaction conditions. All reactions were carried out under a Ar atmosphere for 20 minutes.

Dispersant	Initiator	Molar ratio of initiator to monomer (lactide)	Temperature (°C)	Tin catalyst present (50 ppm)
IsPLA (8)	Isosorbide	1:4	180	Yes
IsPLA (16)	Isosorbide	1:8	180	Yes
IsPLA (24)	Isosorbide	1:12	180	Yes
NaPLA (8)	Sodium hydroxide	1:4	140	No
NaPLA (16)	Sodium hydroxide	1:8	140	No
NaPLA (24)	Sodium hydroxide	1:12	140	No
Sorbitol PLA (1000 Da)	D-sorbitol	1:6	180	Yes
Sorbitol PLA (3000 Da)	D-sorbitol	1:20	180	Yes
Sorbitol PLA (6000 Da)	D-sorbitol	1:40	180	Yes

Kinetic Sampling:

Once the temperature of the reaction mixture was at the reaction temperature, a small sample (*ca.* 30 mg) was taken by inserting a spatula into the reaction mixture at various time intervals. The positive pressure aided in degassing the reaction mixture during sampling. The experiments were repeated at various reaction temperatures and reactant compositions.

Nanoparticle Synthesis:

HA NP's were synthesised using the continuous flow hydrothermal reactor developed by Lester and Azzopardi.[15-17] The reactor consists of a concentric pipe-in-pipe arrangement constructed of 316 stainless steel Swagelok® components. The outer tube had a 3/8 inch

outer diameter (wall thickness = 0.065 inch) and the inner tube a 1/8 inch outer diameter (wall thickness = 0.035 inch). This design facilitates a counter-current flow of the two liquids, enabling rapid mixing at the exit point of the internal pipe. The short residence time limits particle growth and degradation of any organic modifiers that may be present. Hot, pressurised ammonium phosphate/water solution was pumped through the inner pipe (down-flow) and an isopropanol solution of metal salt/organic modifier, at room temperature, was pumped through the outer tube (up-flow). The reactant solutions were prepared at ambient temperatures flowing the method detailed below in the General HA NP reagent synthesis section and the streams were flowed counter-currently with the down-flow pumped at a rate of 20 mL min^{-1} and the up-flow at 10 mL min^{-1}. The ammonium phosphate solution was heated to 200–400 °C and maintained at this temperature during the reaction. Pressure through-out the whole system was controlled by use of a manually operated back pressure regulator (BPR.) The final suspension of particles flowed out of the top of the reactor and cooled to room temperature in flow by a water cooler and was collected in a receiver tank. All NP products were centrifuged and washed with distilled water followed by isopropanol. The residual water was removed by freeze drying for 48 hours.

General HA NP reagent synthesis:

The down-flow stream (see definition above) consisted of ammonium phosphate (2.24 g, 0.015 mol) dissolved in deionised water (1 L) which had a pH = 8 and the up-flow stream (see definition above) consisted of mixture of calcium nitrate tetrahydrate (11.8 g, 0.05 mol) and the required dispersant (e.g. for stearic acid 1.42 g, 0.005 mol) dissolved in isopropanol (1 L). The solutions were prepared by premixing the reagents at ambient temperature and sonicating in a Fisherbrand FB11014 sonicator bath until fully dissolved.

3.3.2 Material Characterisation

NMR:

NMR spectra were recorded at 25 °C using a Bruker AV3-400 spectrometer (^{1}H 400 MHz and ^{13}C 100 MHz). Chemical shifts were recorded in δ_H (ppm). Samples were prepared as solutions in $CDCl_3$ or D_2O and chemical shifts were referenced to the appropriate deuterated solvent. Analysis of the spectra was carried out using MestReNova software.

GPC:

Each sample was dissolved in HPLC grade THF, at a concentration of 2 mg/mL, and filtered through a 0.2 µm PTFE syringe filter. GPC analysis was performed on an Agilent 1260 HPLC with an online vacuum degasser, an Agilent online differential refractometer (DRI) and a Wyatt Helios Dawn 8 multiangle light scattering detector (MALLS.) Two Agilent 3 µm PLgel Mixed E columns (7.5 ×300 mm) were connected in series after an Agilent PLgel 3 µm Guard column (7.5 × 50 mm). The column oven, DRI and MALLS temperature was set to 35 °C and the flow rate was set to 1 mL per minute. The sample injection volume was set to 100 µL. The specific refractive index (RI) increment (dn/dc) of L-lactide and poly(L-lactic acid) was set to 0.05 mL/g and the RI calibration constant was set to 1.5712×10^{-9}. MALLS calibration was performed using HPLC grade toluene, filtered through a 0.02 µm PTFE filter and normalisation was performed in THF using a 30 kDa linear polystyrene narrow dispersity GPC calibration standard. Analysis of the spectra was carried out using Astra software.

X-ray diffraction (XRD):

Powder XRD was carried out using a Bruker AXS D8 Advance diffractometer with a Cu Kα radiation (λ = 0.15418 nm) source. The samples were mounted in a poly(methyl methacrylate) (PMMA) sample holder and the range for 2θ was between 15–65°. The

range interval was 0.04° and the dwell time was 5 s. The results were analysed using DIFFRAC.EVA software and compared to the ICDD database.

Transmission electron microscopy (TEM):

TEM imaging was conducted using a FEI Technai 12 BioTwin with an accelerating voltage of 120 kV. The suspension was dropped onto a copper grid. A suspended solution of 0.1mg ml^{-1} of HA sample in toluene was prepared using a Silverson L5M rotor-stator homogeniser and was pipetted onto the copper grid (300 lines per inch) with a holey carbon film where it was allowed to dry in air at ambient temperatures. Excess toluene was then removed by placing the grids onto filter paper.

Electron energy loss spectroscopy (EELS):

EELS was conducted using a TEM 2100 Plus JEOL instrument at 80 kV with an Oxford X-max attachment. Samples were prepared by sonicating a solution of 0.1mg ml^{-1} of the HA sample in water obtained from a Milli-Q Ultrapure Water System for 10 mins. The solution was pipetted onto the copper grid (300 lines per inch) with a holey carbon film where it was allowed to dry in air at ambient temperatures.

Scanning electron microscopy (SEM):

Images were collected by preparing a powder HA sample was spread onto the surface of a double-sided adhesive carbon tape mounted on an aluminium sample holder. The sample was allowed to dry overnight at room temperature. Platinum was vacuum-evaporated onto the sample using a 0.8 kV argon plasma for 150 s using a Polaron SC7640 sputter coater. Images were collected using a JEOL 6400 SEM at an accelerating voltage of 15 kV.

SEM: Energy-dispersive X-ray (EDX):

EDX data was collected using a Quanta 650 SEM with a 150 mm Xmax attachment at 15 kV and a working distance of 10mm. Samples were prepared by dispersing 1-2 mg of the sample in 3-5 mL of water obtained from a Milli-Q Ultrapure Water System using a sonicator bath for 10 minutes. A drop of the dispersed sample was pipetted onto a mica sheet which was adhered to the SEM stub using carbon tape. Care was taken to keep all of the sample droplet on the mica sheet and away from the carbon backing tape. Samples were then coated with a layer of gold via a LEICA EM SCD00S sputter coater at 25 mA for 300 seconds.

Thermal gravimetric analysis (TGA):

TGA data was collected using a TA instruments Q500 TGA with the samples loaded onto platinum pans. The temperature limit was set to 700 °C with a heating ramp rate of 5 °C per minute. A nitrogen atmosphere was maintained at a flow of 20 mL min^{-1}.

Fourier transform infrared spectroscopy (FTIR):

FTIR data was collected using a Bruker ALPHA FTIR with an attenuated total reflectance (ATR) attachment. Each sample was recorded from 4000 – 400 cm^{-1} using 24 scans.

3.4 Results and Discussion

This study expands on the work conducted with hydrocarbon based dispersants in Chapter 2 and moves into the realm of polylactic acid (PLA) based dispersants. In previous work dispersants were added to the up-flow reservoir and where present in the reactor as the nanoparticles formed. Preliminary work carried out by Gimeno-Fabra established that this method of addition was the most efficient.[16] For consistency, this methodology was also employed in this study. The head groups introduced into the PLA dispersants were chosen

from the range that were assessed in our previous study and consisted of two functional groups; carboxylate sodium salt and isosorbide. Acid ended oligomeric PLA was not used as it is prone to rapid hydrolytic degradation through an autocatalytic process, these processes are typically enhanced by increasing amounts of carboxylate acid end groups.[18] This makes acid ended oligomeric PLA difficult to store for any significant periods of time. Furthermore, when the harsh, aqueous based conditions in the hydrothermal synthesis procedure are considered, it was proposed that it would be counterproductive to include a head group known to speed up this unwanted hydrolytic degradation process. Three chain lengths were chosen to be synthesised for this section of the study. This was to allow an investigation into whether similar patterns would be observed with the polymeric dispersants as had been observed in previous studies with the hydrocarbon dispersants, which demonstrated a trend in performance with dispersant structure. Where longer chain lengths and certain head groups exhibited better performance, i.e. with palmitate isosorbide (C16) emerging as the most effective dispersant. The target PLA chain lengths synthesised consisted of 8, 16 and 24 monomer units corresponding to molecular weights of 600 Da, 1200 Da and 1800 Da, respectively (not including the head group). In addition to these linear PLA dispersants, an additional six-armed star polymer morphology, which involved using sorbitol as the multi-functional initiator, was explored. In the case of the star polymer material, as with the linear PLA dispersants, three different arm chain lengths were also trialled. These consisted of 2, 7 and 14 monomer units per arm and translated to overall molecular weights of 1000 Da, 3000 Da and 6000 Da, respectively. However, the required concentration of the polymer in the hydrothermal process up-stream is 0.005 M, it was found to be impossible to introduce this concentration for 6000 Da sorbitol PLA into the stream. This was because the polymer was found to precipitate out of the water/acetone solution and blockages would quickly form within the reactor. It was possible to use this

6000 M star polymer by lowering the concentration to avoid this issue and a maximum concentration of 0.0025 M was viable for this dispersant. Interactions between the head groups and the HA surface are proposed to be very similar to those depicted in Chapter 2. These interactions include electrostatic attraction, hydrogen bonding, covalent bonding and physical entrainment. Pictorial examples of these different interaction modes can be found below in Figure 3.1.

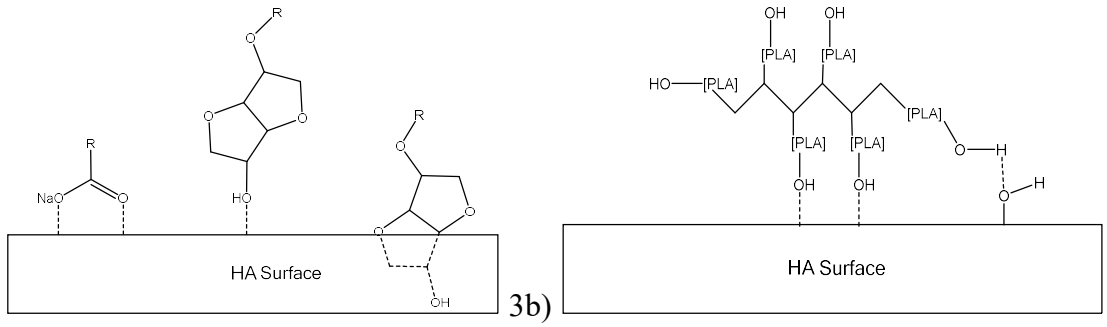


Figure 3.1a and 3.1b. Schematic representation of the potential bonding methods for each head group with the HA surface. 'R' group represents a PLA chain of variable length. From left to right in 1a: PLA-sodium, PLA-isosorbide alcohol group interaction and PLA-isosorbide entrained (one armed isosorbide initiated PLA). 1b shows the interaction mode for the 6-armed star PLA.

The data reported in the previous chapter defined that isosorbide functionalised hydrocarbon products contained a mixture of singly and doubly esterified isosorbide. The data indicated that both of these dispersant molecules were capable of interacting with the HA surface. Therefore, in this chapter, a combination of NMR spectroscopic and GPC analysis was carried out to determine whether the PLA was being initiated from both of the hydroxyl groups of isosorbide during the polymerisation via the coordination-insertion mechanism (described in detail in Chapter 1) and to also fully understand the interactions that could occur with the PLA-Isosorbide and the NP surface. Extensive GPC and NMR analysis on the polymerisation of PLA initiated by isosorbide was conducted with the help

of Dr Alex Ilchev. Figure 3.2 shows the NMR spectrum of isosorbide PLA (IsPLA) at high conversion (87%). The four methylene protons situated on the isosorbide result in a clear, isolated peak at 3.9 ppm and were used to determine the integration values of all other peaks in the spectrum.

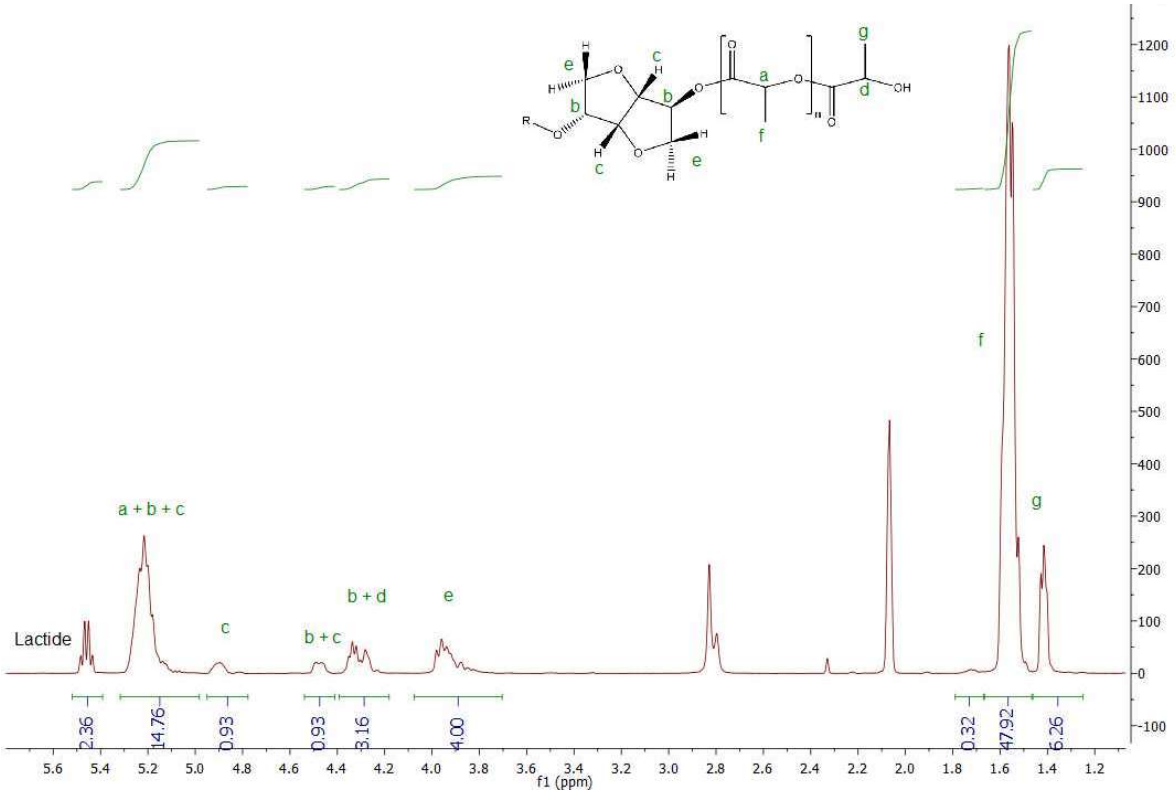


Figure 3.2 ^{1}H NMR spectrum of isosorbide initiated PLA, 1269 Da (20 °C, 400 MHz, $(CD_3)_2CO$). The molecular structure with corresponding labelled peaks is also depicted.

Using these integration values in combination with the correct assignment of each peak, it was possible to determine the level of conversion, the number average molecular weight (M_n) of the polymer, M_n of each arm and consequently the number of arms the polymer contained.[19-21] Table 3.2 summarises the results from both the NMR and GPC analysis at different time intervals during the polymerisation.

Table 3.2 Summary of the GPC and NMR analysis of isosorbide initiated PLA (IsPLA(16)) with 50 ppm catalyst added. Samples were taken at various intervals during the polymerisation.

Sample taken at (minutes):	**Conversion (GPC)**	**Conversion (NMR)**	**M_n (GPC)**	**M_n (NMR)**	**M_n of Arms (NMR)**	**No. of Arms (NMR)**	**No. of Arms (GPC)**
1	0.56	0.56	769	828	402	1.70	1.55
2	0.77	0.74	1050	1084	484	1.94	1.87
4	0.89	0.87	1260	1270	568	1.98	1.96

The data in Table 3.2 showed that both analysis techniques correlate well with each other with no significant deviation in the conversion and M_n values were highlighted. The equations used to determine M_n (NMR) and M_n of Arms (NMR) are shown below as Equations 1 and 2. These two crucial values were then used to determine the number of arms the polymer contained and whether initiation was occurring from both isosorbide hydroxyl groups.

Equation 1 Calculation of Mn (NMR):

$$(\mathbf{f - 3 \times lactide + g - satellite}) \times \frac{\mathbf{72.063}}{\mathbf{3}} + \mathbf{146.14}$$

(f and g represent NMR resonance integrals in Figure 3.2)

The calculation of the M_n (NMR) accounts for the peak at 1.55 ppm, representing the three methyl protons in the polymer chain labelled f in Figure 3.2, containing the methyl protons of any remaining lactide (monomer) in the polymer product. The satellite peak at 1.71 ppm related to the methyl protons on the end group of the polymer chain must also be accounted for (labelled g in Figure 3.2). Using these corrected values, the number of monomer units within the chain can be accurately calculated. Using a combination of how many methyl protons are in the polymer chain and the molecular weight of the monomer units and isosorbide the M_n of the polymer can then be determined.

Equation 2 Calculation of the Mn of Arms (NMR):

$$(\mathbf{f} - \mathbf{3} \times \mathbf{lactide} + \mathbf{g} - \mathbf{satellite}) \times \frac{\mathbf{72.063}}{\mathbf{g} - \mathbf{satellite}}$$

(f and g represent NMR resonance integrals in Figure 3.2)

Equation 3 Calculation of conversion (NMR):

$$\frac{\mathbf{a} + \mathbf{b} + \mathbf{c}}{\mathbf{Lactide} + \mathbf{a} + \mathbf{b} + \mathbf{c}}$$

(a, b and c represent NMR resonance integrals in Figure 3.2)

The calculation for the M_n of Arms (NMR) also utilises the methyl protons contained within the polymer chain to determine the number of monomer units in each arm. The equation deviates from the overall M_n (NMR) equation by using the integral of the end group methyl protons (labelled g in Figure 3.2) and eliminating the molecular weight of the isosorbide group to calculate the molecular weight of just the polymer chain. Should the polymer contain one arm only one set of end group methyl protons would be observed resulting in an integration of 3 for this resonance. For example, the resonance contains a total of 6 protons for the sample taken at 4 minutes indicating that initiation from both hydroxyl groups has occurred creating a two-armed polymer product.

It is interesting to note that at low conversion (<50%) two-armed polymer were not observed. Rather, it is only at higher conversions that the number of arms approaches two which indicates a difference in reactivity between the two isosorbide hydroxyl groups. It was proposed that if both hydroxyl groups reacted equally with the catalyst and monomer the arms would grow at equal rates. These findings agree with previous data related to the hydrocarbon dispersant synthesis, which also suggests a difference in reactivity between these two groups with the endo-hydroxyl being the more reactive of the two. This is discussed in detail in Chapter 2.[22-25]

The synthesis of sodium ended PLA was conducted without the use of the tin octoate catalyst by utilising the anionic ring opening mechanism detailed in Chapter 1. A kinetic study was conducted for all three different chain lengths (8, 16 and 24 monomer units) to establish whether the anionic polymerisation mechanism could produce the required molecular weights with reasonable levels of control i.e. low polydispersity index (PDI). A polymerisation reaction was first conducted at 180 °C to investigate the dynamics of the polymerisation process involving sodium hydroxide. The results are displayed in Table 3.3.

Table 3.3 Summary of the GPC and NMR spectroscopic analysis of sodium hydroxide initiated PLA (NaPLA) at 180°C with samples being taken at various intervals during the polymerisation. The polymer had a target of 16 polymer units (molecular weight target: 1192 Da).

Sample taken at (mins):	**Conversion (GPC)**	**Conversion (NMR)**	**M_n (GPC)**	**M_n (NMR)**	**PDI (GPC)**	**Temperature Change (C°)**
1	0.47	0.75	555	526	1.40	10
2	0.59	0.87	671	781	1.40	5
4	0.57	0.93	671	844	1.40	-1
8	0.65	0.95	730	884	1.60	0
15	0.71	0.95	764	858	1.80	-2

It is interesting to note that the conversion results do not agree between the two analytical techniques. The conversion (NMR) was calculated using Equation 3 which was also used to calculate the conversion (NMR) for the isosorbide PLA kinetic study (Table 3.2). In this polymerisation the conversion results from NMR are over estimating the level of conversion. It is possible that lactic acid dimers may be forming in the anionic ring opening polymerisation process via chain-scission side reactions which could cause a reduction in the level of lactide monomer in the reaction mixture. This would lead to a reduction in the lactide peak in Figure 3.2 and would cause the calculation in Equation 3 to overestimate the conversion. This theory is, in part, supported by the increased PDI values

indicating a wide polymer dispersity and lack of control over the polymerisation process. A significant exotherm was observed within 1 minute of the reaction being initiated. This large exotherm could be playing a role in the lack of control observed during the polymerisation yielding high PDI values and erroneous NMR conversion results. Experiments were subsequently conducted at 140 °C to establish whether this exotherm could be avoided and control over the reaction established. Results for the same polymerisation are seen in Table 3.4.

Table 3.4 Summary of the GPC and NMR analysis of sodium hydroxide initiated PLA (NaPLA) at 140 °C with samples being taken at various intervals during the polymerisation. The polymer had a target of 16 polymer units (molecular weight target: 1192 Da).

Sample taken at (mins):	**Conversion (GPC)**	**Conversion (NMR)**	**M_n (GPC)**	**M_n (NMR)**	**PDI (GPC)**	**Temperature Change (C°)**
1	0.06	0.14	385	171	1.10	0
2	0.11	0.20	359	237	1.20	0
4	0.22	0.32	464	354	1.30	-1
8	0.34	0.54	672	576	1.30	-1
15	0.47	0.75	860	809	1.30	-2

The results shown in Table 3.4 indicate that the large exotherm can be avoided by lowering the reaction temperature and a significant increase in the level of control over the polymerisation is observed in the first 8 minutes of the reaction. The PDI value obtained is lower within this 8 minutes suggesting a decrease in the amount of lactic acid dimers produced. Whilst there is still a disagreement in the conversion results between the two techniques it is primarily seen in the later stages of the reaction. It could be possible that the sodium hydroxide is not only capable of polymerising the lactide monomer but also capable of cleaving the polymer chain to some extent. This side reaction is likely to be more prominent at 180 °C and less so at 140 °C. This cleavage of the chain would lead to the formation of dimers and trimers which could cause the underestimation of conversion

(GPC) should the peaks of these low molecular weight species interfere with the lactide monomer peak. The PDI value, however does not significantly increase as seen in Table 3.3 for the 180 °C polymerisation suggesting that whilst chain cleavage may occur it is not as immediate or as significant at this temperature. Similar studies were carried out for the two other chain lengths (16 and 24 monomer units). Whilst the results and conclusions drawn here are comparable to these higher molecular weight polymers the longest chain length (24 monomer units) required a very large increase in reaction time (60 minutes) to achieve the desired molecular weight.

The synthesis of sorbitol initiated PLA was conducted using the coordination insertion mechanism. The tin octanoate catalyst provided a very good control over the polymerisation producing polymers with a PDI <1.2. Kinetic studies were conducted at 180 °C and targeted two molecular weights 1000 Da and 5000 Da. Three different concentrations of catalysts (40, 60 and 80 ppm) were also investigated at both molecular weights. Analysis was conducted using GPC as the signals in the NMR spectra for this polymer overlapped causing the polymer and initiator peaks to be obscured. The results are presented in Tables 3.5a – 3.5f.

Table 3.5a Summary of the GPC analysis of sorbitol initiated PLA (Sorbitol PLA) using 40 ppm of tin octanoate and targeting a Mn of 1000 Da. Samples were taken at various intervals during the polymerisation. Initiator: monomer ratio was 1:6.

Sample taken at (mins):	**Conversion (GPC)**	**M_n (GPC)**	**PDI (GPC)**
1	0.53	543	1.13
2	0.66	697	1.09
4	0.79	883	1.09
8	0.91	994	1.11
15	0.94	1104	1.10

Table 3.5b. Summary of the GPC analysis of sorbitol initiated PLA using 60 ppm of tin octanoate and targeting a M_n of 1000 Da. Samples were taken at various intervals during the polymerisation. Initiator: monomer ratio was 1:6.

Sample taken at (mins):	Conversion (GPC)	M_n (GPC)	PDI (GPC)
1	0.57	613	1.11
2	0.71	765	1.09
4	0.88	998	1.08
8	0.92	1112	1.09
15	0.97	1137	1.10

Table 3.5c. Summary of the GPC analysis of sorbitol initiated PLA using 80 ppm of tin octanoate and targeting a M_n of 1000 Da. Samples were taken at various intervals during the polymerisation. Initiator: monomer ratio was 1:6.

Sample taken at (mins):	Conversion (GPC)	M_n (GPC)	PDI (GPC)
1	0.58	599	1.12
2	0.71	776	1.08
4	0.86	826	1.30
8	0.95	1091	1.10
15	0.98	1127	1.11

Table 3.5d. Summary of the GPC analysis of sorbitol initiated PLA using 40 ppm of tin octanoate and targeting a M_n of 5000 Da. Samples were taken at various intervals during the polymerisation. Initiator: monomer ratio was 1:34.

Sample taken at (mins):	Conversion (GPC)	M_n (GPC)	PDI (GPC)
1	0.21	905	1.06
2	0.27	1088	1.07
4	0.44	1829	1.08
8	0.80	4179	1.06
15	0.94	5041	1.07

Table 3.5e. Summary of the GPC analysis of sorbitol initiated PLA using 60 ppm of tin octanoate and targeting a M_n of 5000 Da. Samples were taken at various intervals during the polymerisation. Initiator: monomer ratio was 1:34.

Sample taken at (mins):	Conversion (GPC)	M_n (GPC)	PDI (GPC)
1	0.19	775	1.07
2	0.26	820	1.13
4	0.32	1266	1.12
8	0.91	4636	1.06
15	0.96	5032	1.08

Table 3.5f. Summary of the GPC analysis of sorbitol initiated PLA using 80 ppm of tin octanoate and targeting a M_n of 5000 Da. Samples were taken at various intervals during the polymerisation. Initiator: monomer ratio was 1:34.

Sample taken at (mins):	Conversion (GPC)	M_n (GPC)	PDI (GPC)
1	0.32	1890	1.05
2	0.65	3165	1.06
4	0.92	4735	1.08
8	0.96	4859	1.09
15	0.97	5029	1.09

The results show that high conversions (>79%) are seen after 4 minutes for all catalyst concentrations at a target molecular weight of 1000 Da. After 15 minutes, the target M_n is not significantly exceeded and the PDI remains >1.2 indicating a large degree of control over the polymerisation process. For the 5000 Da sorbitol initiated PLA differences in the rate of the reaction are observed according to the catalyst concentration. At 40 ppm catalyst concentration 8 minutes is required to reach conversions of 80% and 15 minutes is needed for >90%. At 60 ppm of catalyst 8 minutes is required to achieve conversions >90%, using 80 ppm of catalyst solution only 4 minutes is needed to reach >90% conversion. It also worth noting that for the 5000 Da sorbitol PLA polymers a significant jump in conversion levels is seen between 4-8 minutes for 40 ppm and 60 ppm catalytic concentrations and between 1-2 minutes for 80 ppm. These jumps in conversion appear to coincide with a M_n >1000 Da being reached and could indicate a phase separation phenomenon between the sorbitol and lactide, were these reactants are not very miscible at the start of the polymerisation. As the sorbitol initiator is consumed the reaction mixture becomes homogenous. Once a molecular weight of approximately 1000 Da is reached it is possible that the growing polymer chains become more miscible with the molten lactide in the melt mixture causing a substantial increase in the rate of chain growth.

To fully understand the surface interactions between the NP and dispersant it is necessary to consider the properties of the PLA chain and its potential to interact with the HA

surface. Figure 3.3 depicts a PLA chain initiated with the isosorbide functional group in a minimised energy configuration. The MM2 force field calculation for determining the molecular mechanics of small organic molecules was used to predict the molecular structure seen in Figure 3.3.[26] Lone pairs of electrons along the chain have been indicated.

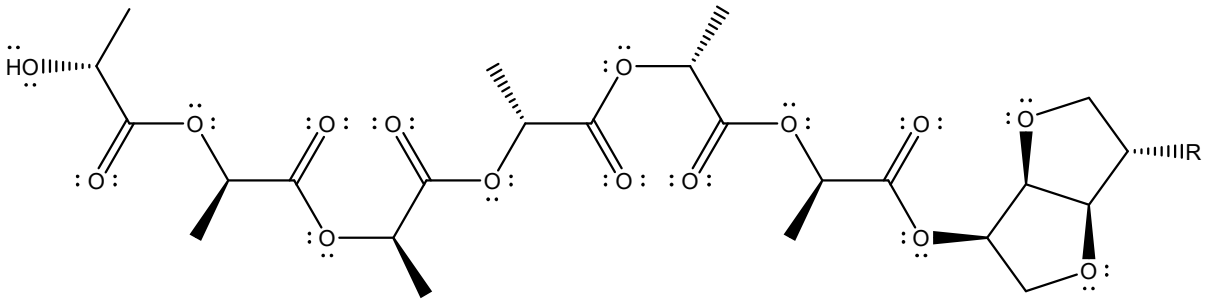


Figure 3.3. Molecular diagram of the PLA chain ended with the isosorbide head group in its lowest energy configuration using a MM2 energy minimisation calculation. R represents another PLA chain initiated from the second isosorbide hydroxyl group.

It is clear from Figure 3.3 that the chemistry of the PLA chain is very different to that of the hydrocarbon chain. With the latter, it was concluded that no potential interaction points with the HA surface were available and that the hydrocarbon chain could be considered an unreactive part of the dispersant molecule in terms of surface interactions with the NP's. The PLA chain, however has multiple lone pairs of electrons that could potentially interact with the positively charged Ca^{2+} ions found on the HA surface leading to a number of potential stearic conformations.[27] Taking this theory into account Figure 3.4 shows a simple diagram of the possible steric conformations that may be formed by the linear (3.4a) and two-armed (3.4b) PLA dispersants on the NP surface.

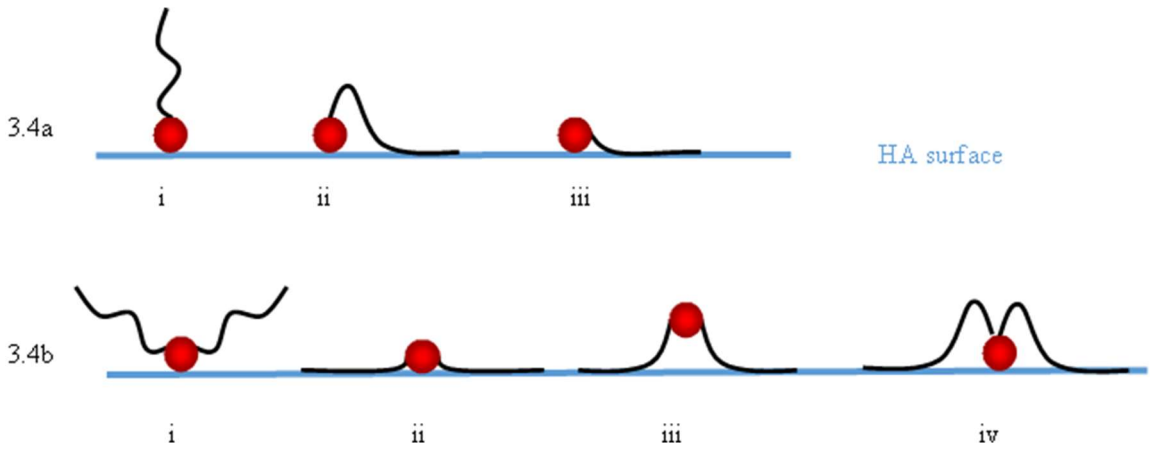


Figure 3.4a. Basic representation of the possible steric conformations linear dispersants can form on the surface of HA. 3.4b. basic representation of the steric conformations of two armed linear dispersants on the HA surface. Red spheres represent the head groups/initiator and the black lines the PLA chain.

Thus, when the conformations of linear PLA dispersants are considered the primary interactions are not limited to the head group and it is probable that the dispersant is interacting through the polymer chain. The data reported by Rimola *et al.* [27] has been discussed in the previous chapter (Chapter 2), which suggested that interactions can occur between electron lone pairs of nitrogen atoms (which can be likened to the lone pairs of oxygen atoms) and the Ca^{2+} ions on the HA surface.[27] Therefore, it is possible that the PLA chain in the dispersant molecule will attempt to lie flat on the surface of HA to maximise these surface interactions decreasing the probability of conformations (i) in both 4a and 4b taking place.

When considering the PLA dispersants which have a sodium salt head group the ionic charges in the highly polar head group will interact with the ions on the HA surface. The isosorbide head group with its lone pairs of electrons is also likely to favourably interact with the HA NP surface making the 4b (iii) conformation unlikely. It is important to discuss the flexibility of the PLA chain when considering possible surface interactions and whether this could influence the preferred stearic conformation. Previous research suggests

that the PLA chain backbone is stiff in nature and not prone to flexibility often producing a brittle polymer product.[28-31] Taking this into consideration the PLA chain may prefer to lie completely flat on the surface, where possible, to avoid any drastic bending/strain of the aliphatic polymer chain. This makes the conformation seen in Figure 3.4a (ii), where the PLA chain bends, less likely to occur when compared to the flat lying conformation on Figure 3.4a(iii). The hypothesis also served to narrow down the most probable steric conformation of the two-armed linear dispersants to the representation seen in 4b (ii) depicting the dispersant lying almost completely flat on the HA surface. The conformation seen in 3.4b (iv) may occur should the steric conformation of the polymer chain prevent the dispersant from lying completely flat. This may be the case for two armed dispersants due to bond angles and increased steric bulk of the molecule. Also, as discussed in the previous chapter (Chapter 2) interactions could occur between the isosorbide head group and the NP surface. Two possible types of interactions were discussed and involved the lone pairs of electrons situated on the oxygen atoms in the head group and the Ca^{2+} fitting into the cavity created by the same oxygen atoms. Both interactions can occur in the isosorbide initiated PLA based dispersants. However, linking back to the discussion above, the inflexibility of the polymer chain may cause significant steric hindrance at longer chain lengths. The longer PLA chains would decrease the likelihood of the cavity situated within the isosorbide being able to successfully interact with the Ca^{2+} surface ion without significant steric hindrance.

By comparison, it was proposed that branched dispersants are more likely to rely on a combination of interactions from the chain and the hydroxyl polymer end groups as the initiator (sorbitol) will be significantly hindered in encountering the surface of the HA by the six polymer chain branches. [37] This dispersant structure means that it can potentially form multiple anchor points onto the HA surface. However, the alcohol hydroxyl groups

found on the end of the PLA chain were not thought the be significantly surface interactive when compared to the charged sodium salt ended PLA and the lone pair containing isosorbide groups. The steric hindrance of six chains within close proximity to each other may also hamper any chain-surface interactions especially when the inflexibility of the polymer chain is considered (discussed above). Shorter chain lengths could prevent all of the hydroxyl end groups forming anchor points to the HA surface. It is expected that an optimal chain length must be achieved to maximise coating level and interaction for this particular dispersant morphology and this factor is discussed in further detail in this chapter.

When considering the stabilisation mechanism of nanoparticles in solutions, research reveals that long-distance interactions are controlled by Brownian motion, gravitational forces and buoyancy.[32] Meanwhile, short range interactions are proposed to be dominated by NP surface charge. According to Einstein's law of diffusion and Stokes law (Equation 4 and 5) the way the NP's will move through a liquid medium will be affected by numerous system conditions, with the most significant being temperature, viscosity and particle size. The highest diffusion coefficients will derive from high temperatures, small particle sizes and low viscosity. It must also be noted that viscosity decreases upon increasing temperature due to the increase in particle velocity. In this project processing of the final composite involves the addition of the coated NP's to matrix polymer in the melt phase via an extruder at high temperatures (220 °C). Therefore, we can establish that the temperature is high, the viscosity relatively low and our particle size small equating to a high diffusion coefficient and an increase the likelihood of NP collisions. However, the viscosity of a material within the extrusion process is subject to many other factors including shear stress and shear rate.[33]

Equation 4 Einstein's law of diffusion:

$$\mathbf{Df = kT}$$

where D = diffusion coefficient, *f* = the frictional coefficient of the particle, k = Boltzmann constant and T = temperature.

Equation 5 Stokes law:

$$\mathbf{f = 6\pi\eta a}$$

where f = frictional force, η = viscosity and a = particle radius.

Due to increasing particle collisions, the rate of aggregation of the NP's would be predicted to increase requiring the NP surface charge to become a significant factor in the systems performance. As HA has a highly-charged surface, collisions would be predicted to have a significantly high chance of resulting in the successful formation of strong interactions, creating the unwanted aggregation of the NP's. Christian *at al.* [32] reveals two primary ways of creating steric barriers between NP's and thus avoiding strong surface interactions: the creation of a charged ionic barrier such as those often used in aqueous based colloidal solutions and the creation of a steric barrier using dispersants (often polymer based).[32] Creation of the latter (the strategy used in this study to prevent aggregation) is demonstrated in Figure 3.5 and requires the NP surface to be completely covered by the chosen dispersant to form an effective steric barrier.

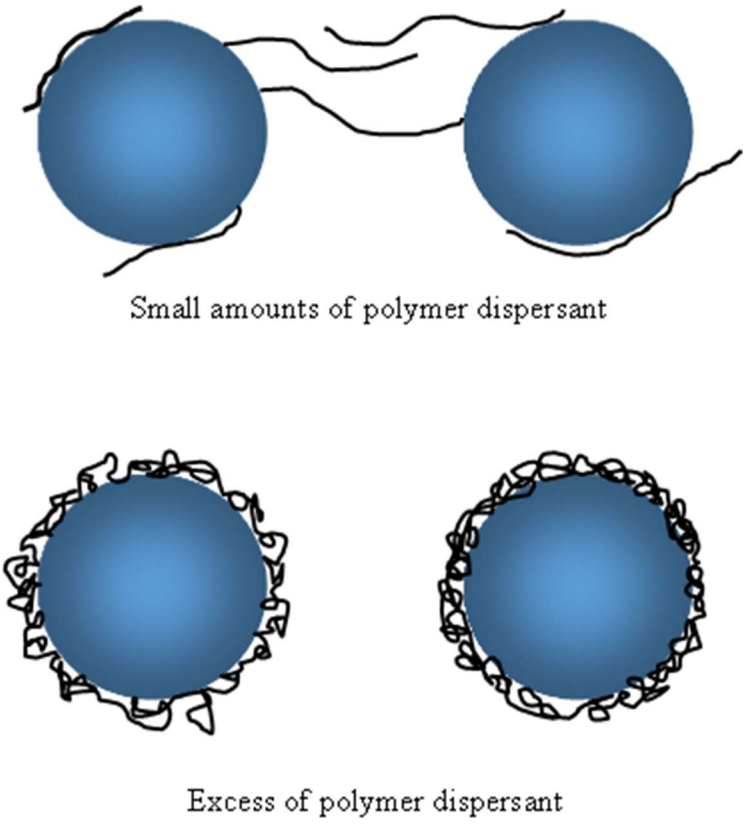


Figure 3.5. Top: mall amounts of dispersant (black lines) creating bridges between the NP's (blue spheres). Bottom: Excess of polymer fully coating the NP surface to create a steric barrier.[34]

It is important that the dispersant is in some part capable of favourably interacting with the "solution" medium or dispersing phase (in our case the PLA matrix) to increase the NP's stabilisation. Figure 3.5 shows the difference between small amounts of polymer dispersants and excess polymer dispersant with the former creating links between NP's and potentially increasing the rate of aggregation. This would see polymer-polymer interactions/entanglements in the coating layer becoming the driving force for aggregation rather than NP surface interactions.

The latter (excess amounts of polymeric dispersant) creates a steric barrier that operates on entropic and osmotic contributions to successfully repel another coated NP. With entropic

contributions relating to volume and configuration restrictions between the two particles. Osmotic contributions are reflected in an increase in the concertation of polymer in the region between the NP's. Both effects act together to create a significant repulsion factor.[34] As previously mentioned an excess of polymeric dispersant can lead to issues within the extrusion process especially if not all the dispersant molecules are properly adsorbed onto the HA NP surface. Taking this into consideration this study also aimed to investigate varying concentrations of dispersants in the up-flow stream of the reactor to find the optimal level of coating.

TGA results for IsPLA at varying chain lengths are shown in Figure 3.6. Degradation temperature is similar for all lengths of dispersant however, an increase in degradation temperature of approximately 120 °C was observed when the dispersants are adsorbed onto the HA surface as a coating. This could indicate a stabilisation of the dispersant molecules via interaction with the NP surface leading to an increased thermal stability. At lower temperatures, the degradation mechanism of PLA involves a chain end located and backbiting reactions, the former with other species such as water whilst the latter are with the chain ester groups and the OH chain end group. Therefore, if the chain and/or head group are adsorbed onto the HA surface this mechanism could require higher temperatures to initiate as the movement of the PLA chains is restricted by their interactions with the HA.[35] Additionally, the shortest chain length of the IsPLA dispersants does not appear to perform as well as the longer lengths suggesting that the chain does indeed play a crucial role in dispersant-NP interactions.

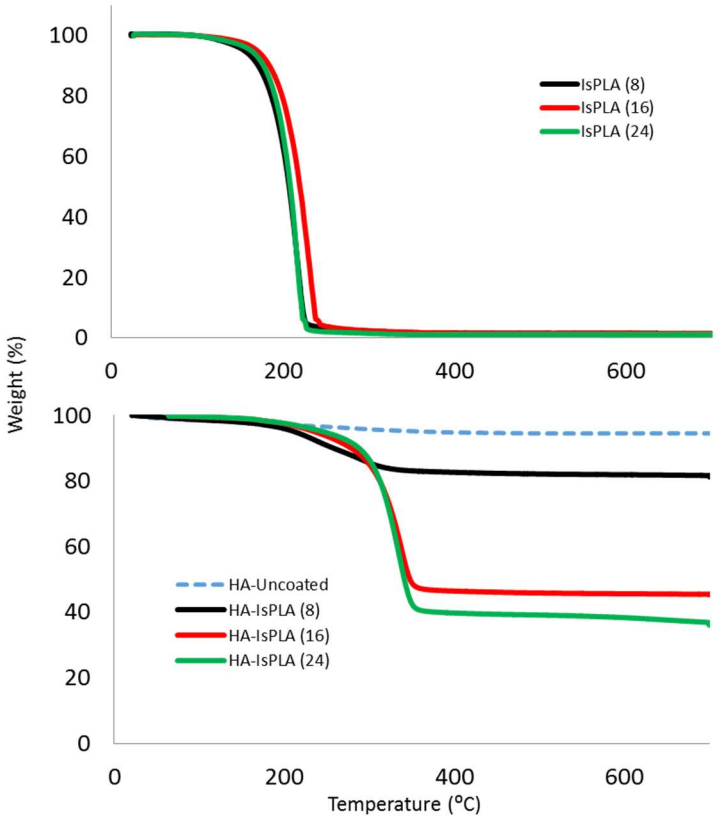


Figure 3.6 TGA plots of total recorded mass loss (weight %) *vs.* temperature for the IsPLA dispersants (top graph) and IsPLA (0.005M) coated NP's (bottom).

The increases in degradation stability can be more clearly defined when the derivative weight % is plotted against temperature as shown in Figure 3.7.

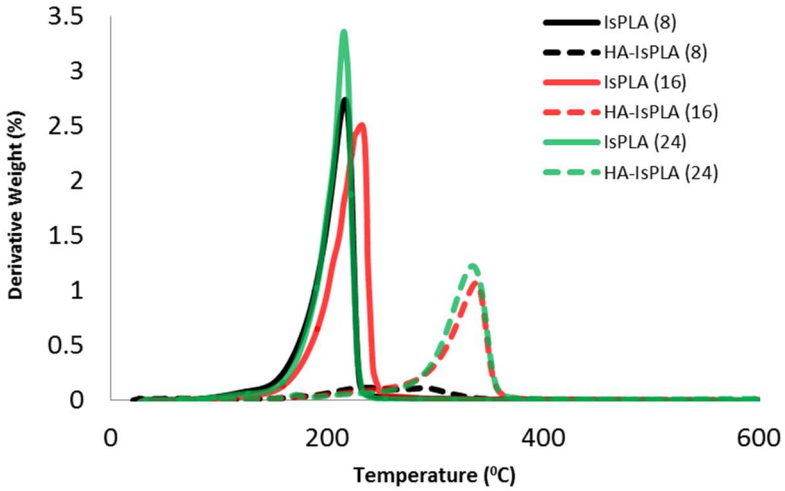


Figure 3.7. TGA plot of total recorded mass loss as a derivative of weight%/temperature vs temperature for the IsPLA dispersants and IsPLA (0.005M) coated NP's.

The poor performance of the shortest chain length PLA material was also more apparent with a sizable portion of the coating degradation occurring at a lower temperature and over a wider range of temperatures. The dispersants with longer chains have sharper degradation profiles occurring at an increased temperature. The lower level of weight loss in the HA sample coated with the shortest chain length indicted that there was a low level of coating coverage achieved with this dispersant. The proposed reasons for this will be discussed later.

TGA results for NaPLA dispersants at varying chain lengths are displayed in Figure 3.8.

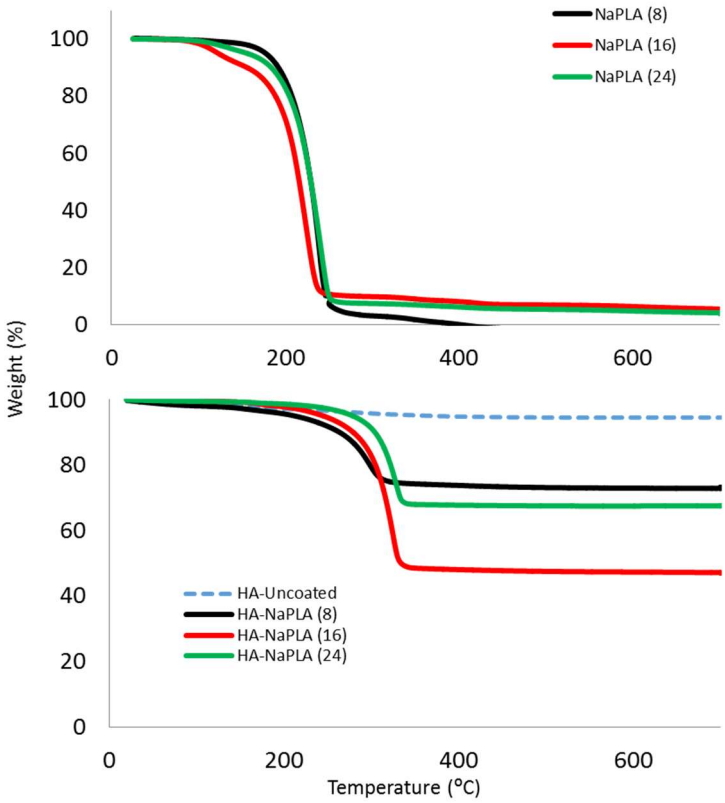


Figure 3.8. TGA plots of total recorded mass loss (weight %) vs. temperature for the NaPLA dispersants (top graph) and NaPLA (0.005M) coated NP's (bottom).

As in the case of the IsPLA dispersants, the degradation temperature is similar for all chain lengths and an increase in degradation temperature of approximately 95 °C was observed when the dispersants are adsorbed onto the HA surface indicating an increased

stabilisation of the dispersant molecules. Again, the shortest chain length dispersant, NaPLA (8), does not appear perform as well as the longer lengths but does perform better in comparison to IsPLA (8). Not only does this dispersant coat the HA to a higher degree than IsPLA (8) but it also degrades at similar temperatures to the longer lengths of NaPLA dispersants once coated onto the NP surface, unlike its IsPLA counterpart. This may indicate that the interactions between the HA surface and NaPLA differ in some respects to the interactions occurring between IsPLA and HA. The sodium salt head group is highly charged and in theory could form ionic bonds with the ions on the NP surface. These bonds would be stronger than the intermolecular bonds (dipole-dipole and hydrogen bonding) that the isosorbide head group could form.[36] The increase in stability was clearly observed in Figure 3.9 which plots the derivative weight % and when compared to Figure 3.7 the onset of degradation of the dispersants is on average 18 °C higher which is indicative of a more stable head group. However, this increased thermal stability of the dispersant was not reflected in an increase in degradation temperature of the coated HA counterparts. When HA-IsPLA (16) and HA-IsPLA (24) were compared to HA-NaPLA (16) and HA-NaPLA (24) they were found to degrade approximately 13 °C higher.

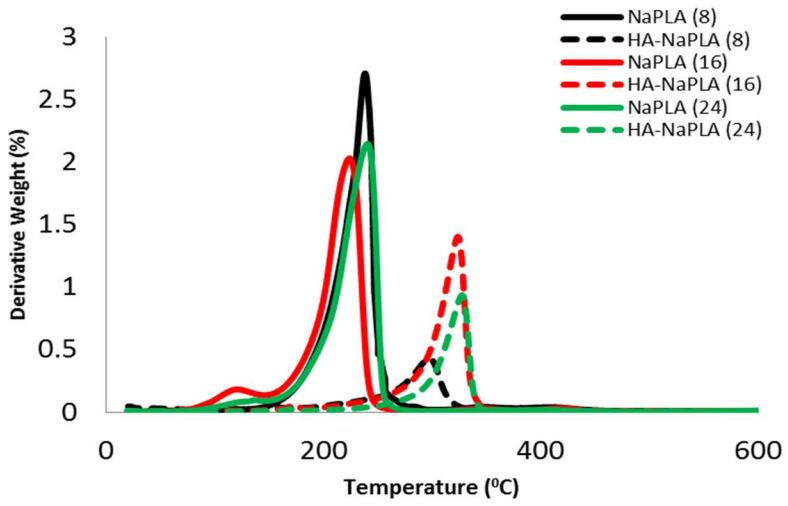


Figure 3.9. TGA plot of total recorded mass loss as a derivative of weight%/temperature *vs.* temperature for the NaPLA dispersants and NaPLA (0.005M) coated NP's.

Figure 3.10 depicts the TGA results of two branched sorbitol PLA dispersants. It was immediately clear that the lowest chain length (1000 Da) did not significantly coat the NP surface whereas the longer chain length of 3000 Da performed well.

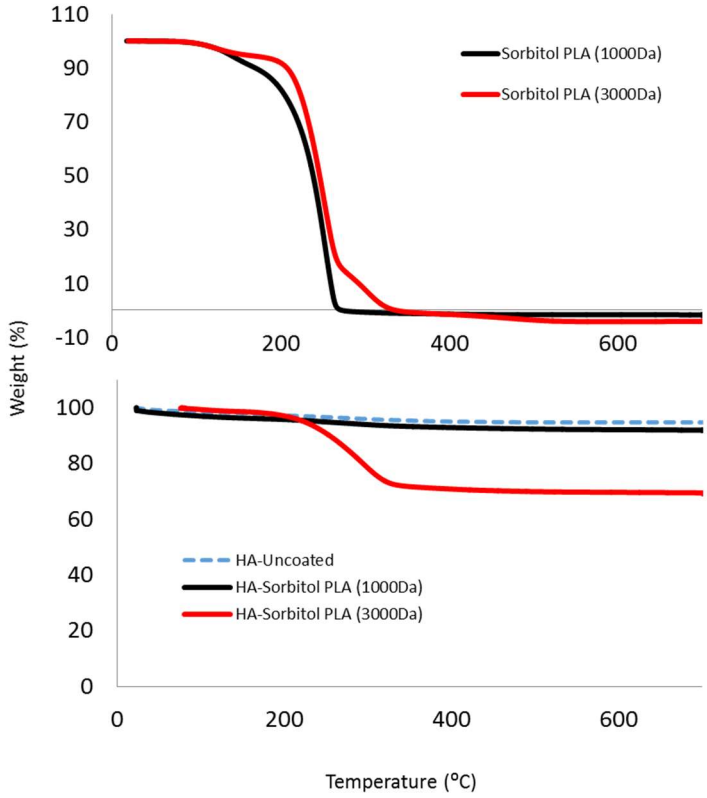


Figure 3.10. TGA plots of total recorded mass loss (weight %) *vs.* temperature for the sorbitol PLA (1000DA) and sorbitol PLA (3000Da) dispersants (top graph) and sorbitol PLA (0.005M) coated NP's (bottom).

As discussed previously the chain length of the branched dispersants are likely to play a key role in their ability to form interactions with the HA surface. A simple diagram representing possible interactions of the branched dispersants with the surface is shown in Figure 3.11. With the difference between these two dispersants being the length of the PLA chains it could be suggested that the shorter chain branched PLA dispersant is unable to form as many surface anchor points due to steric conformation and a severe lack of flexibility in the PLA chain. Longer chains may be able to flex enough to form more anchor points and establish a more stable connection to the surface. Previous research

conducted by Goddard *et al.* [37] suggests that at low molecular weights (<1000 Da) not all hydroxyl groups are able to initiate polymer growth. This work indicated that at a molecular weight of 1000 Da we will only see an average of four branches not six. Therefore, it is possible that there are also physically less anchor points with our lowest molecular weight branched polymer.[37]

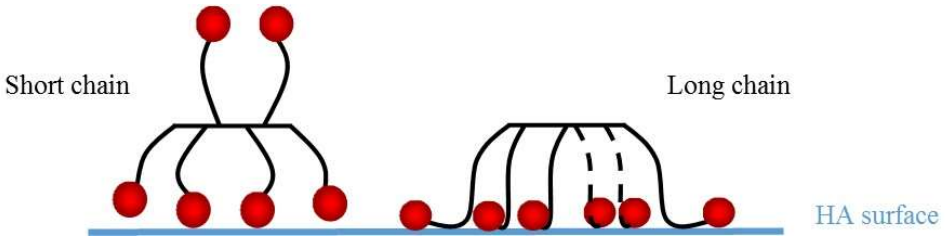


Figure 3.11. Basic representation of the possible steric conformations branched dispersants can form on the surface of HA. Black lines represent polymer chains with dashed lines representing chains going into the plane of the paper. Red spheres represent the alcohol hydroxyl chain end group.

Figure 3.12 plots the derivative weight % of both the branched polymers (Sorbitol 1000 Da and 3000 Da) along with the coated HA counterparts.

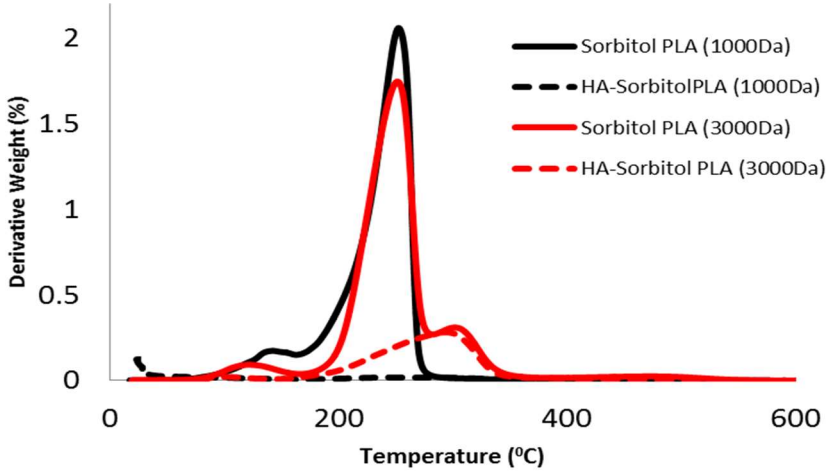


Figure 3.12. TGA plot of total recorded mass loss as a derivative of weight%/temperature *vs*. temperature for the sorbitol PLA (1000 Da) and sorbitol PLA (3000 Da) dispersants and sorbitol PLA coated NP's.

No significant weight loss was observed for the HA coated with the shorter 1000 Da branched polymer and supports the conclusions drawn above. The 3000 Da dispersant performed well with the degradation temperature increasing for the dispersant coating when compared to the pure polymer sample. However, this degradation peak is broad and occurs over a wide range of temperatures and is unlike the previous degradation profiles for the linear dispersants, which give sharp narrow losses at a temperature higher than their pure polymer counterparts. This result points to a lack of thermal stability for a portion of the sorbitol PLA (3000 Da) coating with portions of the dispersant degrading faster than others. It is possible that not all polymeric molecules were able to pack as closely together on the surface due to the steric hindrance of the six PLA chains and therefore, could not form multiple surface attachment points via the OH chain end group.

A breakdown of the TGA analysis for temperatures <400 °C can be found in Table 3.6 for the dispersants found in Figures 3.6-3.12.

Table 3.6 Weight losses in varying temperature regions TGA for the dispersant modified HA.

Nanoparticle (Polymer Chain Length in Monomer Units or M_w in Da)	**Total Weight Loss (%)**	**Total Weight Loss (mol of dispersant)**	**Weight Loss <150 °C**	**Weight Loss 150-200 °C**	**Weight Loss 200-400 °C**
HA- IsPLA (8)	18.63	4.94×10^{-7}	2.08	1.98	13.28
HA- IsPLA (16)	54.63	1.49×10^{-6}	0.99	1.57	51.01
HA- IsPLA (24)	63.78	1.61×10^{-6}	0.91	1.48	57.87
HA- NaPLA (8)	26.78	1.55×10^{-6}	2.70	1.67	21.85
HA- NaPLA (16)	52.94	3.36×10^{-6}	0.79	1.45	49.73
HA- NaPLA (24)	32.42	1.45×10^{-6}	0.77	0.59	30.89
HA- SorbitolPLA (1000Da)	8.15	4.79×10^{-7}	3.78	0.51	2.89
HA- SorbitolPLA (3000Da)	30.79	1.58×10^{-6}	1.49	1.53	26.23
HA - Uncoated	5.34	-	1.99	0.84	2.24

These weight losses are primarily attributed to a combination of surface water and dispersant present in the sample. TGA results indicated that uncoated HA was found to contain approximately 2% surface water with only the HA-SorbitolPLA (1000 Da) sample showing a higher weight % loss within the <150 °C region. Weight loss in the region of 150-200 °C was related to the loss of entrained water in the HA structure and loosely bound dispersant molecules.[38] The TGA analysis performed in this study found that uncoated HA lost a total of 5.34% which can be assigned to water and other surface contaminants related to synthesis and storage procedures. As discovered in the previous chapter detailing the results of the hydrocarbon based dispersants, both the head group and polymer chain length appear to play a role in the level of coating found on the NP surface. For both the isosorbide initiated PLA and the branched sorbitol initiated PLA the shortest chain length had the lowest % weight loss. With a higher portion of the total weight loss observed for SorbitolPLA (1000 Da) occurring at the lower temperature ranges. For IsPLA (8) a large portion of the weight loss was observed at the higher temperature band (200-400 °C) suggesting that a stronger surface interaction had been formed. By cross-referencing this data with the potential modes of attachment presented in Figures 3.4 and 3.11, it is possible to speculate on why the linear chain dispersant could be forming a more stable interaction. In this chapter the potential chain-NP surface interactions have been discussed it was proposed that, not only would it be possible for the chain to form intermolecular interactions with the NP, but that it is very likely that it will do so given the high surface charge of the HA and the lone pair electrons situated along the PLA chain. Figure 3.11 demonstrates Sorbitol PLA (1000 Da) dispersant's inability to adhere effectively to the HA due to the branched structure resulting in a portion of the polymer chain being hindered from reaching the surface due to the steric position of the end groups. Thus, this more highly branched structure would be very unlikely to form as significant

levels of polymer chain: surface interactions. However, Figure 3.4 indicates the strong likelihood of the linear dispersant forming chain-surface intermolecular bonds regardless of chain length. This hypothesis was supported by the TGA data shown above with all linear dispersants capable of coating the NP surface to a larger extent than Sorbitol PLA (1000 Da). Furthermore, a more significant percentage of the linear dispersants distribution of weight loss falls within the higher temperature region of 200-400 °C indicating an increased thermal stability. Upon extension of the branched chains a significant increase in the ability to coat the HA is observed. Sorbitol PLA (3000 Da) performs well and suggests that the longer chain length has enabled an increase in the number of anchor points formed *via* the chain end hydroxyl groups (Figure 3.11). Due to the rigidity of the PLA chain (discussed previously) it is proposed that the longer chained branched polymer may still be unable to form chain-surface interactions to the full extent that the linear species can.

IsPLA (16) and IsPLA (24) have similar weight loss % implying that once a certain chain length is surpassed within the structure of the two-armed linear dispersants the surface interactions formed are quite stable with the longer lengths only capable of small increases in coating levels. It was observed that NaPLA dispersants resulted in significant levels of coatings being deposited on the surface to HA over all chain lengths investigated, but with NaPLA (16) giving the highest weight loss % observed for all dispersants in Table 3.6. This result differs from the pattern observed with IsPLA in terms of the range and may be due to two major differences. IsPLA is a two-armed linear dispersant whereas the NaPLA is one-armed. Furthermore, the head groups vary considerably from each other in terms of both steric nature and reactivity. Both factors could affect the way the two dispersants interact with the surface. However, it was interesting to note that both optimum coatings included the 16 chain length species.

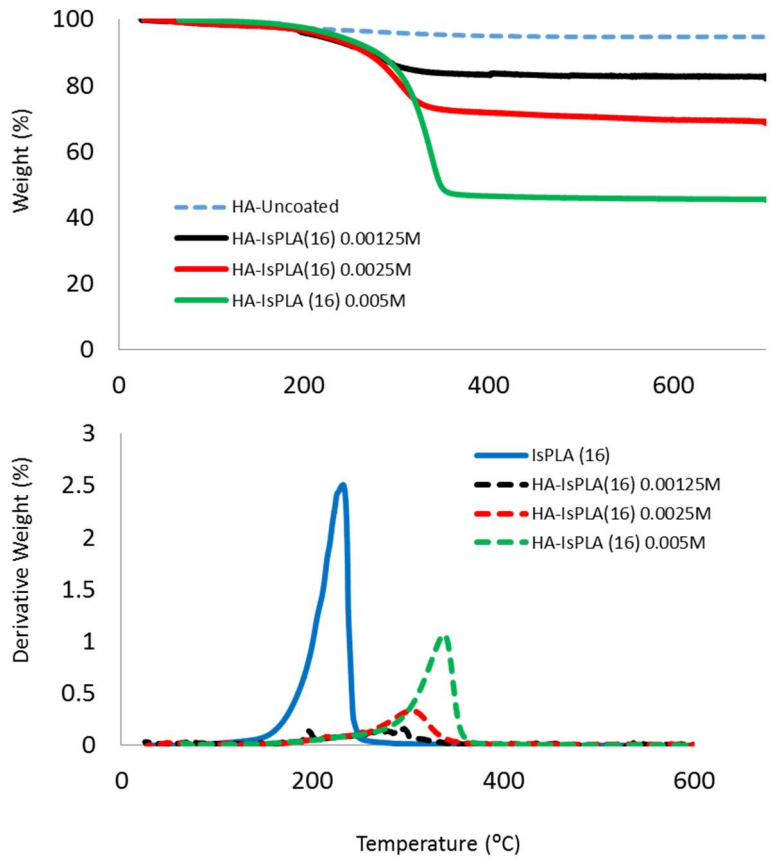


Figure 3.13. TGA plots of total recorded mass loss (weight %) *vs*. temperature for IsPLA (16) coated NP's (top graph) and TGA plot of total recorded mass loss as a derivative of weight%/temperature *vs.* temperature (bottom graph). The dispersant was dosed into the hydrothermal rig at varying concentrations as indicated.

Figure 3.13 depicts the TGA results for coated NP species synthesised using the IsPLA (16) dosed at varying concentrations into the continuous flow rig. As expected the weight % losses decrease with decreasing dispersant concentration. For this linear dispersant, it also became clear that decreasing the concentration had a slight negative effect on the thermal stability of the final coated HA product. The plot of derivative weight % shows that at 0.005M the weight loss is well-defined and occurs within a short range of temperatures. As the concentration was decreased the weight loss occurs over a higher temperature range with the apex of the peak situated at a lower temperature.

Figure 3.14 shows the TGA results for sorbitol PLA (3000 Da) dosed at varying concentrations into the continuous flow rig. Looking exclusively at the top graph the weight % loss appears to decrease with decreasing dispersant concentration. However, it is noted that the HA-Sorbitol PLA (3000 Da) 0.00125 M and 0.0025 M are very close. Upon conversion of the weight loss % to moles of dispersant (Table 3.7) it was revealed that the lower concentration (0.00125 M) coated to a greater molar extent than a concentration of 0.0025M. This indicates that a larger number of polymer molecules are in the coated material. The highest concentration (0.005 M) coated the HA to a significantly higher weight % than all other concentrations both in terms of weight % and weight % as moles of dispersant.

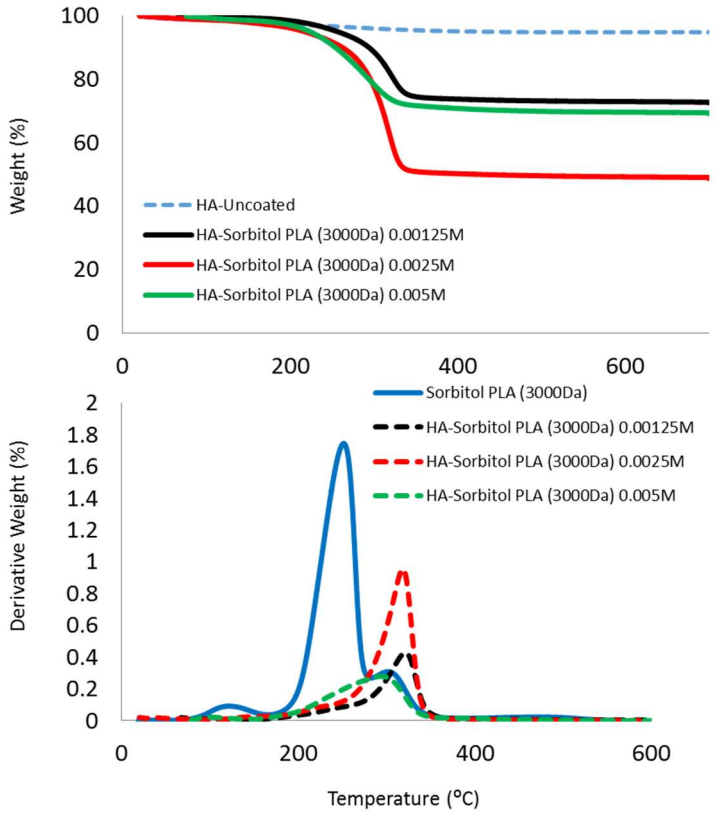


Figure 3.14. TGA plots of total recorded mass loss (weight %) *vs.* temperature for sorbitol PLA (3000Da) coated NP's (top graph) and TGA plot of total recorded mass loss as a derivative of weight%/temperature *vs.* temperature (bottom graph). The dispersant was dosed into the hydrothermal rig at varying concentrations as indicated.

Meanwhile, the plot of derivative weight (%) loss implied that, whilst Sorbitol PLA (3000 Da) 0.0025 M did not give the highest weight % loss, the coating was the most thermally stable on the HA surface. With the Sorbitol PLA (3000 Da) 0.00125 M exhibiting very similar results. The highest concentration (0.005M) appeared to exhibit the least thermal stability with a loss occurring at a lower and broader temperature range. These findings suggest that the binding mechanism for the branched dispersants is different than the nature of the mechanisms adopted by the linear dispersants and has been discussed previously (Figure 3.11). It is also proposed that these results suggest that the overall surface area/volume taken up by the branched dispersant on the HA surface is much larger due to the six branching chains. Thus, this may lead to an excess of coating at the higher concentrations (0.005M) investigated in this study. This was attributed to the ability of the molecules to pack at the surface. Whereas, linear dispersant molecules can pack closely together on the NP surface leading to higher concentrations needed to reach the unfavourable 'excess point' seen for the Sorbitol PLA (3000 Da), this is not the case for the 3D branched structures where packing is less efficient. Furthermore, previous studies conducted by Voit *et al.* [39] indicated that branched polymers are much less crystalline in nature than their linear counterparts suggesting an inability to stack the polymer chains. This leads to the possibility of polymer molecules stacking on top of each other for linear dispersants being much more sterically favourable than for the branched dispersants.[39]

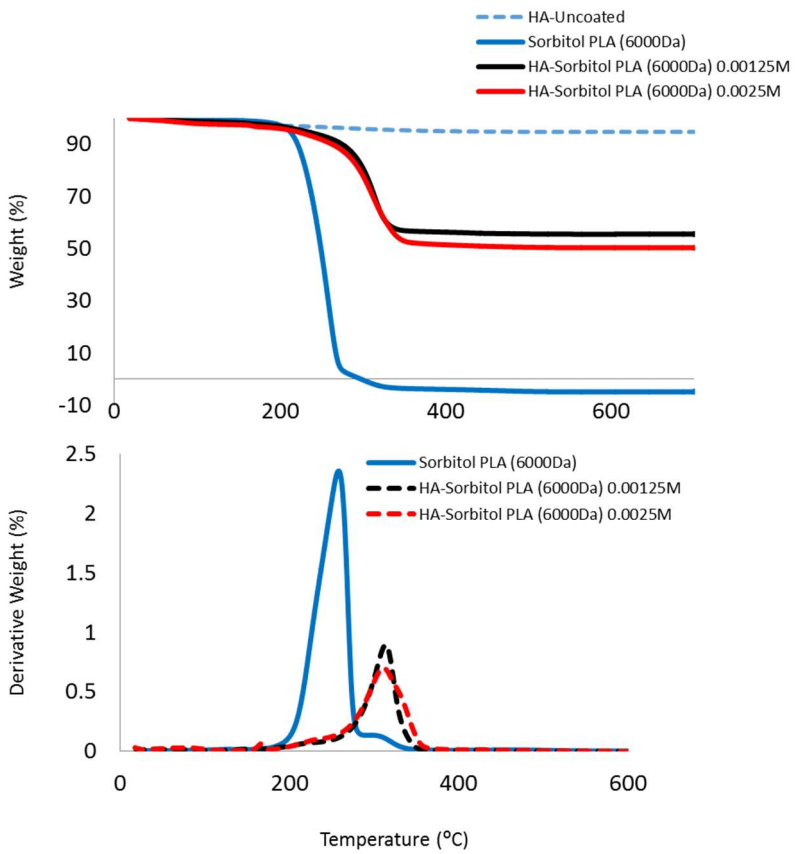


Figure 3.15. TGA plots of total recorded mass loss (weight %) *vs*. temperature for sorbitol PLA (6000Da) coated NP's (top graph) and TGA plot of total recorded mass loss as a derivative of weight%/temperature *vs*. temperature (bottom graph). The dispersant was dosed into the hydrothermal rig at varying concentrations as indicated.

Figure 3.15 shows the TGA results for sorbitol PLA (6000 Da) dosed at varying concentrations into the continuous flow rig. Only two concentrations of sorbitol PLA (6000 Da) could be trialled as any further increase would result in precipitation of the dispersant within the reactor and a failure to safely produce coated HA NP's. TGA analysis suggests that varying the concentration of the HA-Sorbitol PLA (6000 Da) did not significantly affect the amount of coating on the surface of the HA or the degradation profile of the final coated product. Upon conversion of the weight loss % to moles of dispersant (Table 3.6) it was revealed that the higher concentration (0.0025 M) coated to a greater extent, in terms of amount of polymer molecules that are potentially interacting with the HA surface, than a concentration of 0.00125 M. Building on the theory developed

above it is proposed that the lengthening of the PLA chain branches allows a certain amount of crystallinity to form within the polymer dispersant and for a certain amount of overlap of PLA chains on the surface of HA.

The use of acetone as the solvent medium for the dispersants (up flow) was found to have an adverse effect on most of the readily available, low cost o-rings commonly used within our Swagelock fittings. Whilst o-rings that can withstand a combination of harsh solvents, high temperatures and high pressures are available (for example, Kalrez®) they are often significantly more expensive. Therefore, alternative solvents were sought to reduce the overall cost of the synthesis process.[40] Water and isopropanol (IPA) were considered first as water is the primary component of the down flow stream and IPA had been successfully used in the synthesis of hydrocarbon coated HA. Both solvents would cause less wear on the majority of available o-rings. However, both failed to fully dissolve the PLA dispersant and the calcium nitrate tetrahydrate salt required in the up-flow stream despite thorough mixing and sonication of the solution. Methanol was trialled with more success and the resulting coated HA was analysed (see Figure 3.16).

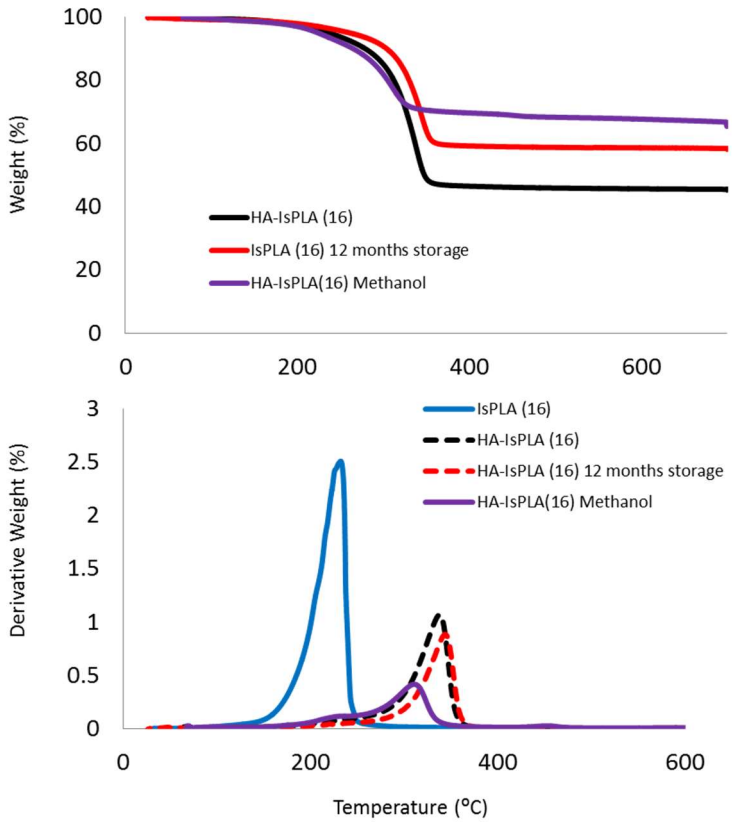


Figure 3.16. TGA plots of total recorded mass loss (weight %) *vs.* temperature for IsPLA (16) coated NP's (top graph) and TGA plot of total recorded mass loss as a derivative of weight%/temperature vs temperature (bottom graph).

The weight % loss for HA-IsPLA (16) processed using methanol appeared to be lower than HA-IsPLA (16) synthesised using acetone. However, the data in Table 3.7 revealed an increase in total weight loss % as moles of dispersant seen on the surface when compared to the results in for HA-IsPLA (16) synthesised via the acetone route in Table 3.5. This indicates that a change in the solvent does affect the coating process with more polymer dispersant molecules coating the HA to a greater extent within a methanol solvent medium. Although, this increase may not transfer into a more effective coating as TGA analysis suggests that the IsPLA (16) via methanol may not be as strongly adhered to the HA surface when compared to the acetone synthesis route. This conclusion was drawn because the derivative weight % *vs.* temperature graph in Figure 3.16 revealed the

degradation profile of the HA-IsPLA (16) methanol product to be widespread over a broad range of temperatures with the apex of the peak at a lower temperature than HA-IsPLA (16) (acetone synthesis). This may indicate that the hydroxyl end groups do play a significant role in the surface adhesion of the dispersant as disrupting these links by the addition of a lower molecular weight alcohol resulted in negative influence upon the TGA results.

Studies conducted by Sato *et al.* [41] investigated the solubility of PLA in various solvent mediums.[41] These studies found that PLA was fully soluble in acetone but insoluble in methanol. Whilst the PLA used in Sato *et al.*[41] study was not oligomeric and was of a significantly higher molecular weight than PLA used in this study, it can be regarded as an indication of how the PLA dispersants used here may behave in the different solvents when processed through the continuous flow apparatus. This data and that reported previously[41] suggests that the binding mechanism is dependent on how efficiently the PLA dispersant is dissolved into the reaction mixture within the hydrothermal reactor, where inefficient solvation of the PLA causes an increase in coating but loss of thermal stability. The loss of thermal stability would suggest that the dispersant molecules could not form strong interactions with the HA surface.

Figure 3.16 also shows the % weight loss profile for a sample of HA-IsPLA (16) stored for one year. The sample was contained within a glass vial situated in a desiccator (calcium chloride drying agent) under normal atmospheric pressure and at room temperature. The graphs show no significant variation of weight loss, with the degradation profile remaining very similar to that of the original analysis. This suggests that significant degradation of the coating has not taken place under these storage conditions. Table 3.7 details the weight loss breakdown of samples seen in Figures 3.13-3.16. When analysing the weight loss in terms of moles of dispersant it is observed that the HA-IsPLA (16) fact gains some

additional mass over the year. As the sample was in contact with the atmosphere it is possible to attribute some of this addition mass to adsorbed water and/or other airborne contaminants. This is reflected by an increase in the proportion of weight loss that occurs <150 °C.

Table 3.7 Weight losses in varying temperature regions TGA for the dispersant modified HA.

Nanoparticle (Polymer Chain Length in Monomer Units or M_w in Da)	**Moles of Polymer in up-flow**	**Total Weight Loss (%)**	**Total Weight Loss (mol of dispersant)**	**Weight Loss <150^{0}C**	**Weight Loss 150-200^{0}C**	**Weight Loss 200-400^{0}C**
HA- IsPLA (16)	0.00125	17.74	2.06×10^{-7}	2.05	2.09	12.73
HA- IsPLA (16)	0.0025	31.46	5.07×10^{-7}	1.97	1.50	24.75
HA- IsPLA (16) 1 Years Storage	0.005	41.76	2.13×10^{-6}	1.15	0.99	38.67
HA- IsPLA (16) Methanol solvent	0.005	34.59	2.37×10^{-6}	1.44	1.63	27.32
HA- SorbitolPLA (3000Da)	0.00125	27.40	9.68×10^{-7}	0.74	0.88	24.68
HA- SorbitolPLA (3000Da)	0.0025	51.2	6.46×10^{-7}	2.17	1.76	45.85
HA- SorbitolPLA (6000Da)	0.00125	44.55	3.75×10^{-7}	1.80	1.38	40.53
HA- SorbitolPLA (6000Da)	0.0025	49.81	6.32×10^{-7}	2.58	1.46	44.52
HA - Uncoated	-	5.34	-	1.99	0.84	2.24

The NP materials were then analysed using Fourier transform infrared (FTIR) spectroscopy. Figure 3.17 contains example FTIR absorbance spectra of unmodified HA NP's and indicates all major IR bands for HA and Figure 3.18 compares this data to that of the coated samples.

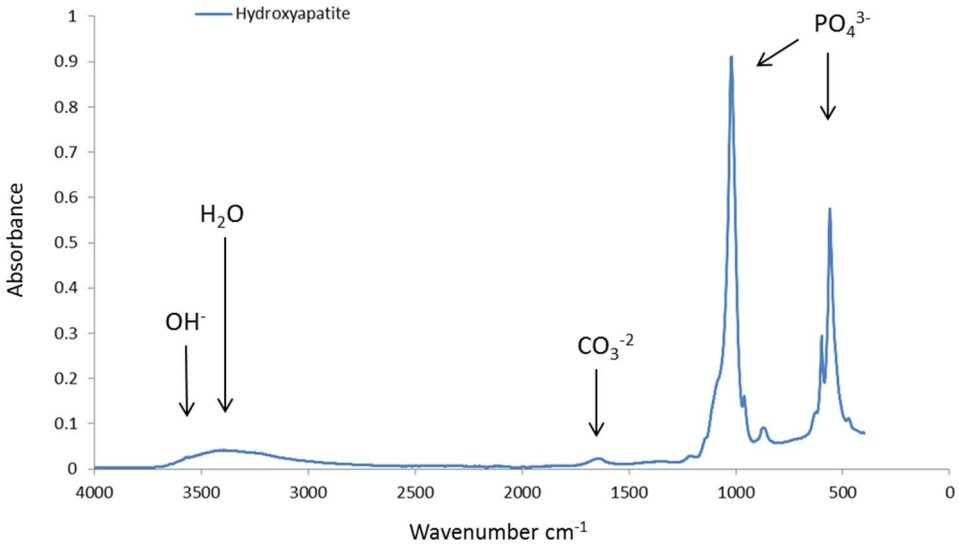


Figure 3.17. FTIR Absorbance spectrum for unmodified HA NP with relevant absorbance bands labelled.

As discussed in Chapter 2 the absorbance bands between 2800 and 3000 cm^{-1} can be attributed to the alkyl C-H stretch related to the CH_3 group in the polymer chain. The absorbance bands between 1700 and 1800 cm^{-1} are associated with the stretching of the C=O bond; this functional group is found within the ester linkages contained within the PLA chain.[42] In Chapter 2 it was observed that different shifts of the C=O peak depending on the type of carbonyl functional group it was a part of with ester functional groups appearing at the upper limits of the C=O wavenumber range. For the IsPLA dispersants featured in Figure 3.18 this functional group appears at 1745-1750 cm^{-1} and is consistent with previous findings. The PLA dispersants also contain a OH group residing at the end of the polymer chain. This band can be observed in the dispersant spectra (2500– 3000 cm^{-1}, broad) but not in the coated HA NP. The possibility that the polymer chain is also interacting with the surface of HA has been previously discussed and that it is likely that where possible the dispersant is lying 'flat' on the surface (see pictorial depiction in Figure 3.4b, centre). As the HA surface is highly charged it is not unfeasible for the polymer chain end OH group to be forming some form of intermolecular

interaction resulting in the OH IR absorbance band to be obscured. All the FTIR spectra for the IsPLA dispersants of varying polymer chain lengths indicate a presence of the dispersant in the final HA NP product and therefore, supports the TGA analysis (Tables 3.6 and 3.7).

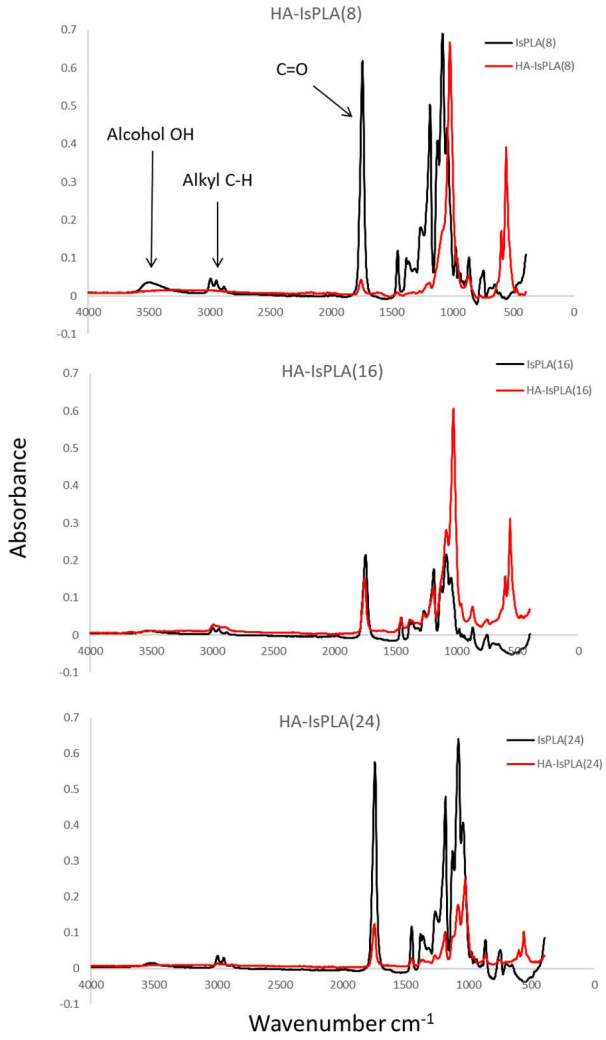


Figure 3.18. FTIR Absorbance spectra for HA NP's coated with IsPLA dispersants. Absorbance bands related to the dispersant are labelled.

In a similar fashion to the peaks observed for IsPLA dispersants in Figure 3.18 the methyl C-H stretch at 2800-3000 cm^{-1} and the ester C=O absorbance band at 1745-1750 cm^{-1} for NaPLA based dispersants (Figure 3.19). It is interesting to note that we do not see a clear OH IR peak in both the NaPLA dispersants and the HA products. Whilst the OH broad

absorbance band can be observed in the NaPLA (8) and (16) it is not as intense (relative to other IR peaks) as those seen for the IsPLA dispersants and is arguably absent in NaPLA (24) spectra. This is likely due to the IsPLA having two branching chains and thus twice the number of OH groups. Once again, the complete absence of this peak when the polymer is interacting with the HA surface implies that the chemical environment of the OH group is being altered and supports previous conclusions of the chain having an important role to play in the intermolecular interactions between dispersant and HA NP.

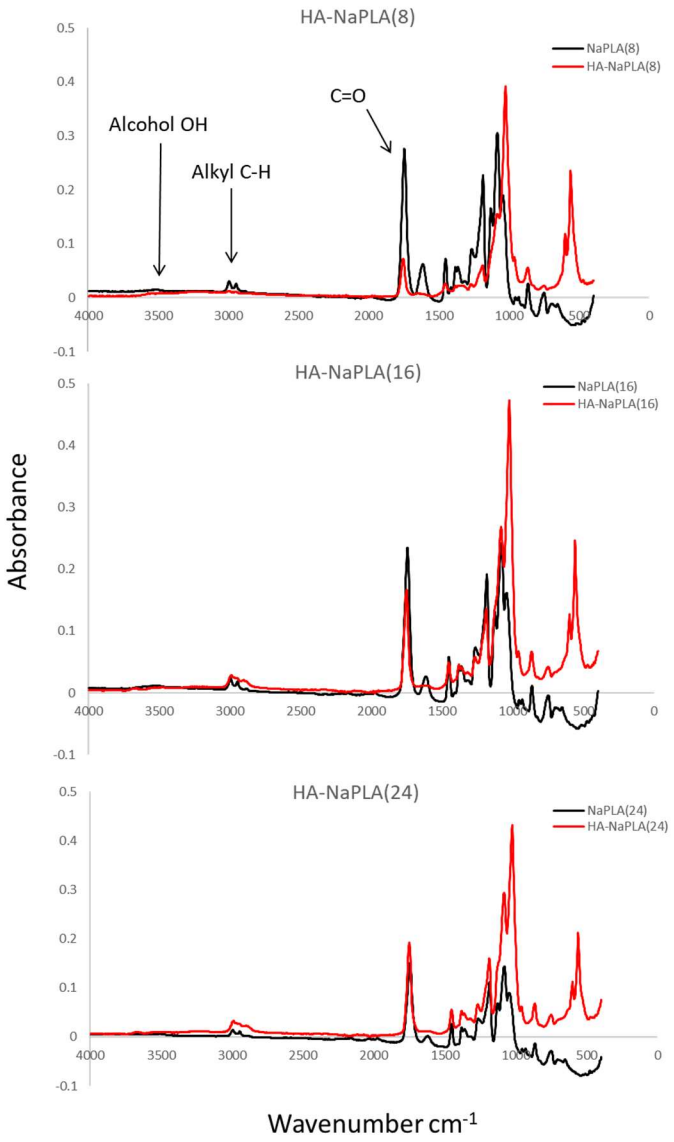


Figure 3.19. FTIR Absorbance spectra for HA NP's coated with NaPLA dispersants. Absorbance bands related to the dispersant are labelled.

Figure 3.20 shows the FTIR spectra for HA-IsPLA (16) synthesised with methanol as the solvent medium. The spectra for the coated product is very similar to that of HA-IsPLA (16) synthesised using acetone. Unfortunately, the FTIR spectrometer used in this study could not clearly determine whether the binding interactions formed between IsPLA and the HA surface differ according to the solvent used during the synthesis process. Figure 3.20 also contains the FTIR analysis of the IsPLA (16) dispersant at varying concentrations. Whilst this analysis is not strictly quantitative the IR peaks relating to the dispersant are harder to distinguish within the coated HA with a lowering of concentration.

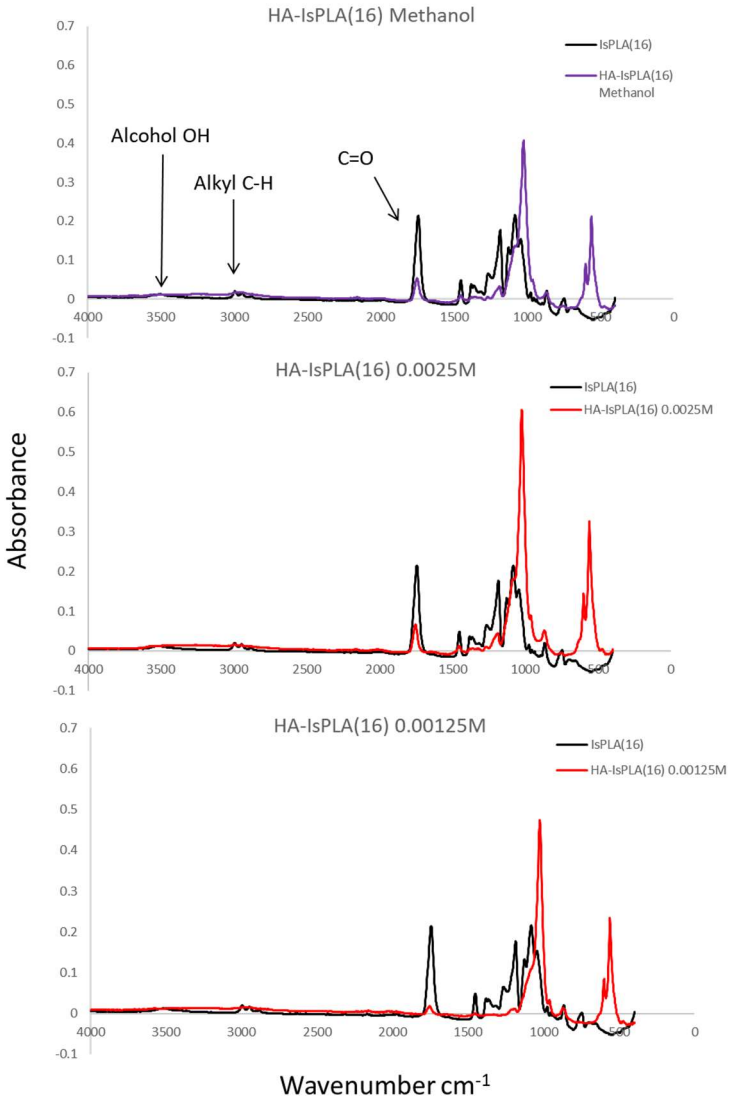


Figure 3.20. FTIR Absorbance spectra for HA NP's coated with IsPLA (16) dispersant in varying reaction conditions. Absorbance bands related to the dispersant are labelled.

Figure 3.21 depicts the FTIR spectra of HA-Sorbitol PLA (1000 Da). As this dispersant contains a total of six OH chain end groups the OH absorbance band observed at 2500 cm^{-1} –3000 cm^{-1} has increased in intensity relative to the other IR bands observed. The TGA analysis showed that very little coating was present on the surface of the HA NP when this dispersant was used. The FTIR of HA-Sorbitol PLA (1000Da) does not show any significant IR peaks relating to the branched dispersant and supports our conclusions from the TGA data.

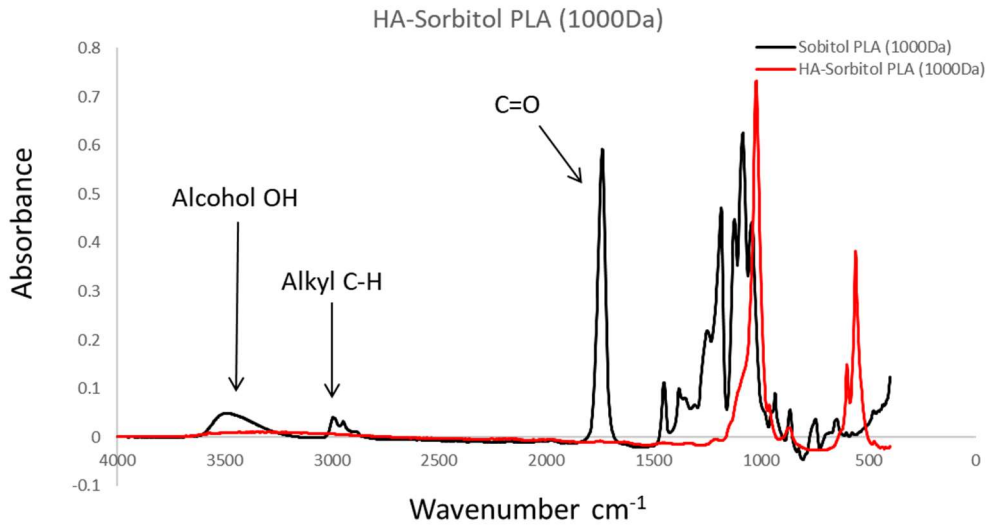


Figure 3.21. FTIR Absorbance spectra for HA NP's coated with the sorbitol PLA (1000 Da) dispersant. Absorbance bands related to the dispersant are labelled.

Figure 3.22 shows the FTIR spectra of HA-Sorbitol PLA (3000 Da) at different concentrations. This dispersant also contains a total of six OH chain end groups and the OH absorbance band observed at 2500 cm^{-1} – 3000 cm^{-1} is clearly observed in the dispersant spectra. However, this absorbance band is not as intense in the Sorbitol PLA (3000 Da) dispersant spectra depicted in Figure 3.21. This is related to the molecular weight increase and proportionally less chain ends groups when compared to the 1000 Da branched PLA. The TGA analysis revealed the dispersant coating was present on the surface of the HA NP at all concentrations and the FTIR spectra corresponds with this

result. The OH chain end group FTIR absorbance band is once again not visible in the coated HA NP spectra and supports the theory that the Sorbitol PLA anchors itself to the surface of the NP through these groups (Figure 3.11).

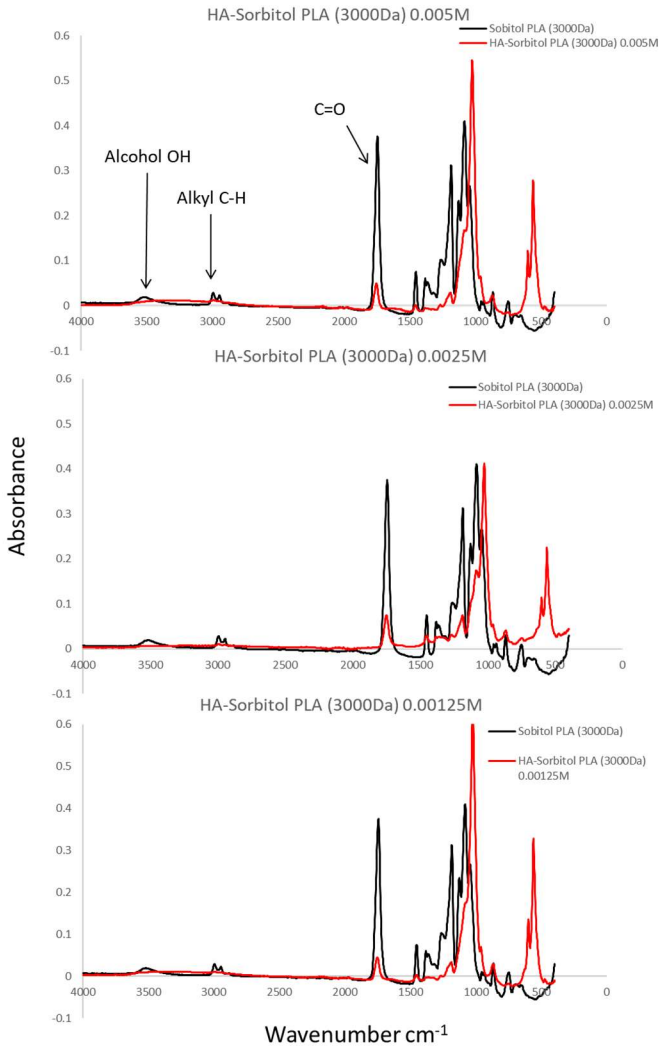


Figure 3.22. FTIR Absorbance spectra for HA NP's coated with sorbitol PLA (3000 Da) dispersant in varying reaction conditions. Absorbance bands related to the dispersant are labelled.

Figure 3.23 shows the FTIR spectra of HA-Sorbitol PLA (6000 Da) at the two concentrations trialled through the continuous flow rig. As expected the OH absorbance band observed in the dispersant spectra has decreased in intensity even further due to the increase in chain length and subsequent decrease in the concentration of the polymer end

group. The TGA analysis revealed the dispersant coating was present on the surface of the HA NP at both concentrations and the FTIR corresponds with this result. The OH chain end group FTIR absorbance band is once again not visible in the HA NP spectra and supports the theory that the sorbitol PLA anchors itself to the surface of the NP via these groups (see pictorial depiction in Figure 3.11).

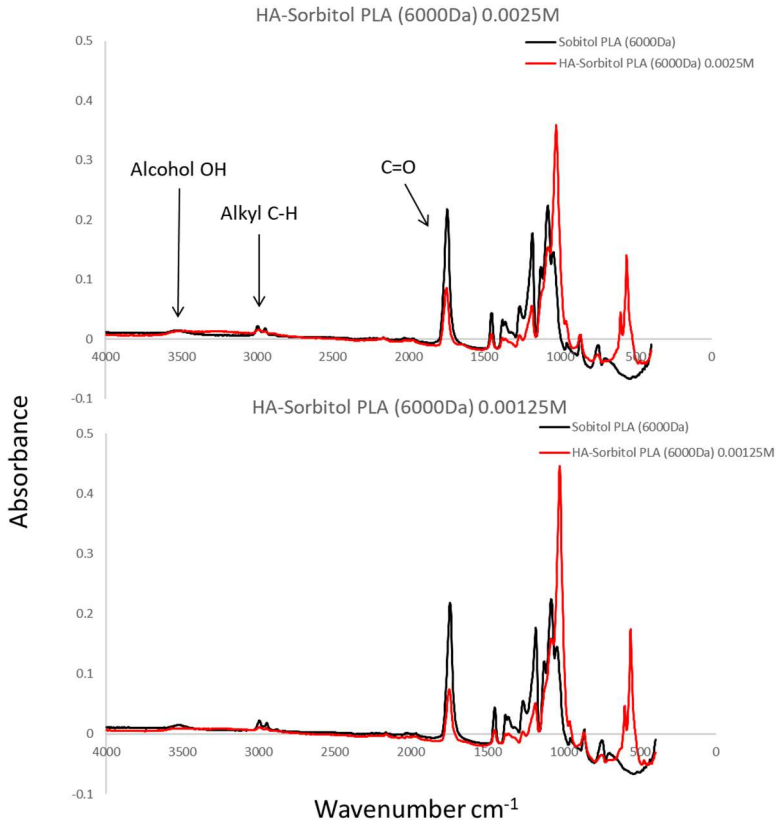


Figure 3.23. FTIR Absorbance spectra for HA NP's coated with sorbitol PLA (6000 Da) dispersant in varying reaction conditions. Absorbance bands related to the dispersant are labelled.

3.5 Material Analysis

XRD data of the synthesised materials was collected to confirm that the crystal structure of the HA had not been altered by the addition of the oligomeric PLA dispersants to the up-flow during the synthesis process. Figure 3.24 contains the XRD patterns for unmodified HA and a representative samples of PLA dispersant modified HA (further XRD analysis can be found in Appendix 1a). All the peaks were found to match with the original HA

exhibiting a hexagonal $Ca_{10}(PO_4)_6(OH)_2$ structure (ICDD ref. 01-074-0565) which matches previous results for the hydrocarbon coated HA and uncoated HA. There were no significant changes in the relative peak intensities observed between each sample indicating similar crystal growth and orientations for each. Therefore, it can be concluded that the addition of the different PLA dispersants and solvents to the up-flow feed of the hydrothermal process did not have a significant effect in the formation of the HA crystal structure.

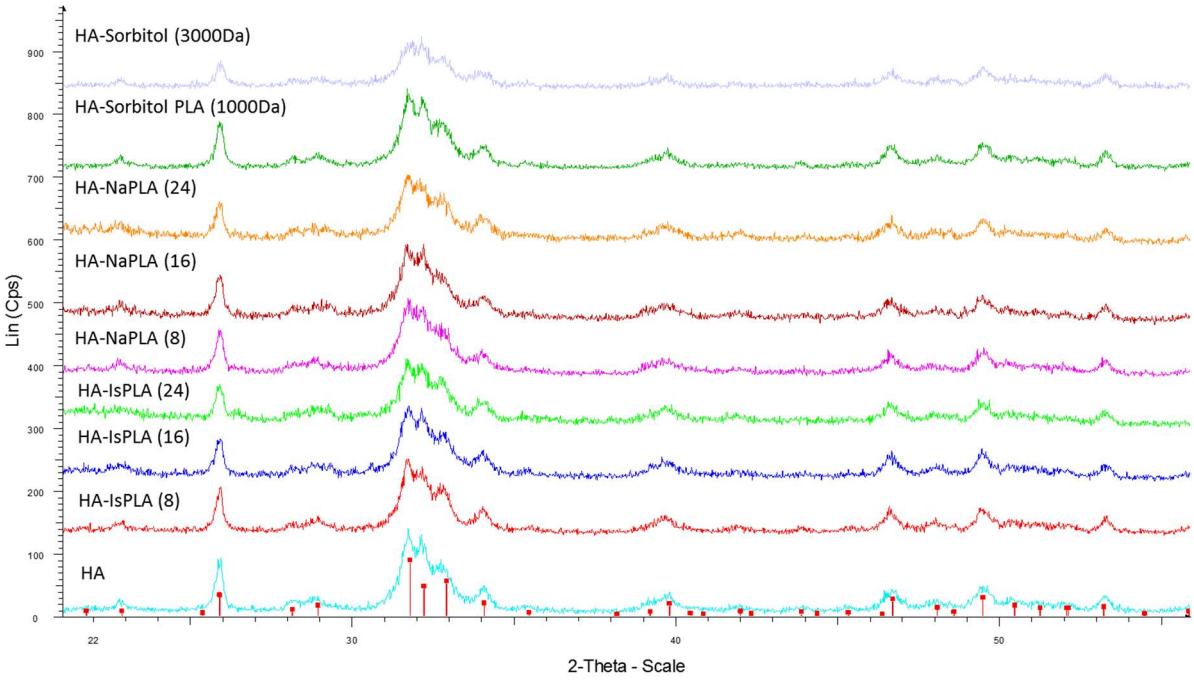


Figure 3.24. XRD patterns for uncoated HA and coated HA for a selection of PLA dispersants. Highlighted marks on the x-axis indicate the predicted peak positions for hexagonal phase hydroxyapatite. Further XRD analysis can be found in the appendix (1a).

SEM and TEM images for a number of the key samples are displayed in Figures 3.25 and 3.26 revealed that the HA NP's were polydisperse in size with average dimensions of 300 × 115 × 20 nm, of a similar morphology (platelets) to each other and similar to those synthesised in Chapter 2.

SEM imaging of the HA-IsPLA (24) sample exhibits large amorphous regions and is unlike the other SEM analysis performed for all other dispersant coated HA. It is likely that these amorphous regions are excess polymer that has failed to coat the surface and instead aggregated to form polymeric structures. This is only particularly evident in HA coated with IsPLA (24) and could be due to the longer polymer chains preferring to interact with each other rather than the NP surface to form visible polymeric clusters.

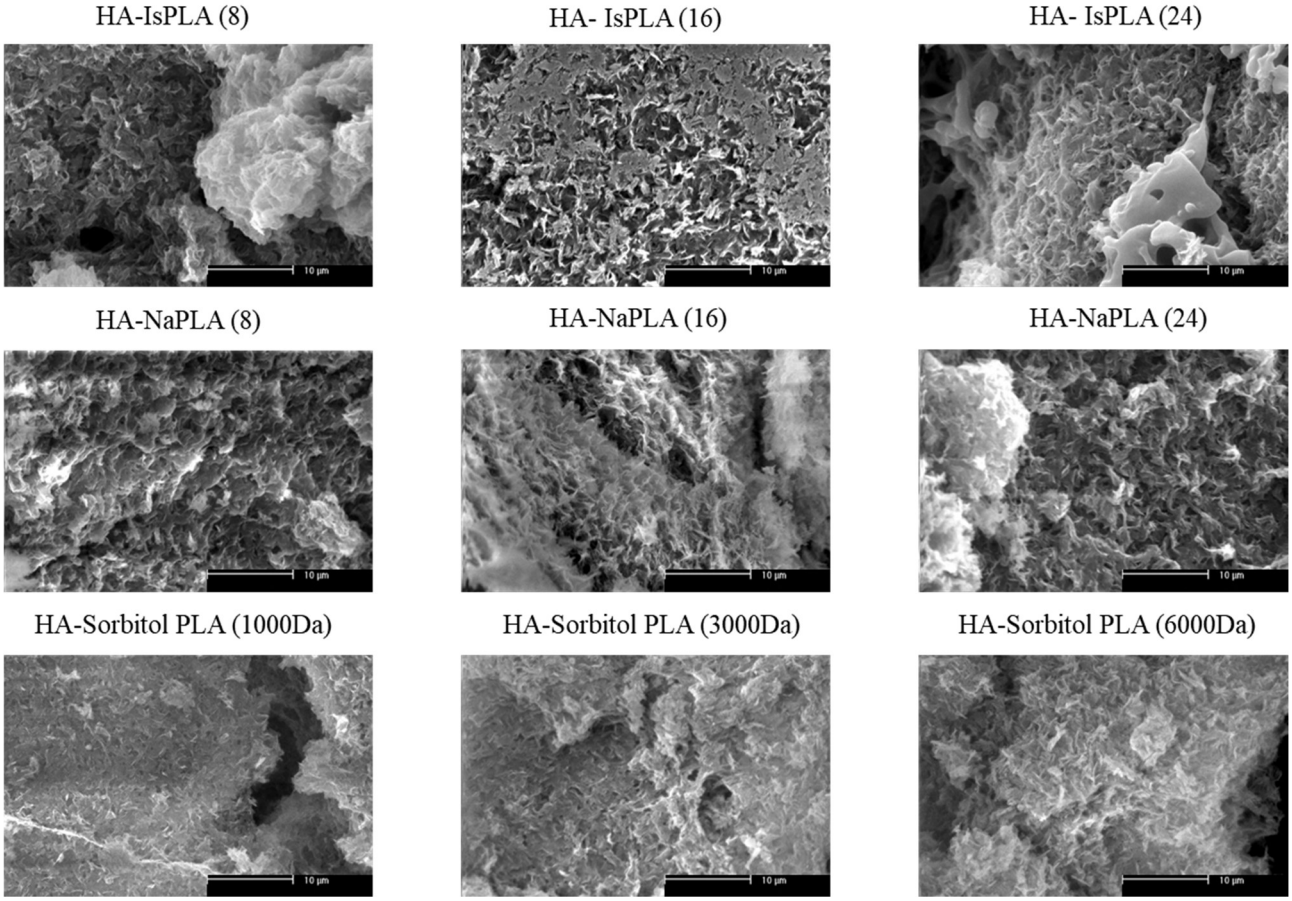


Figure 3.25. SEM images of modified HA. From left to right, top to bottom: HA-IsPLA (8), HA- IsPLA (16), HA- IsPLA (24), HA-NaPLA (8), HA-NaPLA (16), HA-NaPLA (24), HA-Sorbitol PLA (1000Da), HA-Sorbitol PLA (3000Da) and HA- Sorbitol PLA (6000Da) 0.0025M.

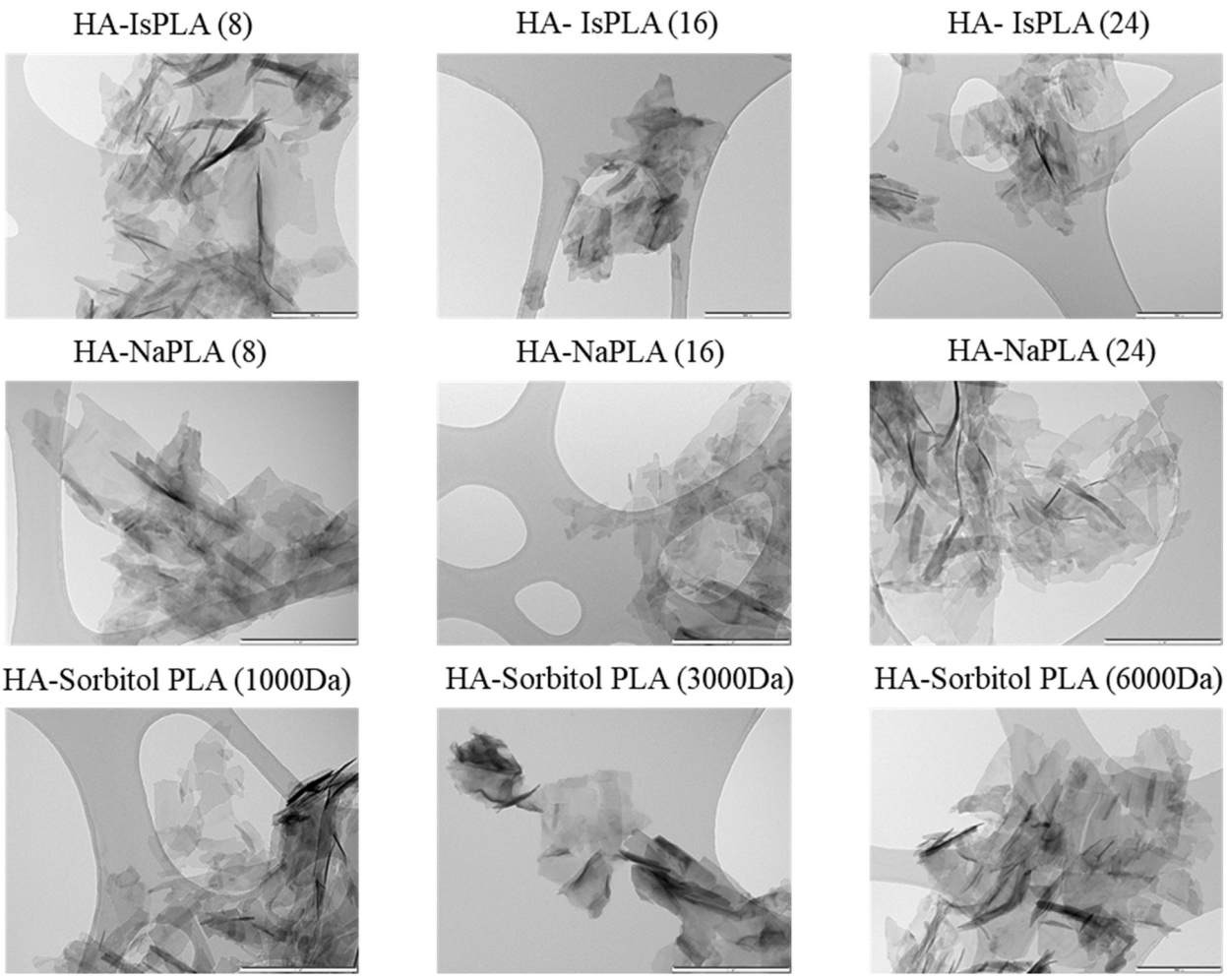


Figure 3.26. TEM images of modified HA. From left to right, top to bottom: HA-IsPLA (8), HA- IsPLA (16), HA- IsPLA (24), HA-NaPLA (8), HA-NaPLA (16), HA-NaPLA (24), HA-Sorbitol PLA (1000Da), HA-Sorbitol PLA (3000Da) and HA- Sorbitol PLA (6000Da) 0.0025M. Scale bar bottom right is equivalent to 500nm. More TEM images can be found in the appendix 1b.

Comprehensive EDX analysis was performed on all the coated HA products synthesised in this chapter and this included analysis on the level of carbon present as a percentage (Table 3.8). It was also found that the Ca:P ratio was slightly high and the HA more calcium enriched than those synthesised in Chapter 2. Uncoated HA presented a carbon % of 6.51 which was attributed to surface contaminants and adsorbed carbon dioxide. All other coated materials showed a significant increase in carbon % composition except HA-Sorbitol PLA (1000 Da) which supports both the TGA and FTIR spectroscopic analysis. Is-PLA (16), IsPLA (24) and NaPLA (24) were concluded to have coated the surface to

large extents as these samples gave exceptionally high carbon % readings. As carbon surface contamination of the HA NP's cannot be completely avoided, it was not possible to view the EDX results as strictly quantitative. However, as storage conditions and sample preparation were consistent throughout the procedure they are comparative to each other within this study. It is interesting to note that whilst HA-NaPLA performed very well in the TGA analysis yielding the highest weight % coating as moles of dispersant it did not give the significantly high results when compared to the three aforementioned dispersants. It may be possible that this dispersant degrades over time and losing some of the coating. Whilst the sodium group succeeds in slowing the catalytic degradation process of PLA when compared to its acid counterpart it is also able to form the basic NaOH in an aqueous solution. Should any of this NaOH remain on the surface of the HA or indeed be formed over time then it may act to speed up the PLA chain degradation through ester bond breakages.

Table 3.8 Average carbon % values and Ca/P ratios for the dispersant modified HA. Results were obtained using EDX analysis.

Sample	**Carbon %**	**Ratio Ca:P**
HA Uncoated	6.51	1.82
HA-IsPLA (8)	13.69	2.02
HA-IsPLA (16)	24.29	2.08
HA-IsPLA (24)	13.29	1.96
HA-IsPLA (16) Methanol	9.29	1.73
HA-IsPLA (16) 0.0025M	23.26	1.98
HA-IsPLA (16) 0.00125M	13.14	1.96
HA-NaPLA (8)	12.19	1.90
HA-NaPLA (16)	14.28	1.94
HA-NaPLA (24)	28.61	1.91
HA-Sorbitol PLA (1000Da)	5.86	1.84
HA-Sorbitol PLA (3000Da)	14.85	1.88
HA-Sorbitol PLA (3000Da) 0.0025M	10.90	1.86
HA-Sorbitol PLA (3000Da) 0.00125M	12.33	1.85
HA-Sorbitol PLA (6000Da) 0.0025M	13.78	1.93
HA-Sorbitol PLA (6000Da) 0.00125M	10.48	1.82

TEM analysis (Figure 3.26) revealed the NP's to be polydisperse plates as previously found to be the case for our hydrocarbon dispersant coated HA. It was concluded that the drying procedures employed in this study could be breaking the platelet structures and contribute to this polydispersity. To confirm this theory a sample of NP's was taken directly from the hydrothermal apparatus and analysed by TEM. Figure 3.27 shows that the NP's synthesised in by the hydrothermal methodology are polydisperse as they exit the continuous flow apparatus and as such it is not the post processing procedures (i.e. freeze drying) that causes the breakage of the HA platelets. The analysis also revealed a significant amount of visible unbound polymer (amorphous regions) that is not seen on the TEM images of the processed products (Figure 3.26) indicating that the post washing processes successfully removes excess dispersant.

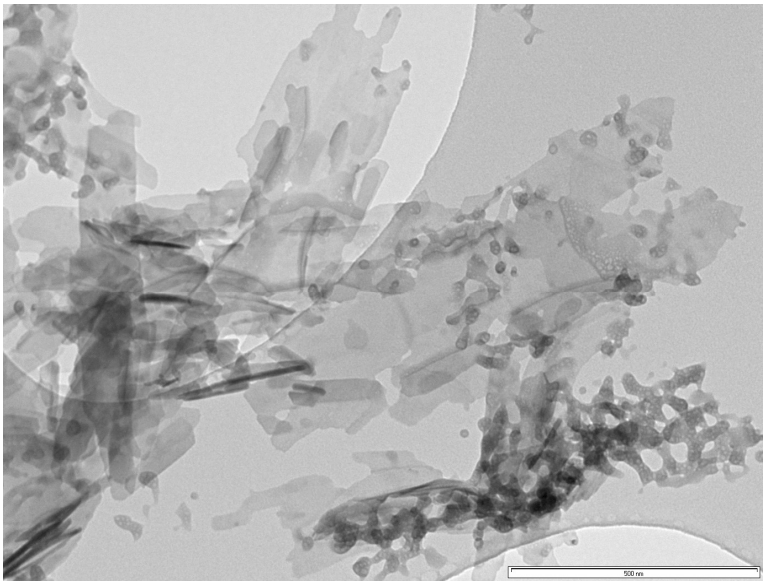


Figure 3.27. TEM image of IsPLA (16) coated HA before any post synthesis processing.

Electron energy loss spectroscopy (EELS) was performed on a selected number of samples to investigate whether the coating was present and if the surface was evenly coated. This technique exposes the sample to a beam of electrons with a narrow range of kinetic energies. The electronic excitations that occur within the material and the subsequent

energy losses within the beam are measured and related to the materials composition. Carbon % mapping was performed using this technique and used to obtain information of the morphology of the coating on the surface of the NP. Figure 3.28 details the EELS analysis of HA-IsPLA (8).

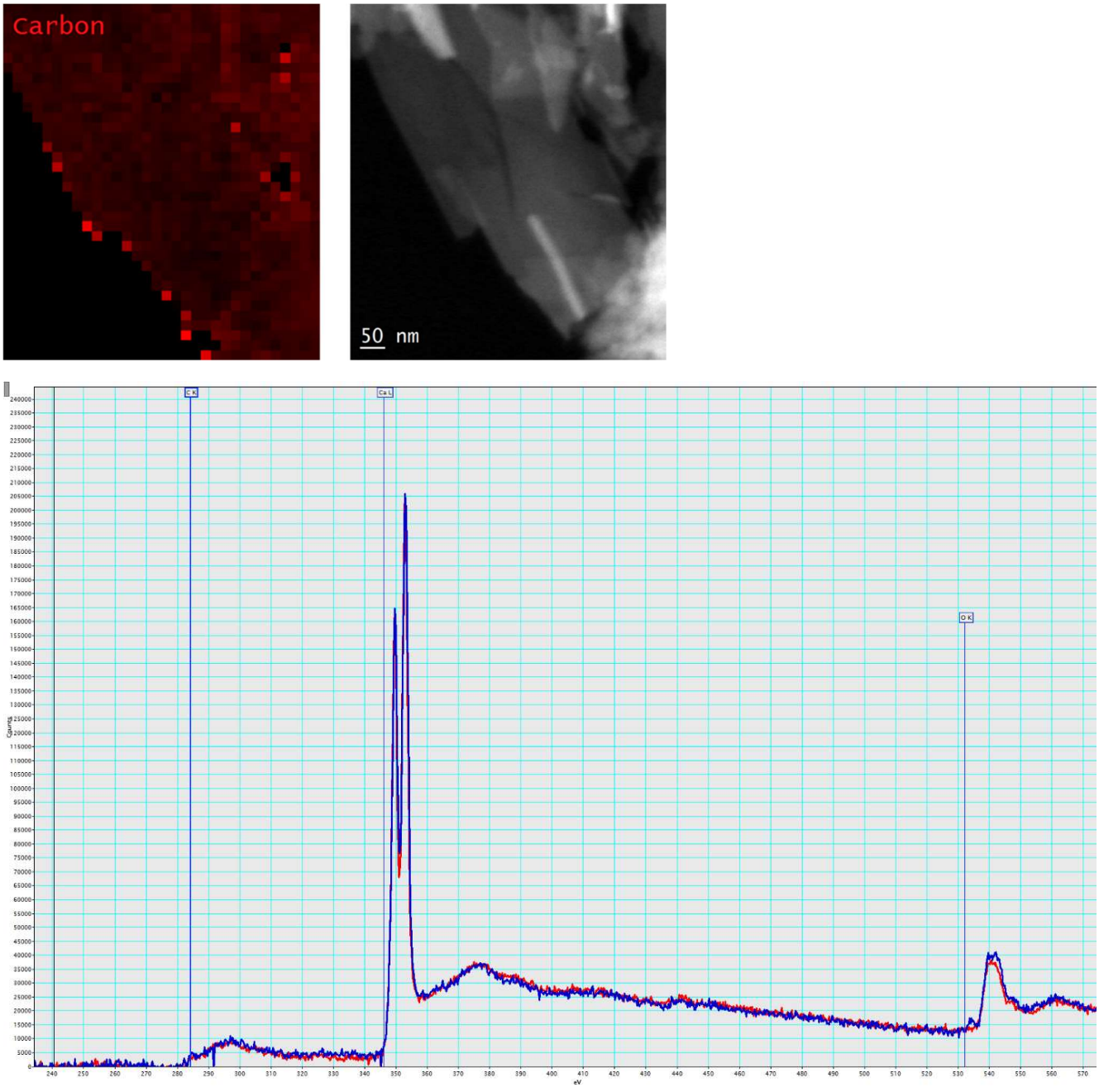


Figure 3.28. EEL analysis of HA-IsPLA (8) with EEL's carbon % mapping image, TEM image of the area examined and a normalised EEL graph or eV *vs.* counts with relevant peaks labelled. With the red line signifying uncoated HA (for reference) and the blue line being the sample.

Whilst an even distribution of surface carbon could be detected in the mapping (red image), the normalised EELS graph shows that the carbon detected was not significantly higher than that detected for uncoated HA. TGA, FTIR and EDX analysis shows that the IsPLA (8) dispersant is present on the surface of HA but not in the quantities seen for dispersants such as IsPLA (16). The EELS cannot detect any convincing increase in the level of carbon and this may be caused by the layer of carbon formed on the surface by the surfactant being very thin. EELS works off the inelastic scattering of electrons as they pass directly through the sample. The type of EELS performed in this study was designed to give a measurement of relative thickness of the carbon layer. Previous conclusions speculate that this dispersant lies flat on the surface of HA and this could explain the analysis inability to detect an increase in carbon. Given the amount of this dispersant present in the sample (Table 3.6) and its short chain length it is not surprising that the surface layer formed would be very thin and almost undetectable.

Figure 3.29 displays the EELS analysis of HA-IsPLA (16). For this dispersant, the TGA and EDX analysis determined a relatively large amount of dispersant coating on the HA. The EELS spectroscopy with this sample could detect a visible increase in the amount of carbon and supports the previous analysis results. Relating back to the discussion above (Figure 3.28) it could be suggested that the significant increased weight % of dispersant present for this chain length of IsPLA (Table 3.5) is in fact caused by the polymer stacking or layering to a certain extent on the HA surface to form a thicker dispersant layer. Should the chain increase in size too much for this dispersant these interactions can become significant and cause the polymer to prefer to interact more with other polymer molecules instead of the HA surface to form the amorphous polymeric regions seen in the SEM analysis (Figure 3.25). The carbon mapping points to the IsPLA (16) dispersant coating forming a comparatively even layer with no obvious regions of polymer aggregates.

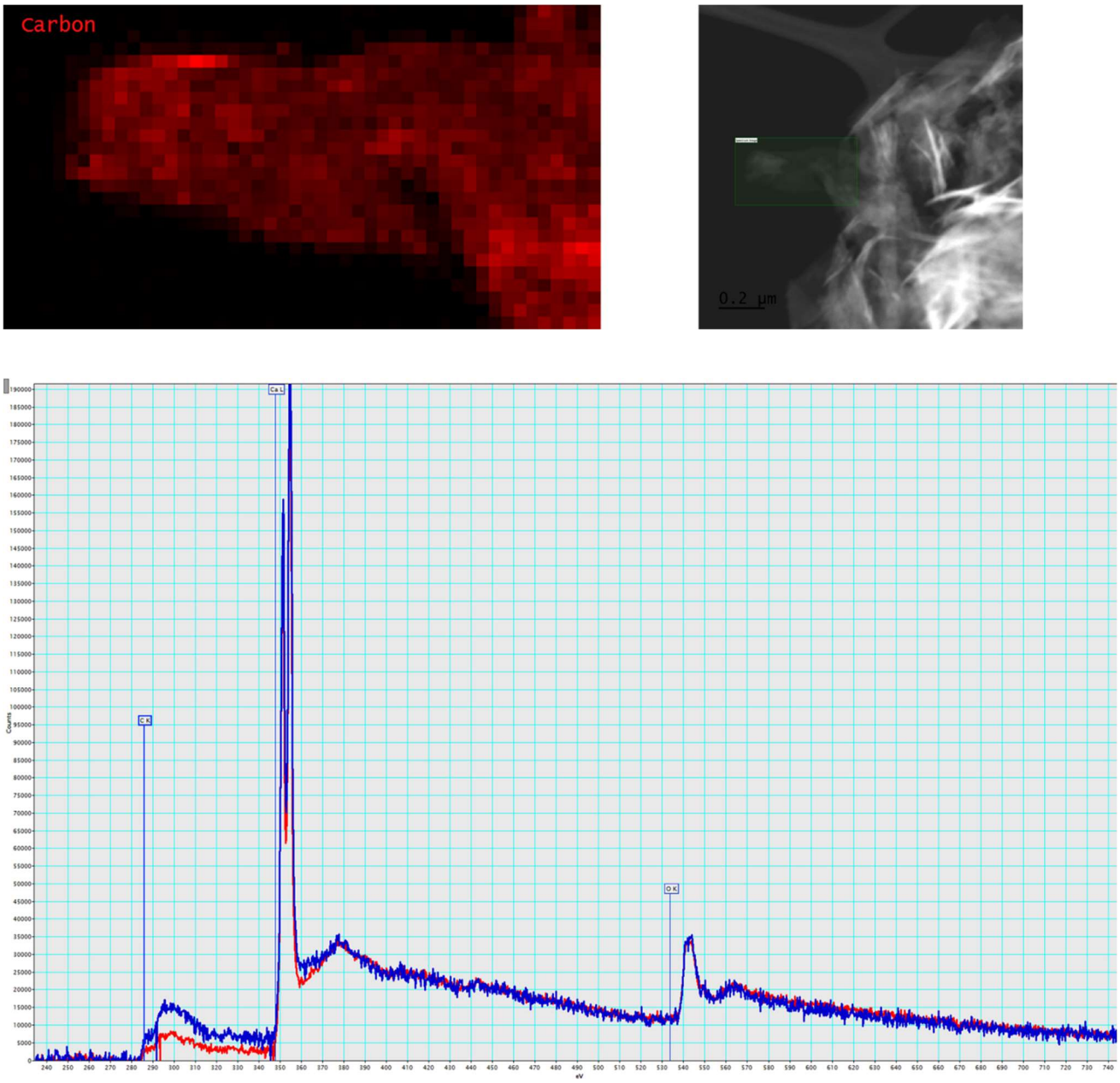


Figure 3.29. EEL analysis of HA-IsPLA (16) with EEL's carbon mapping image, TEM image of the area examined (green box) and a normalised EEL graph or eV *vs.* counts with relevant peaks labelled. With the red line signifying uncoated HA (for reference) and the blue line being the sample.

Figure 3.30 shows the EELS analysis of HA-Sorbitol PLA (3000Da) 0.0025M. For this dispersant, the TGA and EDX analysis determined a below average amount of dispersant coating on the HA. However, the EELS spectroscopy in this sample can detect a visible increase in the amount of carbon present. The thickness of the carbon layer is higher than

that of IsPLA (16) and supports our previous conclusions on both the stacking of linear polymer molecules for IsPLA (16) and our theorised surface interactions for the branched PLA dispersants (Figure 11). If the morphology of the sorbitol PLA and the fact that it is anchoring to the surface via the OH chain end groups means that is in not lying flat on the surface of the HA and creates a thick layer of carbon relative to the linear dispersants. As seen for the previous samples the carbon mapping indicates that the dispersant coating is forming a relatively even layer with no obvious regions of polymer aggregates.

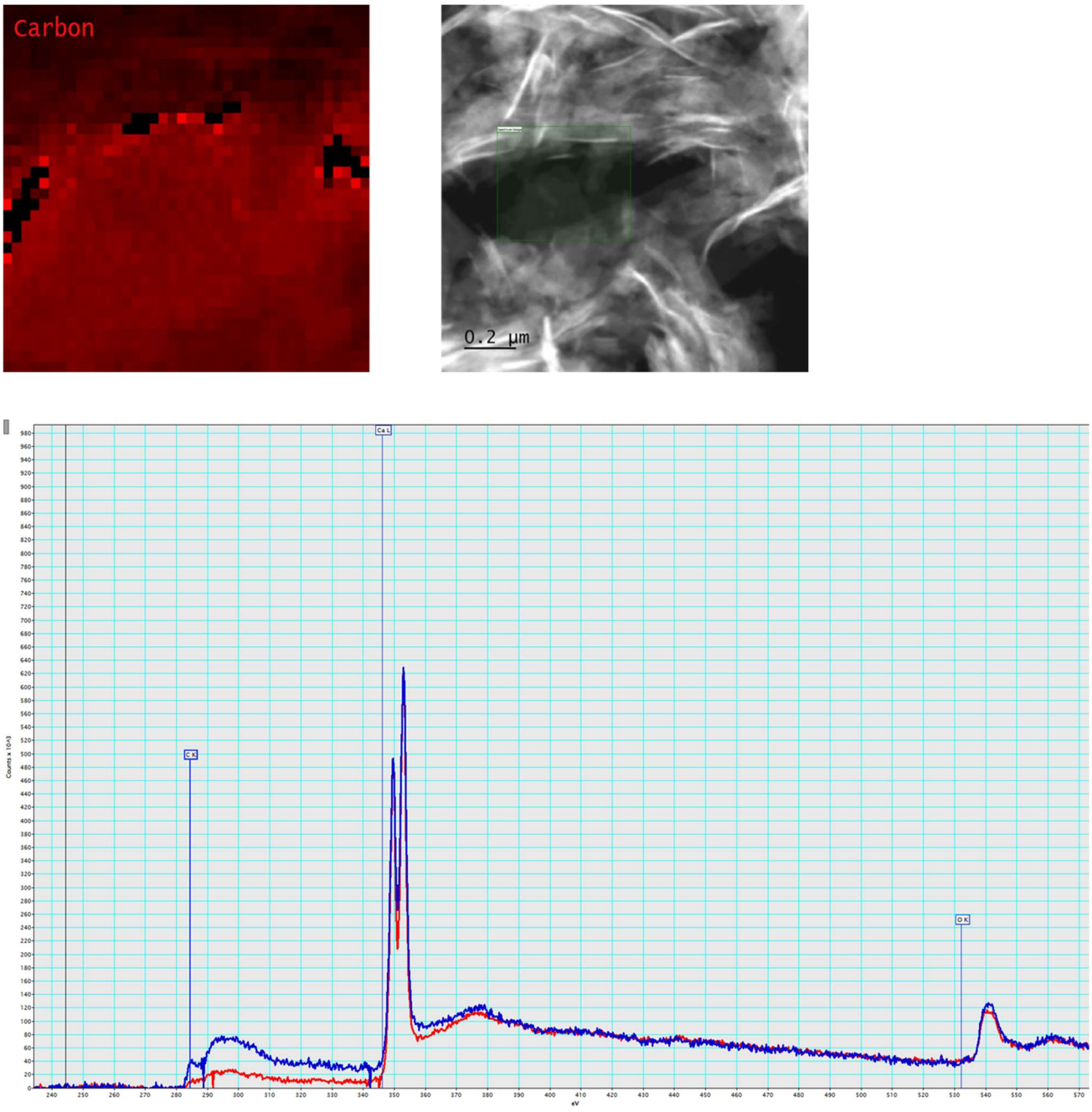


Figure 3.30. EEL analysis of HA-Sorbitol PLA (3000Da) 0.0025M with EEL's carbon mapping image, TEM image of the area examined (green box) and a normalised EEL graph or eV *vs*. counts with relevant peaks labelled. With the red line signifying uncoated HA (for reference) and the blue line being the sample.

3.6 Conclusions

In the previous chapter, work done with DDSA and the synthesis of dispersant coated HA NP's was successfully expanded using multiple hydrocarbon dispersants.[16] It was shown

that a varied range of hydrocarbon dispersants could interact with the HA surface to form a stable coating. This chapter has once again expanded on the range of dispersants capable of modifying the surface properties of HA NP's. Using PLA as the polymer of choice a number of oligomers were synthesised to act as dispersants with the aim of stabilisation of HA NP's in a medical grade PLA matrix composite. By varying polymer chain length, morphology, head group and concentration of the dispersant in the up-flow stream the mechanisms behind forming a stable surface interaction were investigated. The successful synthesis of the modified NP's was found to be sensitive to both the polymer chain length of the dispersant, dispersant morphology (linear, ABA structures and branched) and the composition of the functional head group. The most favourable results relied upon a specific combination of head group and polymer chain length with Is-PLA performing best at 16 monomer units, NaPLA at 24 monomer units and sorbitol PLA at 3000 Da. The level of dispersant coating was affected by the concentration of the dispersant in the up-flow stream. This variation of concentration was used to avoid excess polymer formation in the final product and to stop any potential blockages within the continuous flow rig. Overall the isosorbide initiated PLA dispersants performed most efficiently in terms of both the levels of coating and the stability achieved. IsPLA (16) demonstrated a good extent of surface coating, was thermally stable and could survive long term storage. Whilst NaPLA was also promising, EDX analysis revealed a potential stability and degradation issue arising from the potential formation of NaOH on the HA surface. Substituting the acetone solvent in the up-stream for methanol is not recommended as it negatively affects the dispersants ability to coat the HA. It is proposed that the linear dispersants the primary surface interactions arose from both the head group and the polymer chain causing visible increases in thermal stability of the dispersant on the NP surface. EELS suggests that the dispersants are also coating the HA surface in a relatively even fashion, however TEM and

SEM indicated that should the dispersant be in excess and of a higher chain length amorphous regions of unbound dispersant will form. Whilst most of the dispersants in this study were capable of altering the structure of the HA surface they do not appear to significantly change the crystallinity of the HA NP's but do appear to cause a small increase in the ratio of calcium to phosphorous content.

3.7 References

1. K. Hofvendahl and B. Hahn-Hagerdal, *Enzyme and Microbial Technology*, 2000, **26**, 87-107.
2. N. Sandler, I. Salmela, A. Fallarero, A. Rosling, M. Khajeheian, R. Kolakovic, N. Genina, J. Nyman and P. Vuorela, *International Journal of Pharmaceutics*, 2014, **459**, 62-64.
3. K. A. Athanasiou, G. G. Niederauer and C. M. Agrawal, *Biomaterials*, 1996, **17**, 93-102.
4. W. Groot, J. van Krieken, O. Sliekersl and S. de Vos, in *Poly(Lactic Acid)*, John Wiley & Sons, Inc., 2010, DOI: 10.1002/9780470649848.ch1, pp. 1-18.
5. L. Xiao, B. Wang, G. Yang and M. Gauthier, *Biomedical Science, Engineering and Technology*, 2011, 247-282.
6. R. K. Kulkarni, K. C. Pani, C. Neuman and F. Leonard, *Archives of Surgery*, 1966, **93**, 839-&.
7. F. Carrasco, P. Pages, J. Gamez-Perez, O. O. Santana and M. L. Maspoch, *Polymer Degradation and Stability*, 2010, **95**, 116-125.
8. A. P. Gupta and V. Kumar, *European Polymer Journal*, 2007, **43**, 4053-4074.
9. K. M. Nampoothiri, N. R. Nair and R. P. John, *Bioresource Technology*, 2010, **101**, 8493-8501.
10. S. B. Zhou, X. T. Zheng, X. J. Yu, J. X. Wang, J. Weng, X. H. Li, B. Feng and M. Yin, *Chemistry of Materials*, 2007, **19**, 247-253.
11. D. C. Tancred, B. A. O. McCormack and A. J. Carr, *Biomaterials*, 1998, **19**, 1735-1743.
12. S. Kango, S. Kalia, A. Celli, J. Njuguna, Y. Habibi and R. Kumar, *Progress in Polymer Science*, 2013, **38**, 1232-1261.
13. X. T. Zheng, S. B. Zhou, X. H. Li and H. Weng, *Biomaterials*, 2006, **27**, 4288-4295.
14. J. Li, X. L. Lu and Y. F. Zheng, *Applied Surface Science*, 2008, **255**, 494-497.
15. E. Lester, S. V. Y. Tang, A. Khlobystov, V. L. Rose, L. Buttery and C. J. Roberts, *CrystEngComm*, 2013, **15**, 3256-3260.
16. M. Gimeno-Fabra, F. Hild, P. W. Dunne, K. Walton, D. M. Grant, D. J. Irvine and E. H. Lester, *Crystengcomm*, 2015, **17**, 6175-6182.
17. E. H. Lester and B. J. Azzopardi, *Journal*, 2005.
18. G. L. Siparsky, K. J. Voorhees and F. D. Miao, *Journal of Environmental Polymer Degradation*, 1998, **6**, 31-41.

19. H. Li, J. Chang, Y. Qin, Y. Wu, M. Yuan and Y. Zhang, *International Journal of Molecular Sciences*, 2014, **15**, 2608-2621.
20. A. L. Weikel, S. Y. Cho, N. L. Morozowich, L. S. Nair, C. T. Laurencin and H. R. Allcock, *Polymer Chemistry*, 2010, **1**, 1459-1466.
21. S. H. Zhila Vazifehasl, Mohammadreza Zamanloo, Solmaz Maleki Dizaj, *International Journal of Composite Materials*, 2013, **3**, 100-107.
22. D. A. Atwood, *Sustainable Inorganic Chemistry*, Wiley, 2016.
23. D. Horton, *Advances in Carbohydrate Chemistry and Biochemistry*, Elsevier Science, 1992.
24. N. El Boulifi, J. Aracil and M. Martinez, *Bioresource Technology*, 2010, **101**, 8520-8525.
25. R. U. Lemieux and A. G. McInnes, *Canadian Journal of Chemistry-Revue Canadienne De Chimie*, 1960, **38**, 136-140.
26. N. L. Allinger, *Journal of the American Chemical Society*, 1977, **99**, 8127-8134.
27. A. Rimola, Y. Sakhno, L. Bertinetti, M. Lelli, G. Martra and P. Ugliengo, *Journal of Physical Chemistry Letters*, 2011, **2**, 1390-1394.
28. D. Cohn and A. F. Salomon, *Biomaterials*, 2005, **26**, 2297-2305.
29. O. Martin and L. Averous, *Polymer*, 2001, **42**, 6209-6219.
30. X. Z. Yang, S. H. Kang, S. L. Hsu, H. D. Stidham, P. B. Smith and A. Leugers, *Macromolecules*, 2001, **34**, 5037-5041.
31. J. H. Lee, T. G. Park, H. S. Park, D. S. Lee, Y. K. Lee, S. C. Yoon and J. D. Nam, *Biomaterials*, 2003, **24**, 2773-2778.
32. P. Christian, F. Von der Kammer, M. Baalousha and T. Hofmann, *Ecotoxicology*, 2008, **17**, 326-343.
33. J. M. Dealy and K. F. Wissbrun, in *Melt Rheology and Its Role in Plastics Processing: Theory and Applications*, Springer Netherlands, Dordrecht, 1999, DOI: 10.1007/978-94-009-2163-4_14, pp. 441-490.
34. Z. Q. He and P. Alexandridis, *Physical Chemistry Chemical Physics*, 2015, **17**, 18238-18261.
35. C. Albano, G. Gonzalez, J. Palacios, A. Karam and M. Covis, *Polymer Composites*, 2013, **34**, 1433-1442.
36. G. L. Patrick, *An Introduction to Medicinal Chemistry*, OUP Oxford, 2013.
37. A. R. Goddard, S. Perez-Nieto, T. M. Passos, B. Quilty, K. Carmichael, D. J. Irvine and S. M. Howdle, *Green Chemistry*, 2016, **18**, 4772-4786.
38. C. J. Liao, F. H. Lin, K. S. Chen and J. S. Sun, *Biomaterials*, 1999, **20**, 1807-1813.
39. B. I. Voit and A. Lederer, *Chemical Reviews*, 2009, **109**, 5924-5973.
40. Parker, *Parker O-Ring Handbook. ORD 5700*, Parker Hannifin Corporation, 1991.
41. S. Sato, D. Gondo, T. Wada, S. Kanehashi and K. Nagai, *Journal of Applied Polymer Science*, 2013, **129**, 1607-1617.
42. G. Socrates, *Infrared and Raman Characteristic Group Frequencies: Tables and Charts*, Wiley, 2004.

4 Chapter 4: Continuous Flow, Single Stage Synthesis of Dispersant-Stabilised Hydroxyapatite Platelet Nanoparticles - Solid-state NMR Spectroscopic Analysis

4.1 Aims and Objectives

This chapter focuses on the solid-state NMR spectroscopic studies that were conducted in the hopes of expanding the investigation regarding the surface chemistry of the coated HA NP's. A wide variety of analytical techniques have been employed in this study in the pursuit of fully understanding the coating ability of various organic and polymeric surfactants on the surface of HA and their interactions. Whilst able to give us a general understanding these analytical techniques could not delve into the molecular level. NMR spectroscopy is a powerful technique used in many areas of research to analyse the chemical bonding that occurs between both atoms and molecules. Due to the nature of the coated HA NP's synthesised in this project solution-state NMR spectroscopy could not be utilised without destroying the surface chemistry of interest. Therefore, solid-state ^{1}H-^{31}P correlation NMR spectroscopy was employed with the objective of understanding the bonds that may be forming between the phosphorus groups contained within the HA surface, the hydroxyl groups also present on the surface and the protons situated in the dispersant molecules. The work conducted in this chapter not only supports the theories proposed in the previous chapter but also led to an increased understanding of the surface chemistry that was occurring. A select range of dispersant coated NP's were analysed via solid-state NMR spectroscopy with the help of the Nottingham University solid-state NMR research group led by Associate Professor Jeremy Titman.

4.2 Introduction

Solid-state NMR spectroscopy has been widely used in the medical research field to analyse the crystal structure, interactions and formation of hydroxyapatite.[1-7] Given HA's biocompatibility and reactivity to various biomaterials it is utilised extensively in the medical research field as a bone substitute and as a drug carrier.[7, 8] Investigations of HA and its sought-after properties usually focus on employing microscopic techniques (such as SEM, TEM, EELS), X-ray powder diffraction to look at mineral content and IR spectroscopy to investigate interactions in organic composite materials.[1] However, these techniques often lack the ability to study nanocomposites on a molecular level and often only provide an overall view of what interactions may be taking place. To understand these interactions even further research has been conducted using solid-state NMR spectroscopy which can give a much more localised view of the composite including the surface interactions between HA and the organic dispersant molecules. Within HA systems it has been established that the core of HA particles is an ordered crystalline structure and the surface is a hydrated disordered layer enriched with HPO_4^{-3} species.[9] Solid state NMR spectroscopy using ^{1}H-^{31}P correlation allows for the examination of both synthetic and natural *in-vivo* formation of HA.[2, 3] Solid-state NMR spectroscopy is primarily a bulk technique and surface signals can often be overwhelmed by the signals from the bulk of the material being studied. However, the exceptionally large surface area of the NP's allows for an increase in the signals from the surface allowing an exploration of the types of molecular bonding that could be occurring between dispersants and HA. Previous research conducted by Bradley *et al.* [10] performed solid state NMR on HA precipitated in the presence of polysaccharides and poly(amino acids). They showed that NMR spectroscopy to be particularly effective at studying the complex interactions between the HA surface and the organic polymers.[10]

In this study, a two-dimensional ^{1}H-^{31}P correlation experiment using the DUMBO decoupling method is used. DUMBO decoupling is necessary in the ^{1}H dimension, the first or indirect dimension, because at moderate spinning frequencies magic angle spinning (MAS) alone cannot improve resolution. The technique can remove ^{1}H broadening that occurs due to homonuclear dipolar couplings to give resolved resonances and therefore, site specific information from ^{1}H NMR experiments.[11] The ^{1}H cross sections from these correlation experiments only show protons that are close to (interacting with) ^{31}P nuclei. Any resonances arising from the protons present in the dispersant molecules must be within a close proximity to the phosphorous atoms on the surface of the HA.

4.3 Experimental Setup

Solid-state NMR analysis was carried out by Dr Lyndsey Knight.

^{1}H-^{31}P heteronuclear correlation spectra were acquired at a MAS (magic angle spinning) rate of 12 kHz using the DUMBO decoupling method and the pulse sequence displayed in Figure 4.1. The relaxation delay was set to 3 - 4 s and SPINAL-64 decoupling was applied to the proton channel during acquisition.[12] For LGCP (Lee-Goldberg cross polarisation) the power levels were matched to the ±1 Hartmann-Hahn condition, the offset was between 40544.2 - 36084.39 Hz and a contact time of 5 ms was used. The 90° pulse length was set to 3.4 µs and the magic angle pulse length was set between 1.5 and 1.6 µs.

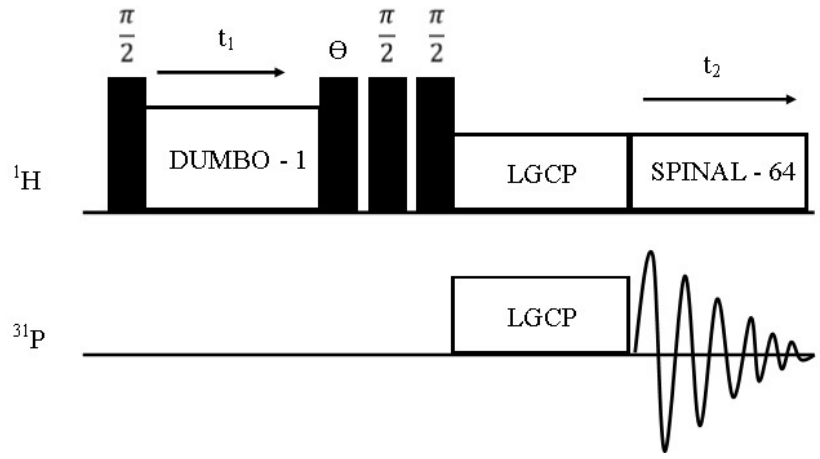


Figure 4.1. Pulse sequence used to acquire the ^{1}H-^{31}P spectra.

The DUMBO pulse length was set to 26 μs and the field used was 96 kHz. The spectra were acquired with 4096 complex data points in the direct dimension and between 176 – 256 complex data points in the indirect dimension. Data was acquired using the States method to generate pure absorption lineshapes.[13] The number of scans used to acquire the experiment was between 176 and 240 per increment giving typical experimental times between 3 - 5 days. The ^{1}H-^{31}P correlation spectra are all plotted using 100 contour levels linearly arrayed between the maximum peak height and 2% of this value.

4.4 Results and Discussion

Previous analysis has led to various theories on how the surfactant molecules were arranging themselves on the surface of the HA NP's. Using the broad range of data collected the most probable theories were formed. These theories then enabled two primary conclusions to be formed: a) hydrocarbon based dispersants are likely to be dominated by head group – surface interactions and b) polymeric dispersants would prefer to interact through both head group and polymer chain. Whilst the overall analysis appeared to support these two conclusions they failed to provide a deeper picture of the

specific types of chemical bonding occurring on the HA surface. Therefore, ^{1}H-^{31}P correlation spectra of the HA was acquired to establish what form of interactions were arising on between the dispersants and the HA NP's. Solid-state NMR spectroscopy was first performed on pure HA.

The solid-state NMR spectra of HA has been widely investigated in previous literature. [2] The literature relates the dominant peak seen in the proton spectra at 0 ppm (Figure 4.2) to the OH groups contained within HA. It is proposed that these OH groups form ordered structures, stacking in columns with little hydrogen bonding occurring between molecules due to the distance between them[2] and results in a narrow peak at a lower proton shift than hydrogen bonded hydroxyl groups. The broad peak observed at approximately 5 ppm is attributed to hydrogen bonded water, most likely residing near to or adsorbed onto the surface of HA and interacting with calcium phosphate groups.[6] Another broad contribution to the proton spectra was observed at 8-13 ppm and was assigned to HPO_4^{2-}.[14] This region is believed to be related to disordered surface HPO_4^{2-}. Defects containing HPO_4^{2-} groups that are incorporated into the bulk crystal material are assigned to a peak at 3.1 ppm.[9] Figure 4.2 also displays narrow resonances between 1-2 ppm. Literature suggests that these resonances could be originating from highly structured water on the surface of HA that is able to align with the hydroxyl columns of the bulk HA.[9]

To surmise, from this data it was possible to identify five main resonances contained within the HA ^{1}H spectrum in Figure 4.2: 1) 0 ppm assigned to OH^- in the HA 2) 5-8 ppm assigned to surface adsorbed water 3) the tail end of the 5-8 ppm peak that extends above 10 ppm is attributed to a disordered surface layer of HPO_4^{2-} 4) HPO_4^{2-} groups contained within defect in the crystal structure are assigned to 3.1 ppm 5) 1-2 ppm is related to highly structured surface water. This spectrum displays all ^{1}H present in the sample and therefore, water is particularly prevalent. In a ^{1}H-^{31}P correlation spectra this ^{1}H cross

section would only show the protons that are within close proximity to phosphorous which will result in a reduction in the resonances related to protons in water.

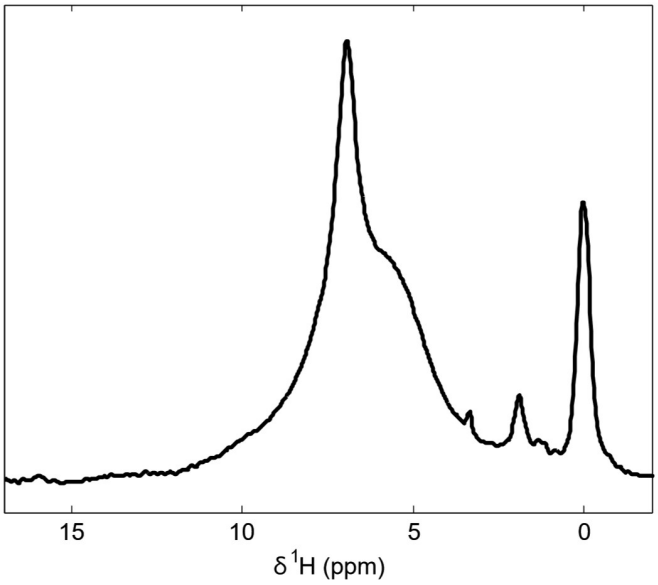


Figure 4.2. ^{1}H spectrum of HA NP's.

Figure 4.3 shows the ^{1}H-^{31}P correlation spectrum for HA, which only displays resonances of protons that are within close proximity to phosphorous nuclei. The dominating resonance at 0-2 ppm can be assigned to the interactions between the bulk phosphate and OH protons in the HA and water structured along these channels. A broad, less intense resonance is observed between 5-15 ppm and is caused be correlations between phosphate groups and surface adsorbed water along with the presence of HPO_4^{2-} on the HA surface. From this spectrum two distinct types of phosphorous environments are identified: an intense, narrow resonance at 0-2 ppm corresponding to phosphate contained within the bulk HA and the much broader resonance cause by surface phosphate groups. The broad resonance observed is the result of the disorder occurring on the surface giving rise to a larger distribution of chemical shift values. The ordered crystal structure gives rise to a much narrower distribution resulting in sharper resonances. Using the HA spectrum and its assigned peaks new resonances can be easily observed once a dispersant is introduced.

Evidence of any chemical interactions between the HA surface and the dispersant should result in the emergence of new resonances within the ^{1}H-^{31}P correlation spectra.

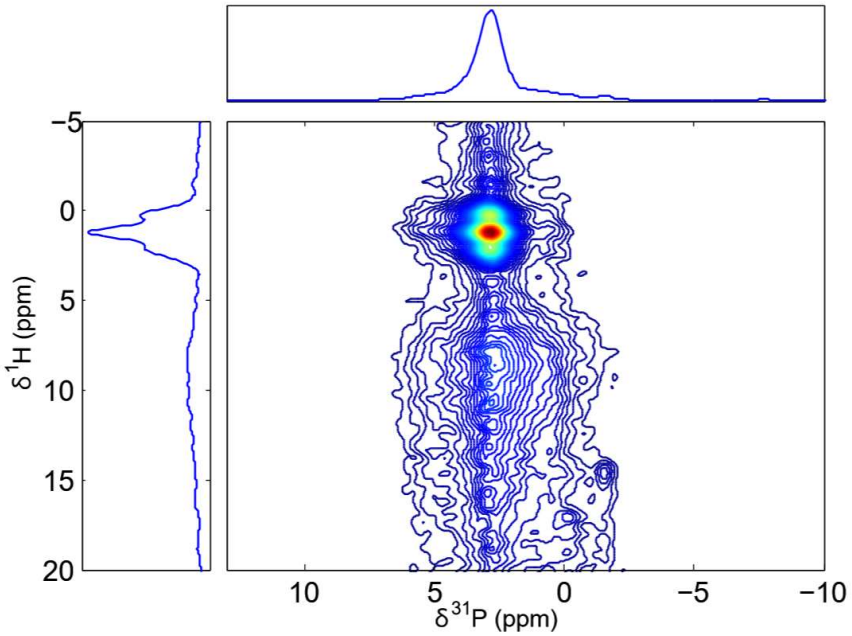


Figure 4.3. ^{1}H-^{31}P correlation spectrum of the HA nanoparticles. Skyline projections of both dimensions are also displayed.

Figure 4.4 displays the ^{1}H-^{31}P correlation spectrum of HA coated with DDSA. The DDSA dispersant has been discussed previously in Chapter 2 and investigated as a dispersant in Gimeno-Fabra *et al.*[15] The functional head group of DDSA is a dicarboxylate containing two potential interaction points with the HA surface. The aliphatic carbon chain in hydrocarbon based dispersants, as discussed previously in Chapter 2, are proposed to have little to no interaction with the HA surface. Therefore, the interactions occurring should primarily rise from the diacid head group. The spectrum in Figure 4.4 contains a distinct resonance at 9-10 ppm in the proton dimension that overshadows signals originating from the hydroxyapatite surface hydrogen bonded water. This was not seen in the HA spectrum in Figure 4.2 and suggests that it is originating from interactions between DDSA and HA on the NP surface. The functional groups capable of forming surface interactions are

contained within the acidic groups in the DDSA. The proton shift of the new resonance could occur because a greater number of hydroxyl contacts are being formed on the surface or the distances between hydroxyl groups and surface phosphate groups have been reduced shortening the distance over which polarisation transfer takes place. Both of which would lead to a strong peak in the 5-15 ppm (^{1}H) region. The appearance of a strong peak at 9-10 ppm (^{1}H) lends evidence to interaction occurring between the protons contained within hydroxyl groups situated in the dicarboxylate functional group.

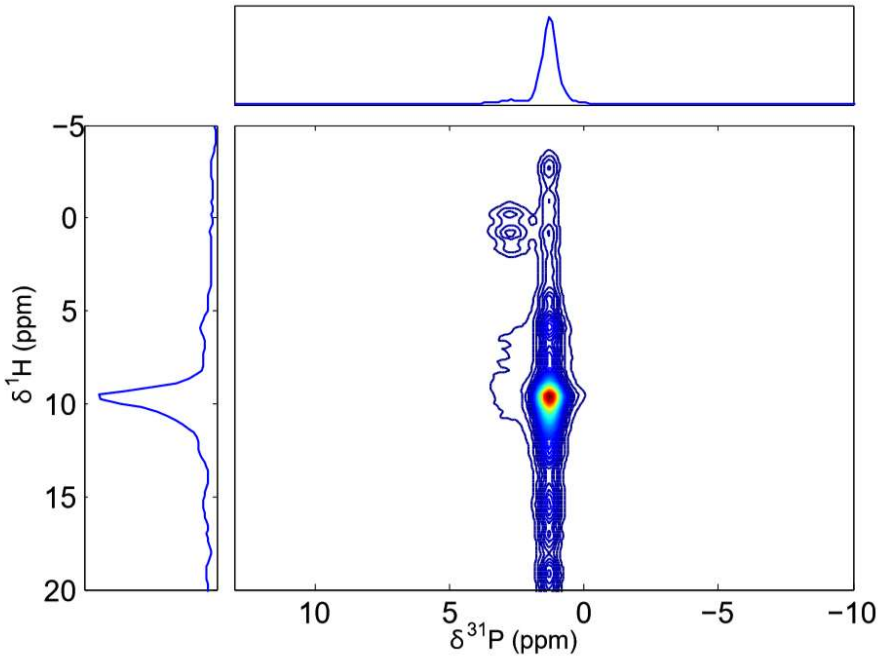


Figure 4.4. ^{1}H-^{31}P correlation spectrum of the HA nanoparticles coated with DDSA. Skyline projections of both dimensions are also displayed.

Figure 4.6 depicts the ^{1}H-^{31}P correlation spectrum for laurate isosorbide; another hydrocarbon based dispersant. The theory that the head groups dominate dispersant – HA surface interactions for aliphatic carbon-based dispersants was also evidenct in this NMR spectra. Two new resonances are observed in Figure 4.5 between -0.5 - -1.7 ppm in the ^{31}P and at 13.25 and 15.5 in the ^{1}H spectrum. When comparing the different head groups in

DDSA and laurate isosorbide there are hydroxyl groups of two different chemistries: carboxylate for the former and alcohol for the latter. Each head group can interact with the surface of HA in different ways and would then be reflected in the ^{1}H-^{31}P NMR spectra. The spectra for each clearly shows two different forms of interactions lending evidence to the theory that it is the head groups that are dominating the surface interactions between the HA NP's and dispersants. Should the protons in the hydrocarbon chain be in close proximity to the surface of the HA they would be seen in both solid-state NMR spectra. As they are not observed it is proposed that these dispersants are likely creating a micellar type structure (Figure 4.5) with the headgroup interacting with the HA surface and the hydrocarbon chain orientated away from the surface. This would also explain our ability to extract such materials into an organic medium as seen in Chapter 2.

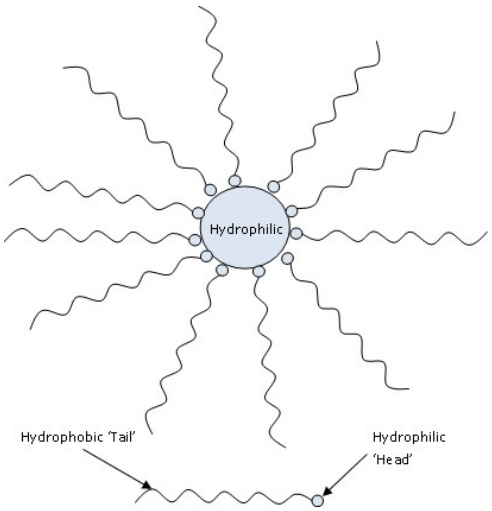


Figure 4.5. Dispersant molecules interacting with a small hydrophilic particle to form a micellar type structure.

Whereas it was relatively easy to speculate on the form of interaction occurring between the dicarboxylate group in DDSA and the HA surface in Figure 4.4 it is not as clear as to what specific surface interaction between ^{1}H and ^{31}P nuclei would cause the emergence of two distinct resonances in Figure 4.6. However, a high delta value of >10 pmm usually

indicates a hydrogen bonded environment so it is possible to speculate that this is the primary mode of interaction between the laurate isosorbide and HA surface.[16]

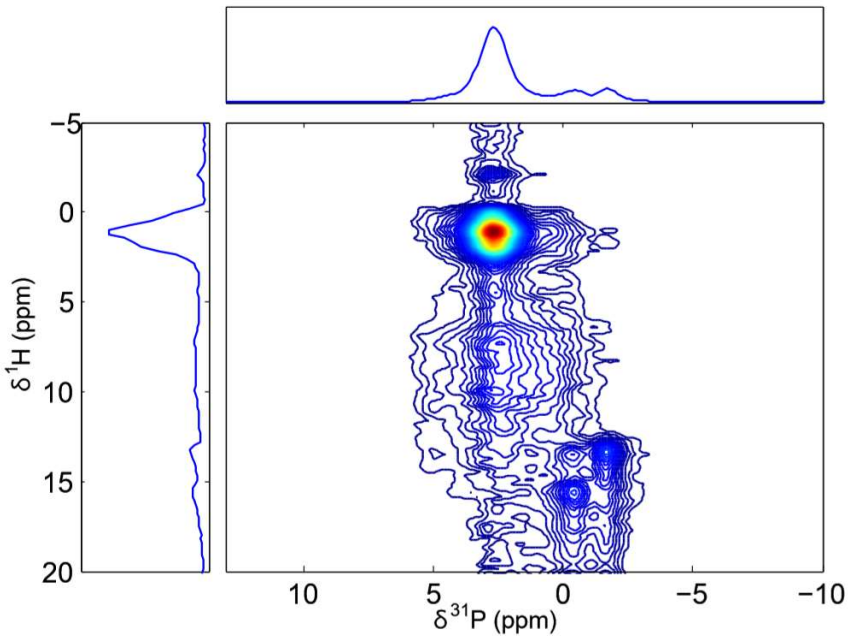


Figure 4.6. ^{1}H-^{31}P correlation spectrum of the HA nanoparticles coated with Laurate Isosorbide (C12). Skyline projections of both dimensions are also displayed.

Figure 4.7 displays the NMR spectrum for HA-NaPLA (8). Previous analysis had indicated that chain interactions would dominate for polymer based surfactants. Once again, a new resonance that is not present in the uncoated HA spectra (Figure 4.3) is observed. This resonance appears at a lower phosphorous chemical shift (1.5 ppm) than seen for uncoated HA and extends over a slightly higher range of proton shifts (5-16 ppm) with a sharp resonance occurring at approximately 11 ppm. This high proton chemical shift value suggests that this interaction originates from strong hydrogen bonds and are likely to be caused by the polymeric surfactant interacting with surface phosphate groups on the HA NP. This new resonance differs from those seen for DDSA (Figure 4.4) and laurate isosorbide (Figure 4.6) implying a different form of hydrogen bonding is taking place.

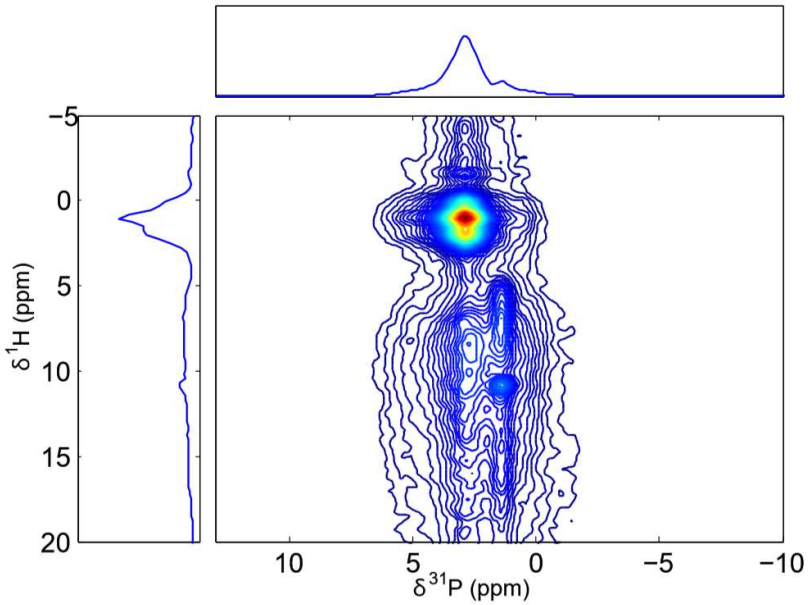


Figure 4.7. ^{1}H-^{31}P correlation spectrum of the HA nanoparticles coated with NaPLA (8) Skyline projections of both dimensions are also displayed.

The spectra of HA-NaPLA (8) alone does not lend evidence to the primary theory that polymer based dispersants interact primarily through chain – surface interactions. To prove this theory subsequent NMR spectroscopic analysis of PLA based dispersants with varying head groups were acquired. Figure 4.8 shows the ^{1}H-^{31}P correlation spectrum for HA-IsPLA (8). The dispersant has the same chain length and composition but a different head group in the form of isosorbide. If the theory is correct a very similar spectrum to the one seen in Figure 4.7 for HA-NaPLA (8) should be observed as the mode of interaction with the surface will be very similar for each dispersant. Figure 4.8 reveals a resonance that is in the same region as the new resonance observed in Figure 4.7 (1.5 ppm for ^{31}P shift and a proton shift in the range of 5-16 ppm with a sharp resonance at approximately 11 ppm). Interestingly the two resonances at -0.5 - -1.7 ppm in the ^{31}P and at 13.25 and 15.5 ppm in the ^{1}H spectrum seen in Figure 4.6 (HA- laurate isosorbide) are absent. These resonances are attributed to the isosorbide head group. The HA-IsPLA (8) spectrum appears to be dominated by the same resonance observed in HA-NaPLA (8), strongly suggesting that it

originates from polymer chain - HA surface interactions and not from the head groups. Head groups interactions may also be taking place (as discussed in Chapter 3) but they are almost certainly not the primary mode of interaction.

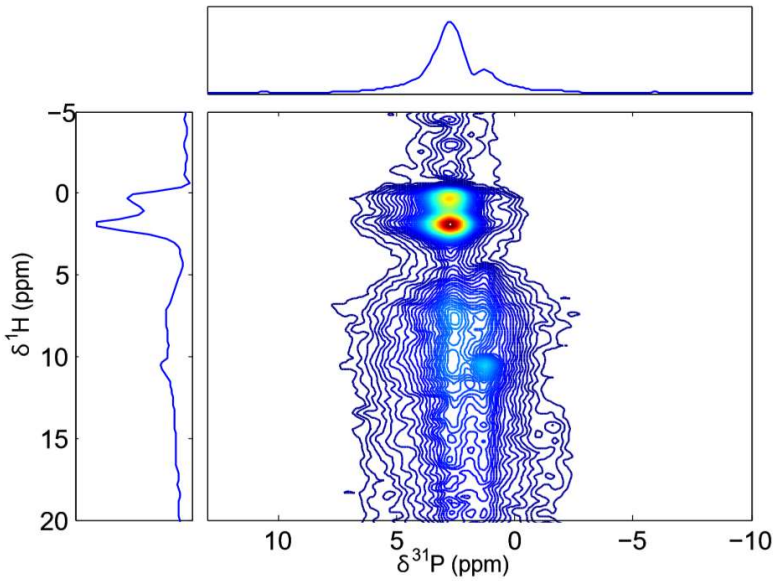


Figure 4.8. ^{1}H-^{31}P correlation spectrum of the HA nanoparticles coated with IsPLA (8) Skyline projections of both dimensions are also displayed.

To investigate the proposal further, the polymer coated HA analysis of a PLA dispersant containing a longer polymer chain was performed. If the polymer surfactants are lying in 'flat' formations on the surface of HA with chain interactions dominating, extending the length of the polymer chain should enhance the resonance attributed to the chain. Figure 4.9 displays the NMR spectrum for HA-IsPLA (24) and it was observed that the resonance at a phosphorous shift of 1.5 ppm and proton shift between 5-16 ppm was significantly enhanced. This enhancement lends evidence to the conclusion of chain interactions being the dominating factor and resolves the interaction in three different regions of proton intensity allowing for further investigation on the exact nature of the interaction. The resonance at approximately 10 ppm is still present and can be assumed to originate from a

strongly hydrogen bonded proton. The stripe of intensity seen at 6-7 ppm can be assigned to correlations between protons in the polymer with water molecules on the surface and surface phosphate groups. A newly resolved resonance at approximately 5 ppm, not seen in the previous spectra (Figures 4.7 and 4.8), is likely to originate from an interaction occurring between the phosphate groups on the HA surface and the methoxy protons in the PLA chain. This interaction between the surface and the methoxy protons in the chain suggests that the chain is in close proximity to the HA surface indicating that at least part (if not all) of the polymer chain is lying in a flat conformation on the surface.

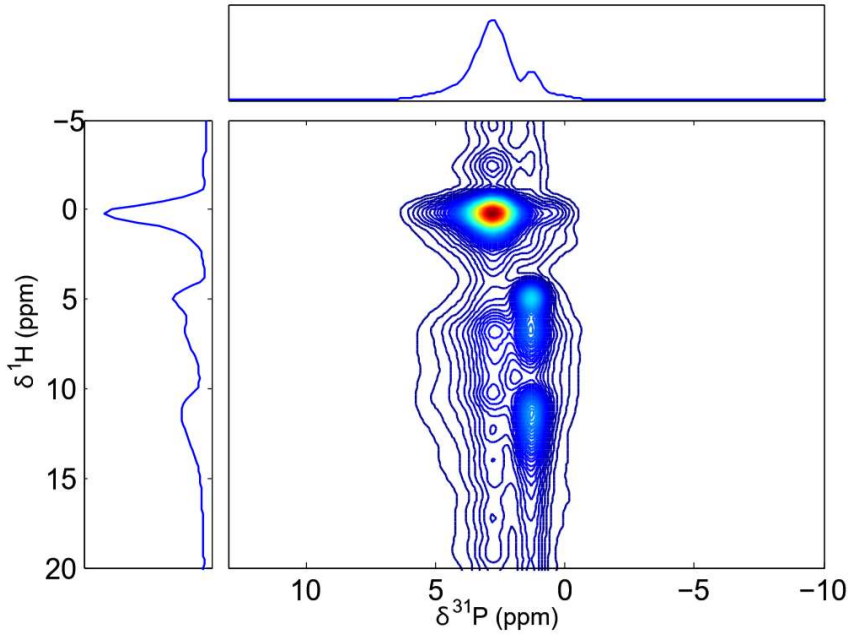


Figure 4.9. ^{1}H-^{31}P correlation spectrum of the HA nanoparticles coated with IsPLA (24) Skyline projections of both dimensions are also displayed.

4.5 DNP Solid-State NMR

Dynamic Nuclear Polarisation (DNP) NMR spectroscopic analysis is a technique used to significantly amplify the signal intensities resulting from the polarisation of nuclear spins. DNP enables this higher signal intensity by transferring electron spin polarisation to the nuclei which have increased magnetic moments and therefore, an increased polarisation.[17]

The spin polarisation from these electrons is transferred to the nuclei (usually protons) in the sample by using microwave radiation at or near the electron paramagnetic resonance frequency (Larmor Frequency). As this technique requires high frequency, high power sources it was not until recently that it became more widely utilised in the field of solid-state NMR. Whilst standard solid-state NMR experiments (such as DUMBO) are able to provide detailed information about surface mechanisms in solids the low signal to noise ratio caused by the small magnetic moments exhibited by common nuclei (^{1}H, ^{13}C, ^{31}P etc) limits the ability to study such mechanisms.[18] In the 1980's DNP was combined with magic angle spinning (MAS) to provide the capability to perform solid-state DNP experiments. These were conducted using relatively low magnetic fields (low-field experiments), however over the years, as the capability of producing high frequency, high power microwaves to perform the polarisation transfer step (previously mentioned) have advanced. This has given rise to increased resolutions (high-field experiments) and sensitivity in the solid-state NMR field.[19]

To prepare a sample for DNP analysis a radical most be introduced to the system. This is usually achieved by wetting the surface of the sample with a solution containing a radical. As such, this causes a preferential enhancement of surface signals as the radicals congregate on the surface of the solid. Signal intensities from the bulk of the material will be observed but will not be as prominent as those emanating from the surface. This is in contrast to standard solid-state NMR experiments where the signal primarily dominated from the main constituent of the sample (the bulk) which can often obscure surface signals. As surface mechanisms are of primary interest in this study into DNP offers an analysis technique that could provide a deeper insight as to what interactions are occurring on the surface of the HA NP's when an organic dispersant was introduced. Another advantage of

DNP is its capability of producing high resolutions in a relatively short time, reducing days' worth of acquisition time to hours.

4.5.1 DNP Experimental Method

Samples of HA-IsPLA (8) and HA-DDSA were prepared by wetting 30 mg of each sample with 30 µL of 10 mmol Amupol solution with 90/10 % by volume D_2O/H_2O. When not in use samples were stored in the freezer to slow the decomposition of the radical.

All the DNP experiments were performed on a wide-bore AVIII 600 MHz (^{1}H Larmor frequency) Bruker spectrometer equipped with a 395 GHz gyrotron, a transmission line and a low temperature 3.2 mm HX MAS probe operating at ≈107 K.

The ^{1}H-^{31}P correlation spectra were acquired using the pulse sequence displayed in Figure 4.10 The principal difference between this sequence and the sequence displayed in Figure 4.1 is that an R-sequence was applied in the indirect dimension to carry out the homonuclear proton decoupling. The basic element of the R-sequence, R_φ, was a composite pulse of the form $90_{45}90_{135}90_{45}$. This sequence was used instead of DUMBO as it produced superior resolution under the conditions present in the DNP experiment.

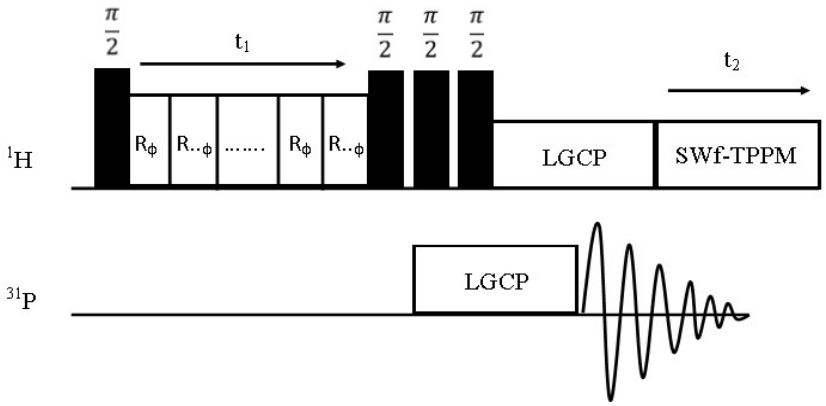


Figure 4.10. Pulse sequence used to acquire the DNP enhanced ^{1}H-^{31}P correlation spectra. $[R_\varphi][R_{-\varphi}] = [90_{45}90_{135}90_{45}][90_{-45}90_{-135}90_{-45}]$.

All the DNP spectra were recorded at a MAS rate of 12 kHz with a recycle delay of 5 s. The 90° pulse length was set to 2.6 μs and SWf-TPPM (swept-frequency two-pulse phase modulated) decoupling was applied to the proton channel during acquisition.[20] TPPI (time-proportional phase incrementation) was used to generate pure absorption lineshapes. The spectra were acquired using eight scans and the number of complex data points acquired in the direct and indirect dimension was 1024 and 150, respectively. For LGCP an offset of -37137Hz was used and the contact time was set to 4.12 ms. The ^{1}H-^{31}P correlation spectra are all plotted using 100 contour levels linearly arrayed between the maximum peak height and 5% of this value.

4.5.2 4.5.2 DNP: Results and Discussion

The direct excitation spectra of protons in the HA-IsPLA (8) sample can be found in Figure 4.11a. The resonance seen at 0 ppm arises from the hydroxyl groups of the HA and the broad resonance at approximately 7 ppm corresponds to water. Upon the application of microwave irradiation, a fivefold increase was observed in the signal intensity due to the transfer of spin polarisation from electrons to the proton nuclei (DNP effect). Figure 4.11b displays the phosphorous spectrum of the same sample. An increase in the intensity of the signal with microwave irradiation is still observed, however it is only a threefold increase. The is due to the phosphorous residing mainly in the bulk of the material and therefore, further away from the radical polarising agent.

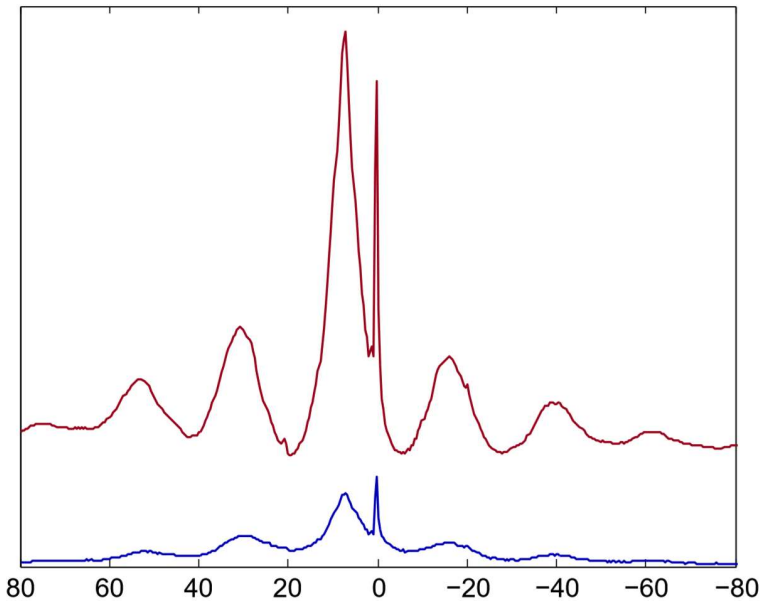


Figure 4.11a. ^{1}H spectra of HA-IsPLA (8) recorded with the microwaves off (blue) and the microwaves on (red)

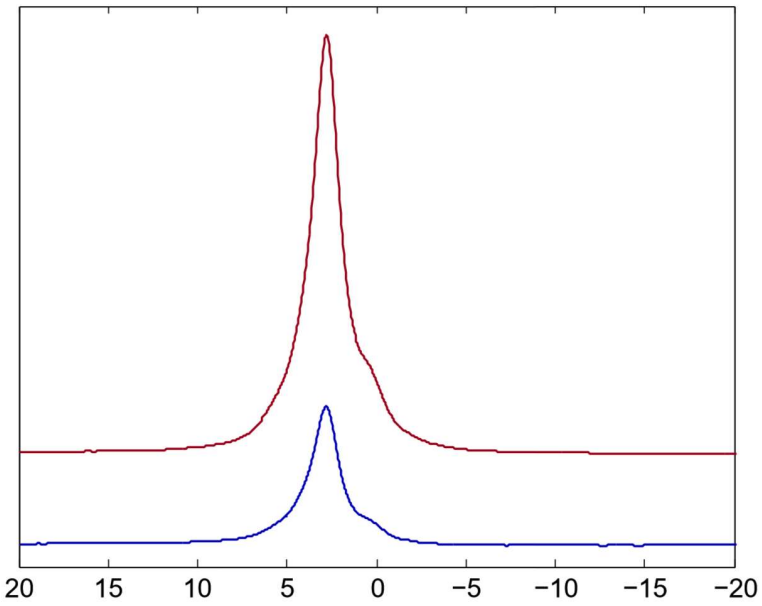


Figure 4.11b. ^{31}P spectra of HA-IsPLA (8) recorded with the microwaves off (blue) and the microwaves on (red).

The ^{1}H-^{31}P correlation spectrum of HA-DDSA with the DNP enhancement is displayed in Figure 4.12. Figure 4.4 shows the standard solid-state NMR spectrum for this sample and we see significant differences. These differences arise for a variety of reasons one of which includes the way samples are prepared for the DNP spectra compared to standard NMR.

When performing a standard solid-state NMR analysis, the sample is completely untreated; neither solvent nor agent is needed to obtain a spectrum. However, DNP requires the radical polarising agent to be added and this is achieved by wetting the samples with a solution of 90/10% D_2O/H_2O. This of course can lead to changes in the intensity of the water resonance at approximately 6 ppm normally observed for the HA sample. It is also important to note that the spectra are acquired at a much lower temperature (approximately 107 K) than standard solid-state NMR experiments (room temperature) and this could also affect the interactions that are occurring in the sample. What is thought to be a temperature affect is observed in Figure 4.12 with the hydrogen bonded protons, assigned to the resonances at 10-11 ppm in the standard solid-state NMR experiments, are shifted to a slightly higher ppm. Furthermore, the radical polarising agent congregates primarily on the surface and this proximity to the surface molecules could lead to an enhancement of the resulting resonances.

Comparing the spectra observed in Figure 4.12 to the uncoated HA standard solid-state NMR spectra displayed in Figure 4.3 the signal intensity of the two primary phosphorous environments differ. In Figure 4.3 the predominant narrow resonance at 0-2 ppm (^{1}H), 0-5 ppm (^{31}P) was due to phosphate groups within the bulk material interacting with the OH groups within the HA crystal structure. The broad resonance between 5-15 ppm (^{1}H) in the same spectra is caused by surface phosphate groups interacting primarily with surface water. This broad resonance is significantly less intense in signal. In Figure 4.12 this intensity switches, with the predominant resonance being the broad 5-15 ppm arising from surface interactions. The narrow resonance all but disappears from this spectrum as the signal from the surface overwhelms that of the bulk material. The spectra in Figure 4.12 is essentially a surface enhanced version of the standard solid-state NMR spectra and was expected considering the nature of the DNP experiments. On its own it only reveals limited

information and therefore, a DNP spectrum of a polymer coated HA material was also acquired.

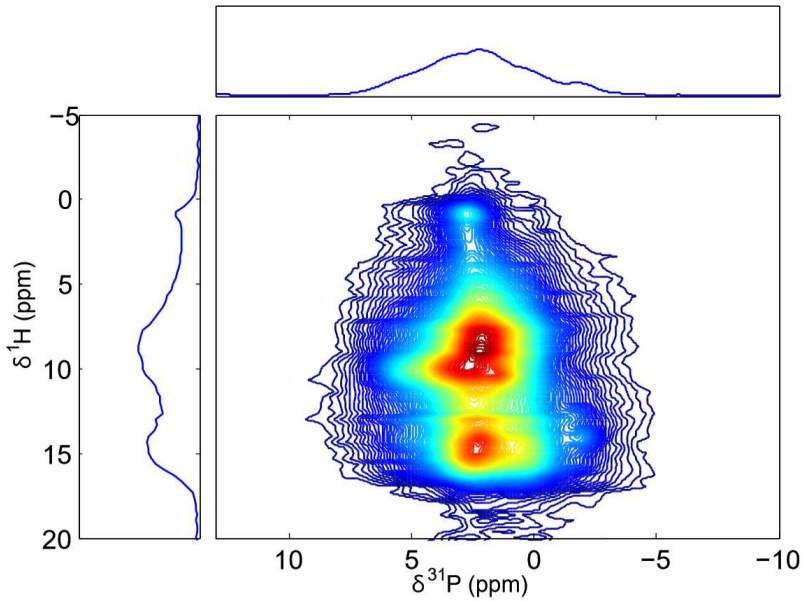


Figure 4.12. ^{1}H-^{31}P correlation spectrum of HA-DDSA acquired using DNP. Skyline projections of both dimensions are also displayed.

Figure 4.13 shows the DNP enhanced ^{1}H-^{31}P correlation spectra of HA-IsPLA (8). The first notable difference between this spectrum and that of the HA-DDSA (DNP enhanced) observed in Figure 4.12 is that the narrow resonance at 0-2 ppm (^{1}H) originating from bulk phosphate – OH interactions is much larger in signal intensity. The broad surface resonance observed at 5-15 ppm (^{1}H) is enhanced when compared to the standard solid-state NMR spectra of HA-IsPLA (8) (Figure 4.8); this narrow resonance dominates the spectra seen in Figure 4.12. Referring to the theory that the hydrocarbon dispersants interact primarily via the headgroup to form micellar like structures and PLA based dispersants lie flat/much closer to the surface it would be logical that the bulk material is the dominating resonance in HA-IsPLA (8). It was speculated that this is because the radicals in the polarising agent can sit in a much closer proximity to the bulk material as

the polymeric dispersant on the surface is also close to the bulk material. Whereas, the hydrocarbon chain does not reside in close proximity to the surface and the radicals sit much further away from the bulk causing a much greater enhancement of surface interactions.

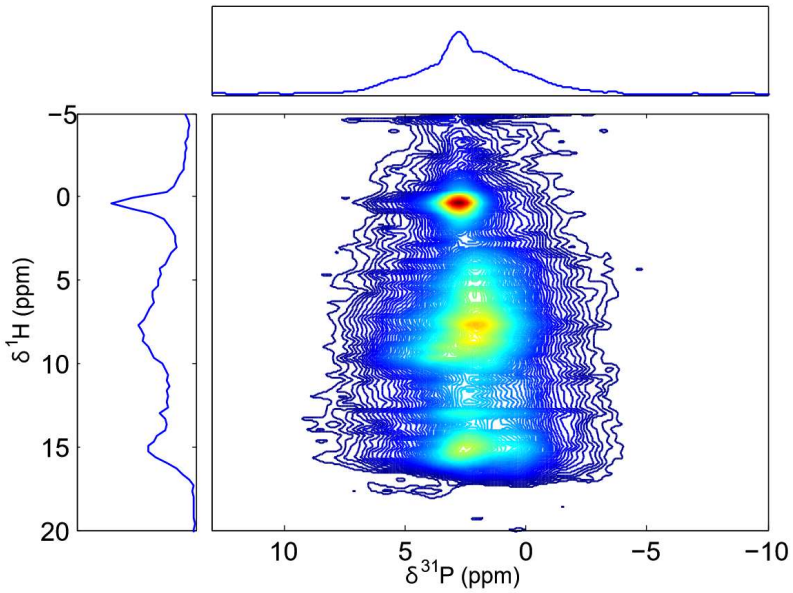


Figure 4.13. ^{1}H-^{31}P correlation spectrum of HA-IsPLA (8) acquired using DNP. Skyline projections of both dimensions are also displayed.

4.6 Conclusions

This chapter has investigated the use of solid-state NMR spectroscopy in determining the molecular interactions occurring on the surface of both uncoated and coated HA NP's. Our uncoated HA spectrum corroborated with those seen in previous literature and was used as a basis for determining whether any molecular interaction had occurred between the organic dispersants and the inorganic NP. All five coated HA materials analysed by standard solid state ^{1}H-^{31}P correlation NMR spectroscopy new resonances within the HA spectrum. In previous chapters, data has indicated that all the dispersants analysed in this chapter had, to varying extents, interacted and coated the HA NP's. The NMR spectroscopic studies reported in this chapter support these previous conclusions. It was

also proposed that the interactions between the HA surface and the aliphatic hydrocarbon dispersants were significantly different to the interactions occurring for our polymeric dispersants. With the head group interactions dominating for hydrocarbon dispersants and polymer chain interactions dominating these surface bonds for the polymer based dispersants. Standard solid-state NMR analysis revealed that the DDSA and laurate isosorbide molecules resulted in very different resonances in the HA NMR spectra. It was suggested that this gave evidence to this theory and it was likely that the hydrocarbon dispersants are forming structures like those formed by micelles. HA coated with PLA based dispersants gave rise to a different spectrum to those seen for both hydrocarbon based dispersants, however the PLA coated HA NP's all revealed the same resonance forming despite a change in head groups. This resonance was further enhanced by the addition of a longer polymer chain indicating a significant interaction occurring between the methoxy protons in the polymer chain and HA phosphate surface groups. As discussed in previous chapters the ability of the hydrocarbon chain to interact with the HA surface was very limited, especially once its relative hydrophobic nature was considered. In contrast, the PLA chain contained sites, such as the ester bonding between monomers, that were theoretically capable of forming various bonds with the HA surface. The interactions revealed in this NMR spectroscopic analysis explains the differences observed between these materials and gives another layer of understanding regarding the behaviour of our various nanocomposites.

The use of the novel solid-state DNP NMR analysis lent further evidence to support the conclusions that have been drawn throughout this study. In these surface enhanced NMR spectra, the radical polarising agent was situated much closer to the bulk material when the HA was coated in a polymeric dispersant and sat much further away in the hydrocarbon coated HA material.

In conclusion, solid-state NMR spectroscopy has been a powerful tool in revealing the interactions between the HA and the dispersant molecules on a molecular level. This analysis has provided the final piece in the puzzle and supports the overall conclusions drawn from the more conventional techniques in previous chapters.

4.7 References

1. A. Vyalikh, P. Simon, T. Kollmann, R. Kniep and U. Scheler, *Journal of Physical Chemistry C*, 2011, **115**, 1513-1519.
2. J. Kolmas and W. Kolodziejski, *Chemical Communications*, 2007, DOI: 10.1039/B708317C, 4390-4392.
3. Y. Wang, S. Von Euw, G. Laurent, C. Crevant, L. Bonhomme-Coury, M. M. Giraud-Guille, F. Babonneau, N. Nassif and T. Azais, *Materials Horizons*, 2014, **1**, 224-231.
4. G. Y. Cho, Y. T. Wu and J. L. Ackerman, *Science*, 2003, **300**, 1123-1127.
5. J. R. Long, W. J. Shaw, P. S. Stayton and G. P. Drobny, *Biochemistry*, 2001, **40**, 15451-15455.
6. C. Jager, T. Welzel, W. Meyer-Zaika and M. Epple, *Magnetic Resonance in Chemistry*, 2006, **44**, 573-580.
7. R. N. Panda, M. F. Hsieh, R. J. Chung and T. S. Chin, *Journal of Physics and Chemistry of Solids*, 2003, **64**, 193-199.
8. F. Pourpoint, C. Gervais, L. Bonhomme-Coury, T. Azais, C. Coelho, F. Mauri, B. Alonso, F. Babonneau and C. Bonhomme, *Applied Magnetic Resonance*, 2007, **32**, 435-457.
9. M. Ben Osman, S. Diallo-Garcia, V. Herledan, D. Brouri, T. Yoshioka, J. Kubo, Y. Millot and G. Costentin, *Journal of Physical Chemistry C*, 2015, **119**, 23008-23020.
10. J. V. Bradley, L. N. Bridgland, D. E. Colyer, M. J. Duer, T. Friscic, J. R. Gallagher, D. G. Reid, J. N. Skepper and C. M. Trasler, *Chemistry of Materials*, 2010, **22**, 6109-6116.
11. E. Salager, R. S. Stein, S. Steuernagel, A. Lesage, B. Elena and L. Emsley, *Chemical Physics Letters*, 2009, **469**, 336-341.
12. T. Bräuniger, P. Wormald and P. Hodgkinson, in *Current Developments in Solid State NMR Spectroscopy*, eds. N. Müller and P. K. Madhu, Springer Vienna, Vienna, 2003, DOI: 10.1007/978-3-7091-3715-4_4, pp. 69-74.
13. J. Keeler, *Understanding NMR Spectroscopy*, Wiley, 2005.
14. S. Maltsev, M. J. Duer, R. C. Murray and C. Jaeger, *Journal of Materials Science*, 2007, **42**, 8804-8810.
15. M. Gimeno-Fabra, F. Hild, P. W. Dunne, K. Walton, D. M. Grant, D. J. Irvine and E. H. Lester, *Crystengcomm*, 2015, **17**, 6175-6182.
16. A. D. Cohen and C. Reid, *Journal of Chemical Physics*, 1956, **25**, 790-791.
17. A. B. Barnes, G. De Paepe, P. C. A. van der Wel, K. N. Hu, C. G. Joo, V. S. Bajaj, M. L. Mak-Jurkauskas, J. R. Sirigiri, J. Herzfeld, R. J. Temkin and R. G. Griffin, *Applied Magnetic Resonance*, 2008, **34**, 237-263.
18. R. G. Griffin, *Nature*, 2010, **468**, 381-382.

19. C. T. Farrar, D. A. Hall, G. J. Gerfen, S. J. Inati and R. G. Griffin, *Journal of Chemical Physics*, 2001, **114**, 4922-4933.
20. R. S. Thakur, N. D. Kurur and P. K. Madhu, *Chemical Physics Letters*, 2006, **426**, 459-463.

5 Chapter 5: Summary and Outlook

This thesis has sought to investigate the synthesis of biocompatible HA NP's and a range of dispersant molecules with the aim of grafting such dispersants onto the HA surface using a continuous flow method. The study was successful in this aspect and a wide range of techniques were subsequently utilised with the aim of understanding the mechanisms involved in effectively coating the HA NP's.

The study was first focused on the synthesis of hydrocarbon based dispersants. Previous work conducted within the group had shown the successful coating of HA with the di-acid hydrocarbon, DDSA. This was used as a foundation for the investigation detailed throughout this thesis and it was deemed logical to use a selected range of hydrocarbon based dispersants to expand understanding of the surface chemistry involved in the coating process. These dispersants were easily sourced or synthesised and provided an insight into what types of dispersant chemistry provided the ideal coating material for our HA NP's. They were also able to survive the conditions in our hydrothermal flow process and all coated the HA NP's to varying degrees. The data revealed that the hydrocarbon chain length, its morphology and the chemical composition of the head group all had a role to play in the coating mechanisms observed. It was noted that a range of analytical techniques were needed in order to understand the interactions taking place between the HA surface and the dispersant molecules, with no one technique able to exclusively provide this information. The results from this chapter (Chapter 2) indicated that the most favourable dispersant was composed of an isosorbide head group and the shortest hydrocarbon chain (C_{12}). It was proposed that the head group would be the main point of interaction with the NP surface and the chain effect would be limited to its steric influence.

Chapter 3 moved the investigation into the realm of polymeric dispersants. As the overall aim of the project was to eventually disperse the HA NP's into a PLA matrix to form a biocompatible composite the dispersants chosen were composed of oligomeric PLA. The PLA dispersants would be composed of a headgroup that favourably interacted with the HA surface and a tail group that favoured the matrix polymer. Building upon the study conducted into the effectiveness of hydrocarbon dispersants (Chapter 2) similar head groups (initiators) were selected however; the range of dispersant morphology was expanded into the realm of a six-armed oligomeric polymers. New challenges arose in analysing such dispersants and their surface interaction with some techniques, such as extraction efficiency, being rendered impractical due to the polymer dispersant's preference to polar solvents. Advanced electron microscopy techniques, including electron energy loss and energy-dispersive X-ray spectroscopy, were employed to provide an overall understanding of the complex combination of morphology, steric and chemical composition that provided an effective coating material for the HA NP's. The concentration of polymer dispersant in the hydrothermal process was also found to affect the grafting of dispersant onto the HA surface with certain concentrations of the six-armed oligomer hindering the synthesis process completely. Solvent choice was revealed to be a factor in the coating mechanism with methanol reducing the thermal stability of the dispersant on the surface of HA. Once again both chain length of the polymer, the head group chemistry and the dispersant morphology all played a role in the dispersants effectiveness. It was revealed that not all polymer based dispersants were able to graft onto the HA surface with sorbitol PLA 1000 Da completely unable to form any bonding interaction. IsPLA (16) demonstrated a good extent of surface coating, was thermally stable and could survive long term storage. This dispersant was easily synthesised and did not excessively coat the HA to such an extent as to be visible under SEM and TEM

spectroscopy. It was proposed that, unlike the hydrocarbon based dispersants, the dispersant 'chain' was able to interact with the HA surface as PLA contained functional groups with lone pairs of electrons and potential dipoles formed between the carbon and oxygen bonds found in the ester groups.

Whilst a large range of analytical techniques were explored in Chapters 2 and 3 none could fully reveal the nature of the chemical bonds forming between dispersant and NP surface. Solid-state NMR spectroscopy is a unique method of observing the chemical bonding that occurs in solids. With the help of Dr Lindsey Knight and Nottingham University's Solid-State NMR research group the mechanisms behind the surface bonding occurring within our materials was revealed and evidence was provided in support of the theories drawn from the many analytical techniques employed throughout this study. ^{1}H-^{31}P correlation NMR spectroscopy revealed the formation of new peaks within the HA spectrum when dispersants were added to the hydrothermal synthesis. Most importantly this specialised NMR analysis revealed significant differences between hydrocarbon coated HA materials and PLA coated HA. The ^{1}H-^{31}P correlation spectra showed the formation of completely different resonances depending on the type of headgroup for the hydrocarbon based dispersant. However, the PLA coated HA spectra revealed the same resonance despite variations in the headgroup functionality. This resonance was enhanced by a longer polymer chain. Solid-state NMR spectroscopy supported the theory that hydrocarbon dispersants were not interacting via the chain group and instead formed bonds to the HA surface though the headgroup. The technique also demonstrated that the PLA based dispersants were dominated by polymer chain – HA surface interactions. From these results, a picture of how the dispersants molecules had arranged themselves on the surface was formed that lent evidence to discussions in previous chapters. Hydrocarbon dispersant

coated HA are thought to form micelle like structures and PLA dispersants are speculated to lie relatively flat on the surface with possible ‘polymer stacking’ taking place.

The work conducted in this thesis could be expanded by investigating numerous avenues. One of which includes extending the polymeric dispersants used into the branched area as this would not only create more functional end groups to act as surface anchor points but would also increase the steric boundary created by the dispersant. It has been established in this work that the PLA chain shows affinity to the HA surface causing the polymer chain to lie in close proximity to the NP surface. Whilst this results in a relatively strongly bonded dispersant it does not provide a large steric boundary between the highly charged HA surface and the hydrophobic PLA matrix used in the final composite materials. A larger steric boundary could provide further stabilisation properties and was discussed in Chapter 3. It is important to note however, that the polymer should not create too much steric hindrance as this would cause the dispersant coated HA NP’s to interact via chain entanglement to form aggregates.

The study could expand into the realm of copolymers and utilise another well researched biopolymer such as polycaprolactone (PCL). PCL has an increased aliphatic portion in the polymer chain and would in theory be less attracted to the highly charged HA. This may produce a dispersant with a polymeric chain that would not prefer to be in close proximity to the HA surface unlike the PLA based dispersants. Furthermore, it is of course possible to expand the range of functional head groups along with altering the polymer backbone to further refine the desirable chemical properties. For example, using the six-armed polymers discussed in Chapter 3 and altering the hydroxyl end groups to produce the diacid functional group seen in DDSA may increase the strength of the polymer-surface bonds significantly.

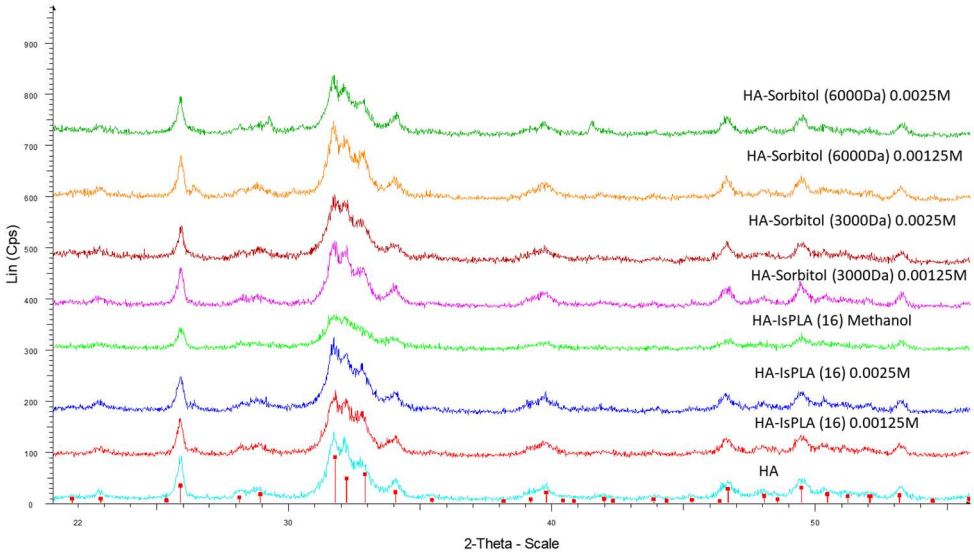
The method of producing dispersant coated nanoparticles via a continuous hydrothermal process can also be investigated further. The process has been shown to be capable of producing various inorganic nanomaterial's which could be of interest in medical applications.[1, 2] The method of introducing the dispersant is capable of modification; it has been briefly mentioned in Chapter 2 that the hydrothermal reactor has a 'capping' point where other reactants can be introduced.[3] Introduction of dispersants at this point was not investigated in this thesis due to time constraints and the failure of this introduction method to produce DDSA coated HA.[4] However, it would be beneficial for this route to be explored in more depth should different morphologies of HA NP's be desired. In order to alter the morphology of the HA plates to form rods and scrolls the pH of the downstream (containing ammonium phosphate) must be increased. In a brief investigation, it was found that an increase in pH would result in an unsuccessful coating, most likely caused by the degradation of the dispersant due to the harsh conditions within the reactor (high pressure, temperature) combined with the increased pH. It may be possible to use the capping point, which is at a lower temperature than the reactor, to introduce the dispersant to the preformed HA NP's. Different morphologies of HA could perform differently within the final polymer composite.

5.1 References

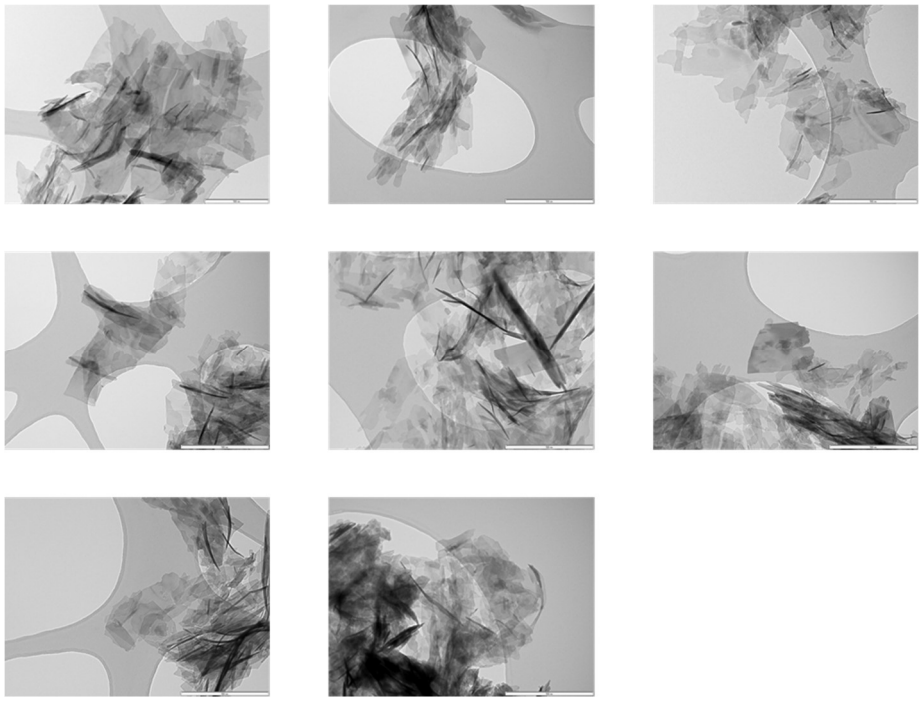
1. P. Caramazana-Gonzalez, P. W. Dunne, M. Gimeno-Fabra, M. Zilka, M. Ticha, B. Stieberova, F. Freiberg, J. McKechnie and E. H. Lester, *Green Chemistry*, 2017, **19**, 1536-1547.
2. I. Clark, P. W. Dunne, R. L. Gomes and E. Lester, *Journal of Colloid and Interface Science*, 2017, **504**, 492-499.
3. E. Lester, S. V. Y. Tang, A. Khlobystov, V. L. Rose, L. Buttery and C. J. Roberts, *CrystEngComm*, 2013, **15**, 3256-3260.
4. M. Gimeno-Fabra, F. Hild, P. W. Dunne, K. Walton, D. M. Grant, D. J. Irvine and E. H. Lester, *Crystengcomm*, 2015, **17**, 6175-6182.

6 Appendix

1a) XRD patterns for uncoated HA and coated HA for a selection of PLA dispersants. Highlighted marks on the x-axis indicate the predicted peak positions for hexagonal phase hydroxyapatite.



1b) TEM images of modified HA. From left to right, top to bottom: HA-Sorbitol (6000Da) 0.0025M, HA-Sorbitol (6000Da) 0.00125M, HA-Sorbitol (3000Da) 0.0025M, HA-Sorbitol (3000Da) 0.00125M, HA-IsPLA (16) Methanol, HA-IsPLA (16) 0.0025M, HA-IsPLA (16) 0.00125M and unmodified HA. Scale bar on the bottom right is equivalent to 500 nm



6.1 Further analysis of the esterified hydrocarbon dispersants

Lauric isosorbide:

ATR FTIR (Neat) ν 1083, 1170, 1730, 2848, 2916, 3394 cm^{-1}; ^{1}H NMR (400 MHz; $CDCl_3$) δ_H ppm 0.85-0.90 (6H, t, **CH_3**$(CH_2)_8(CH_2)_2$OC=OCHCH_2OCHCHOCH_2CHOC=O$(CH_2)_2(CH)_8$**CH_3**), 1.20-1.35 (32H, m, CH_3**$(CH_2)_8$**$(CH_2)_2$OC=OCHCH_2OCHCHOCH_2CHOC=O$(CH_2)_2$**$(CH_2)_8$**CH_3), 1.54-1.68 (8H, m, $CH_3(CH_2)_8$**$(CH_2)_2$**OC=OCHCH_2OCHCHOCH_2CHOC=O**$(CH_2)_2$**$(CH_2)_8CH_3$), 2.28-2.39 (4H, m, $CH_3(CH_2)_8$**$(CH_2)_2$**OC=OCHCH_2OCHCHOCH_2CHOH), 3.54-3.60 (1H, m, $CH_3(CH_2)_8(CH_2)_2$OC=OCHCH_2OCHCHOCH_2CH**OH**), 3.84-3.99 (4H, m, $CH_3(CH_2)_8(CH_2)_2$OC=OCH**CH_2**OCHCHO**CH_2**CHOC=O$(CH_2)_2(CH_2)_8CH_3$), 4.00-4.02 (2H, m, $CH_3(CH_2)_8(CH_2)_2$OC=OCHCH_2OCHCHO**CH_2**CHOH), 4.28-4.49 (4H, m, CH3$(CH2)_8$(CH2)2OC=O**CH**CH2O**CHCH**OCH2**CH**OH), 4.61-5.25 (4H, m, $CH_3(CH_2)_8(CH_2)_2$OC=O**CH**CH_2O**CHCH**OCH_2**CH**OC=O$(CH_2)_2(CH_2)_8CH_3$); ^{13}C NMR (100 MHz; $CDCl_3$) δ_C ppm 14.3, 22.8, 25, 29.7, 32.1, 34.32, 70.5, 72.5, 73.9. Melting point: 46°C.

Palmitate isosorbide:

ATR FTIR (Neat) ν 1091, 1165, 1730, 2848, 2918, 3382 cm^{-1}; ^{1}H NMR (400 MHz; $CDCl_3$) δ_H ppm 0.85-0.92 (6H, t, **CH_3**$(CH_2)_{12}(CH_2)_2$OC=OCHCH_2OCHCHOCH_2CHOC=O$(CH_2)_2(CH)_{12}$**CH_3**), 1.20-1.36 (48H, m, CH_3**$(CH_2)_{12}$**$(CH_2)_2$OC=OCHCH_2OCHCHOCH_2CHOC=O$(CH_2)_2$**$(CH_2)_{12}$**CH_3), 1.51-1.59 (8H, m, $CH_3(CH_2)_{12}$**$(CH_2)_2$**OC=OCHCH_2OCHCHOCH_2CHOC=O**$(CH_2)_2$**$(CH_2)_{12}CH_3$), 2.28-2.39 (4H, m, $CH_3(CH_2)_{12}$**$(CH_2)_2$**OC=OCHCH_2OCHCHOCH_2CHOH), 3.54-3.60 (1H, m, $CH_3(CH_2)_{12}(CH_2)_2$OC=OCHCH_2OCHCHOCH_2CH**OH**), 3.84-3.99 (4H, m, $CH_3(CH_2)_{12}(CH_2)_2$OC=OCH**CH_2**OCHCHO**CH_2**CHOC=O$(CH_2)_2(CH_2)_{12}CH_3$), 4.00-4.03 (2H, m, $CH_3(CH_2)_{12}(CH_2)_2$OC=OCHCH_2OCHCHO**CH_2**CHOH), 4.28-4.49 (4H, m, CH3$(CH2)_{12}$(CH2)2OC=O**CH**CH2O**CHCH**OCH2**CH**OH), 4.61-5.26 (4H, m, $CH_3(CH_2)_{12}(CH_2)_2$OC=O**CH**CH_2O**CHCH**OCH_2**CH**OC=O$(CH_2)_2(CH_2)_{12}CH_3$); ^{13}C NMR (100 MHz; $CDCl_3$) δ_C ppm 14.3, 22.8, 25, 29.8, 32.1, 70.5, 73.9. Melting point: 66.4°C.

Stearic isosorbide:

ATR FTIR (Neat) ν 1083, 1165, 1728, 2850, 2919, 3382 cm^{-1}; ^{1}H NMR (400 MHz; $CDCl_3$) δ_H ppm 0.85-0.91 (6H, t, **CH_3**$(CH_2)_{14}(CH_2)_2OC{=}OCHCH_2OCHCHOCH_2CHOC{=}O(CH_2)_2(CH)_{14}$**$CH_3$**), 1.20-1.36 (56H, m, CH_3**$(CH_2)_{14}$**$(CH_2)_2OC{=}OCHCH_2OCHCHOCH_2CHOC{=}O(CH_2)_2$**$(CH_2)_{14}$**$CH_3$), 1.51-1.59 (8H, m, $CH_3(CH_2)_{14}$**$(CH_2)_2$**$OC{=}OCHCH_2OCHCHOCH_2CHOC{=}O$**$(CH_2)_2$**$(CH_2)_{14}CH_3$), 2.27-2.39 (4H, m, $CH_3(CH_2)_{14}$**$(CH_2)_2$**$OC{=}OCHCH_2OCHCHOCH_2CHOH$), 3.54-3.61 (1H, m, $CH_3(CH_2)_{14}(CH_2)_2OC{=}OCHCH_2OCHCHOCH_2CH$**OH**), 3.84-3.99 (4H, m, $CH_3(CH_2)_{14}(CH_2)_2OC{=}OCH$**$CH_2$**$OCHCHO$**$CH_2$**$CHOC{=}O(CH_2)_2(CH_2)_{14}CH_3$), 4.00-4.03 (2H, m, $CH_3(CH_2)_{14}(CH_2)_2OC{=}OCHCH_2OCHCHO$**$CH_2$**$CHOH$), 4.27-4.49 (4H, m, CH3$(CH2)_{14}$(CH2)2OC=O**CH**CH2O**CHCH**OCH2**CH**OH), 4.59-5.25 (4H, m, $CH_3(CH_2)_{14}(CH_2)_2OC{=}O$**CH**$CH_2O$**CHCH**$OCH_2$**CH**$OC{=}O(CH_2)_2(CH_2)_{14}CH_3$); ^{13}C NMR (100 MHz; $CDCl_3$) δ_C ppm 14.3, 22.8, 25, 29.9, 32.1, 34.3, 72.5, 73.9. Melting point: 73.0°C.

6.2 Further analysis of the polymeric dispersants

IsPLA(8):

ATR FTIR (Neat) ν 1085, 1188, 1746, 2936, 3478 cm^{-1}; ^{1}H NMR (400 MHz; $CDCl_3$) δ_H ppm 1.37-1.62 (24H, m, HOCH**CH_3**$(OC{=}OCH$**CH_3**$)_3OCHCH_2OCHCHOCH_2CHO(OC{=}OCH$**$CH_3$**$)_3$**$CH_3$**$CHOH$), 3.73-4.02 (4H, m, $HOCHCH_3(OC{=}OCHCH_3)_3OCH$**$CH_2$**$OCHCHO$**$CH_2$**$CHO(OC{=}OCHCH_3)_3CH_3CHOH$), 4.27-4.49 (3H, m, HO**CH**$CH_3(OC{=}OCHCH_3)_3OCHCH_2OCHCHOCH_2$**CH**$O(OC{=}OCHCH_3)_3CH_3$**CH**OH), 4.78-4.87 (1H, m, $HOCHCH_3(OC{=}OCHCH_3)_3O$**CH**$CH_2OCHCHOCH_2CHO(OC{=}OCHCH_3)_3CH_3CHOH$) 5.00-5.10 (1H, m, $HOCHCH_3(OC{=}OCHCH_3)_3OCHCH_2OCH$**CH**$OCH_2CHO(OC{=}OCHCH_3)_3CH_3CHOH$) 5.11-5.28 (7H, m, $HOCHCH_3(OC{=}O$**CH**$CH_3)_3OCHCH_2O$**CH**$CHOCH_2CHO(OC{=}O$**CH**$CH_3)_3CH_3CHOH$). GPC (THF), Mw 816, Mn 688, Đ 1.19.

IsPLA(16):

ATR FTIR (Neat) ν 1078, 1186, 1748, 2934 , 3508 cm^{-1}; ^{1}H NMR (400 MHz; $CDCl_3$) δ_H ppm 1.34-1.61 (51H, m, HOCH**CH_3**(OC=OCH**CH_3**)$_7$OCHCH_2OCHCHOCH_2CHO(OC=OCH**CH_3**)$_7$**CH_3**CHOH), 3.72-4.01 (4H, m, HOCHCH_3(OC=OCHCH_3)$_7$OCH**CH_2**OCHCHO**CH_2**CHO(OC=OCHCH_3)$_7$CH_3CHOH), 4.28-4.46 (3H, m, HO**C**HCH_3(OC=OCHCH_3)$_7$OCHCH_2OCHCHOCH_2**C**HO(OC=OCHCH_3)$_7$CH_3**C**HOH), 4.77-4.85 (1H, m, HOCHCH_3(OC=OCHCH_3)$_7$O**C**HCH_2OCHCHOCH_2CHO(OC=OCHCH_3)$_7$CH_3CHOH) 5.01-5.08 (1H, m, HOCHCH_3(OC=OCHCH_3)$_7$OCHCH_2OCH**C**HOCH_2CHO(OC=OCHCH_3)$_7$CH_3CHOH) 5.10-5.26 (16H, m, HOCHCH_3(OC=O**C**HCH_3)$_7$OCHCH_2O**C**HCHOCH_2CHO(OC=O**C**HCH_3)$_7$CH_3CHOH). GPC (THF), Mw 1238, Mn 1040, Đ 1.19.

IsPLA(24):

ATR FTIR (Neat) ν 1077, 1179, 1748, 2934, 3499 cm^{-1}; ^{1}H NMR (400 MHz; $CDCl_3$) δ_H ppm 1.40-1.65 (63H, m, HOCH**CH_3**(OC=OCH**CH_3**)$_8$OCHCH_2OCHCHOCH_2CHO(OC=OCH**CH_3**)$_8$**CH_3**CHOH), 3.80-4.02 (4H, m, HOCHCH_3(OC=OCHCH_3)$_8$OCH**CH_2**OCHCHO**CH_2**CHO(OC=OCHCH_3)$_8$CH_3CHOH), 4.34-4.50 (3H, m, HO**C**HCH_3(OC=OCHCH_3)$_8$OCHCH_2OCHCHOCH_2**C**HO(OC=OCHCH_3)$_8$CH_3**C**HOH), 4.81-4.89 (1H, m, HOCHCH_3(OC=OCHCH_3)$_8$O**C**HCH_2OCHCHOCH_2CHO(OC=OCHCH_3)$_8$CH_3CHOH) 5.01-5.09 (1H, m, HOCHCH_3(OC=OCHCH_3)$_8$OCHCH_2OCH**C**HOCH_2CHO(OC=OCHCH_3)$_8$CH_3CHOH) 5.10-5.26 (20H, m, HOCHCH_3(OC=O**C**HCH_3)$_8$OCHCH_2O**C**HCHOCH_2CHO(OC=O**C**HCH_3)$_8$CH_3CHOH). GPC (THF), Mw 1525, Mn 1341, Đ 1.14.

IsPLA representative ^{13}C NMR (100 MHz; $CDCl_3$) δ_C ppm 16.3, 17.1, 31.4, 67.1,69.5, 72.9, 75.4, 86.2, 170.0, 207.

NaPLA(8):

ATR FTIR (Neat) ν 1077, 1190, 1604, 1740, 2938 cm^{-1}; ^{1}H NMR (400 MHz; $CDCl_3$) δ_H ppm 1.34-1.64 (36H, m, HOCH**CH_3**(OC=OCH**CH_3**)$_{10}$OCH**CH_3**OC=ONa), 4.29-4.42 (1H, m, HO**C**HCH_3(OC=OCHCH_3)$_{10}$OCHCH_3OC=ONa), 4.82-4.96 (1H, m, HOCHCH_3(OC=OCHCH_3)$_{10}$O**C**HCH_3OC=ONa), 5.10-5.28 (10H, m, HOCHCH_3(OC=O**C**HCH_3)$_{10}$OCHCH_3OC=ONa). GPC (THF), Mw 956, Mn 758, Đ 1.26.

NaPLA(16):

ATR FTIR (Neat) ν 1075, 1190, 1605, 1748, 2979 cm^{-1}; ^{1}H NMR (400 MHz; $CDCl_3$) δ_H ppm 1.35-1.64 (54H, m, HOCH**CH_3**(OC=OCH**CH_3**)$_{16}$OCH**CH_3**OC=ONa), 4.32-4.41 (1H, m, HO**CH**CH_3(OC=OCHCH_3)$_{16}$OCHCH_3OC=ONa), 4.88-4.96 (1H, m, HOCHCH_3(OC=OCHCH_3)$_{16}$O**CH**CH_3OC=ONa), 5.10-5.28 (16H, m, HOCHCH_3(OC=O**CH**CH_3)$_{16}$OCHCH_3OC=ONa). GPC (THF), Mw 1092, Mn 860, Đ 1.27.

NaPLA(24):

ATR FTIR (Neat) ν 1075, 1179, 1610, 1750, 2983 cm^{-1}; ^{1}H NMR (400 MHz; $CDCl_3$) δ_H ppm 1.34-1.62 (73H, m, HOCH**CH_3**(OC=OCH**CH_3**)$_{22}$OCH**CH_3**OC=ONa), 4.31-4.41 (1H, m, HO**CH**CH_3(OC=OCHCH_3)$_{22}$OCHCH_3OC=ONa), 4.85-4.94 (1H, m, HOCHCH_3(OC=OCHCH_3)$_{22}$O**CH**CH_3OC=ONa), 5.09-5.27 (22H, m, HOCHCH_3(OC=O**CH**CH_3)$_{22}$OCHCH_3OC=ONa). GPC (THF), Mw 1373, Mn 1025, Đ 1.34.

NaPLA representative ^{13}C NMR (100 MHz; $CDCl_3$) δ_C ppm 15.8, 16.7, 20.5, 66.6, 72.5, 30.9, 69.0, 169.4, 206.9.

Sorbitol PLA (1000 Da):

ATR FTIR (Neat) ν 1081, 1181, 1736, 2949, 3482 cm^{-1}; ^{1}H NMR (400 MHz; $CDCl_3$) δ_H ppm 1.42-1.72 (48H, m, (HOCH**CH_3**(OC=OCH**CH_3**)$_2$)$_6$$CH_2(CH)_4$$CH_2$), 4.30-4.44 (6H, m, (HO**CH**CH_3(OC=OCHCH_3)$_2$)$_6$$CH_2(CH)_4$$CH_2$), 5.08-5.54 (11H, m, (HOCHCH_3(OC=O**CH**CH_3)$_2$)$_6$$CH_2(CH)_4$$CH_2$). GPC (THF), Mw 1211, Mn 1104, Đ 1.10.

Sorbitol PLA (3000 Da):

ATR FTIR (Neat) ν 1077, 1180, 1740, 2936, 3530 cm^{-1}; ^{1}H NMR (400 MHz; $CDCl_3$) δ_H ppm 1.42-1.66 (130H, m, (HOCH**CH_3**(OC=OCH**CH_3**)$_6$)$_6$$CH_2(CH)_4$$CH_2$), 4.30-4.40 (6H, m, (HO**CH**CH_3(OC=OCHCH_3)$_6$)$_6$$CH_2(CH)_4$$CH_2$), 5.08-5.29 (36H, m, (HOCHCH_3(OC=O**CH**CH_3)$_6$)$_6$$CH_2(CH)_4$$CH_2$). GPC (THF), Mw 3347, Mn 3123, Đ 1.07.

Sorbitol PLA (6000 Da):

ATR FTIR (Neat) ν 1073, 1186, 1740, 2969, 3514 cm^{-1}; ^{1}H NMR (400 MHz; $CDCl_3$) δ_H ppm 1.44-1.64 (231H, m, (HOCH**CH_3**(OC=OCH**CH_3**)$_{11}$)$_6$$CH_2(CH)_4$$CH_2$), 4.30-4.40 (6H, m, (HO**CH**CH_3(OC=OCHCH_3)$_{11}$)$_6$$CH_2(CH)_4$$CH_2$), 5.06-5.29 (68H, m, (HOCHCH_3(OC=O**CH**CH_3)$_6$)$_{11}$$CH_2(CH)_4$$CH_2$). GPC (THF), Mw 6458, Mn 6223, Đ 1.04.

Sorbitol PLA representative ^{13}C NMR (100 MHz; $CDCl_3$) δ_C ppm 15.8, 16.7, 20.4, 66.8, 69.0, 72.5, 167.4.

6.3 Polymer DSC

All polymeric dispersants synthesised were amorphous in nature and did not exhibit a melting point when analysed by DSC. Figure 6.1 displays the DSC trace for IsPLA (16) and is a representative example of a polymer dispersant DSC trace.

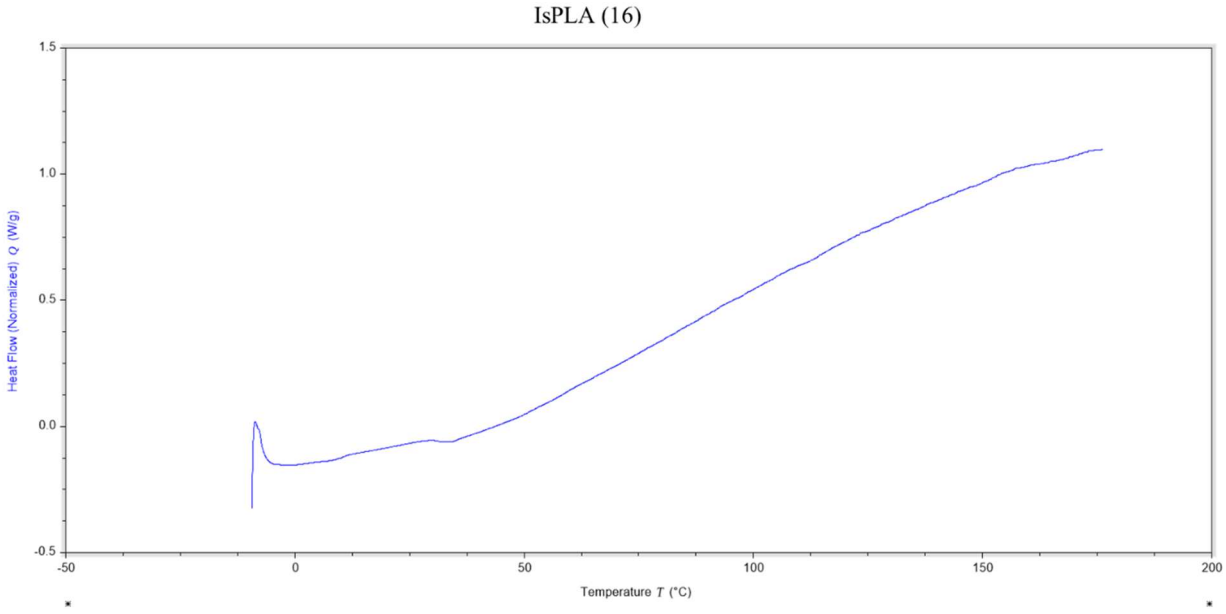


Figure 6.1 DSC trace of IsPLA(16)